**EUMETSAT Satellite Application Facility on Climate Monitoring**


# Validation Report

# SEVIRI cloud products

# CLAAS Edition 2

DOI: 10.5676/EUM_SAF_CM/CLAAS/V002

| | |
|---|---|
| **Fractional Cloud Cover** | **CM-21011** |
| **Joint Cloud property Histogram** | **CM-21021** |
| **Cloud Top level** | **CM-21031** |
| **Cloud Phase** | **CM-21041** |
| **Liquid Water Path** | **CM-21051** |
| **Ice Water Path** | **CM-21061** |


| | |
|---|---|
| Reference Number: | SAF/CM/KNMI/VAL/SEV/CLD |
| Issue/Revision Index: | 2.1 |
| Date: | 10.06.2016 |

## Document Signature Table

| | Name | Function | Signature | Date |
|---|---|---|---|---|
| Authors | Stephan Finkensieper<br>Timo Hanschmann<br>Martin Stengel<br>Nikos Benas<br>Gerd-Jan van Zadelhoff<br>Jan Fokke Meirink | CM SAF scientist (DWD)<br>CM SAF scientist (DWD)<br>CM SAF scientist (DWD)<br>CM SAF scientist (KNMI)<br>CM SAF scientist (KNMI)<br>CM SAF scientist (KNMI) | | 20/04/2016<br>10/0672016 |
| Editor | Jan Fokke Meirink | CM SAF scientist (KNMI) | | 10/06/2016 |
| Approval | Rainer Hollmann | Science Coordinator | | 10/06/2016 |
| Release | Martin Werscheck | Project Manager | | |

## Distribution List

| Internal Distribution | |
|---|---|
| **Name** | **No. Copies** |
| DWD Archive | 1 |
| CM SAF Team | 1 |

| External Distribution | | |
|---|---|---|
| **Company** | **Name** | **No. Copies** |
| PUBLIC | | 1 |

## Document Change Record

| Issue/Revision | Date | DCN No. | Changed Pages/Paragraphs |
|---|---|---|---|
| 1.0 | 20/04/2016 | SAF/CM/KNMI/VAL/SEV/CLD/2/1.0 | First official version submitted for DRR 2.4 |
| 1.1 | 10/06/2016 | SAF/CM/KNMI/VAL/SEV/CLD/2.1 | Update addressing DRR 2.4 RIDs |

## Table of Contents

## List of Figures

## List of Tables

## Applicable documents

| Reference | Title | Code |
|---|---|---|
| AD 1 | EUMETSAT CM SAF CDOP 2 Product Requirements Document (PRD) | SAF/CM/DWD/PRD/2.7 |
| AD 2 | Requirements Review RR 2.4 document | SAF/CM/CDOP2/KNMI/RR24, v1.2 |

## Reference Documents

| Reference | Title | Code |
|---|---|---|
| RD 1 | Product User Manual SEVIRI Cloud Products Edition 2 (CLAAS-2) | SAF/CM/DWD/PUM/SEV/CLD/2.1 |
| RD 2 | Algorithm Theoretical Basis Document SEVIRI cloud products processing chain | SAF/CM/DWD/ATBD/SEV/CLD/2.3 |
| RD 3 | Algorithm Theoretical Basis Document SEVIRI cloud physical products | SAF/CM/KNMI/ATBD/SEV/CPP/2.2 |
| RD 4 | Algorithm Theoretical Basis Document SAFNWC/MSG “Cloud mask, Cloud Type, Cloud Top Temperature, Pressure, Height” | SAF/NWC/CDOP/MFL/SCI/ATBD/01, v3.2 |
| RD 5 | Algorithm Theoretical Basis Document Joint Cloud property Histograms AVHRR/SEVIRI | SAF/CM/SMHI/ATBD/JCH/2.0 |
| RD 6 | Validation Report SEVIRI cloud products Edition 1 | SAF/CM/DWD/VAL/SEV/CLD/1.2, dated 16/10/2013. |

# 1 The EUMETSAT SAF on Climate Monitoring

The importance of climate monitoring with satellites was recognized in 2000 by EUMETSAT Member States when they amended the EUMETSAT Convention to affirm that the EUMETSAT mandate is also to “contribute to the operational monitoring of the climate and the detection of global climatic changes". Following this, EUMETSAT established within its Satellite Application Facility (SAF) network a dedicated centre, the SAF on Climate Monitoring (CM SAF, http://www.cmsaf.eu).

The consortium of CM SAF currently comprises the Deutscher Wetterdienst (DWD) as host institute, and the partners from the Royal Meteorological Institute of Belgium (RMIB), the Finnish Meteorological Institute (FMI), the Royal Meteorological Institute of the Netherlands (KNMI), the Swedish Meteorological and Hydrological Institute (SMHI), the Meteorological Service of Switzerland (MeteoSwiss), and the Meteorological Service of the United Kingdom (UK MetOffice). Since the beginning in 1999, the EUMETSAT Satellite Application Facility on Climate Monitoring (CM SAF) has developed and will continue to develop capabilities for a sustained generation and provision of Climate Data Records (CDR’s) derived from operational meteorological satellites.

In particular, the generation of long-term data records is pursued. The ultimate aim is to make the resulting data records suitable for the analysis of climate variability and potentially the detection of climate trends. CM SAF works in close collaboration with the EUMETSAT Central Facility and liaises with other satellite operators to advance the availability, quality and usability of Fundamental Climate Data Records (FCDRs) as defined by the Global Climate Observing System (GCOS). As a major task the CM SAF utilizes FCDRs to produce records of Essential Climate Variables (ECVs) as defined by GCOS. Thematically, the focus of CM SAF is on ECVs associated with the global energy and water cycle.

Another essential task of CM SAF is to produce data records that can serve applications related to the Global Framework of Climate Services initiated by the WMO World Climate Conference-3 in 2009. CM SAF is supporting climate services at national meteorological and hydrological services (NMHSs) with long-term data records but also with data records produced close to real time that can be used to prepare monthly/annual updates of the state of the climate. Both types of products together allow for a consistent description of mean values, anomalies, variability and potential trends for the chosen ECVs. CM SAF ECV data records also serve the improvement of climate models both at global and regional scale.

As an essential partner in the related international frameworks, in particular WMO SCOPE-CM (Sustained COordinated Processing of Environmental satellite data for Climate Monitoring), the CM SAF - together with the EUMETSAT Central Facility, assumes the role as main implementer of EUMETSAT’s commitments in support to global climate monitoring. This is achieved through:

- Application of highest standards and guidelines as lined out by GCOS for the satellite data processing,
- Processing of satellite data within a true international collaboration benefiting from developments at international level and pollinating the partnership with own ideas and standards,
- Intensive validation and improvement of the CM SAF climate data records,
- Taking a major role in data record assessments performed by research organisations such as WCRP (World Climate Research Program). This role provides the CM SAF

with deep contacts to research organizations that form a substantial user group for the CM SAF CDRs,

- Maintaining and providing an operational and sustained infrastructure that can serve the community within the transition of mature CDR products from the research community into operational environments.

A catalogue of all available CM SAF products is accessible via the CM SAF webpage, http:/www.cmsaf.eu/. Here, detailed information about product ordering, add-on tools, sample programs and documentation is provided.

## 2 Executive Summary

This CM SAF report provides information on the validation of cloud products of the CLAAS-2 data record (CLAAS-2: CLoud property dAtAset using SEVIRI, Edition 2). All CLAAS-2 products are derived from measurements taken by the Spinning Enhanced Visible and InfraRed Imager (SEVIRI) onboard the EUMETSAT Meteosat Second Generation (MSG) satellites. The covered time period ranges from 2004 to 2015, and includes MSG-1, -2, and -3 (Meteosat-8, -9, and -10, respectively).

This report presents an evaluation of the following cloud products:

| | | |
|---|---|---|
| Fractional Cloud Cover | CM-21011 | (CFC) |
| Joint Cloud property Histogram | CM-21021 | (JCH) |
| Cloud Top level | CM-21031 | (CTO) |
| Cloud Phase | CM-21041 | (CPH) |
| Liquid Water Path | CM-21051 | (LWP) |
| Ice Water Path | CM-21061 | (IWP) |

The reference datasets, used to evaluate CLAAS-2 cloud products, were taken from ground-based observation sources (SYNOP) as well as from other satellite-based sources (incl. CALIPSO, CloudSat, AMSR-E, and MODIS). The comparisons to MODIS products have to be viewed as inter-comparisons, because the MODIS type of measurements (passive visible and infrared imagery) are similar to SEVIRI. The comparisons to the other products come much closer to validation of the SEVIRI products because of their assumed superior measurement principle and quality, although these other products also have their uncertainties and pitfalls, which will be outlined in this report.

The evaluation includes both Level-2 and Level-3 comparisons (except JCH, which by definition only exists as monthly representations), to not only demonstrate the applicability concerning the aggregated products, but also to allow a more in-depth analysis of the cloud properties provided on a high temporal resolution. All evaluations presented were done in the light of the product requirements. The evaluation scores and their compliance to the target requirements of accuracy and precisions are given in Table 1-1 and Table 1-2, and are briefly summarized in the following:

- **Fractional Cloud Cover (CFC)**
  - The CLAAS-2 level-3 CFC product fulfils the target requirements when compared with all references. Optimal requirements are also fulfilled for SYNOP and MODIS.
  - The level-2 cloud mask validation scores with CALIOP fulfil the threshold requirements.

- **Cloud Top level (CTO)**
  - The CLAAS-2 CTH product fulfils target requirements when compared to CALIOP (level-2) and optimal requirements for comparisons with MODIS (level-3). These results hold for both bias and bc-RMS.
  - The CLAAS-2 CTP product fulfils optimal accuracy requirements and threshold precision requirements against CALIOP (level-2). Against MODIS level-3 data the threshold accuracy requirement and target precision requirement are fulfilled.
  -

- **Cloud Thermodynamic Phase (CPH)**
  - The CLAAS-2 CPH product mostly achieves target and optimal requirements for POD and FAR when compared to CALIOP. When evaluated against MODIS, optimal requirements for both bias and bc-RMS are fulfilled.

- **Liquid Water Path (LWP)**
  - The CLAAS-2 LWP product meets target requirements for bias and bc-RMS when validated against the UWisc data set. The bias and bc-RMS with respect to MODIS fulfil optimal requirements.
  - The level-2 target precision requirement is fulfilled against AMSR-E data.

- **Ice Water Path (IWP)**
  - The CLAAS-2 IWP product fulfils optimal bias and bc-RMS requirements when compared to MODIS. Both CLAAS-2 and MODIS IWP show similar trends.

**Table 1-1:** Summary of CLAAS-2 validation results compared to target **accuracy** requirements for each cloud product. The accuracies are formulated in terms of biases. Results from consistency checks / inter-comparisons (using MODIS data, which, due to the sampling, cannot be seen as absolute reference) are marked in **blue**. * = ICOT>0 applied for CALIOP filtering; ** = ICOT>0.2 applied for CALIOP filtering.

| Product | | Accuracy requirement (bias) | Achieved accuracies |
|---|---|---|---|
| Cloud Fractional Cover | (CFC) | 10% | ≈ 3% (CALIOP*)<br>3.8 % (SYNOP)<br>-1.1 % (MODIS) |
| Cloud Top Height | (CTH) | 800 m | -520 m (CALIOP**)<br>307 m (MODIS) |
| Cloud Top Pressure | (CTP) | 45 hPa | -2.2 hPa (CALIOP**)<br>-58.6 hPa (MODIS) |
| Cloud Phase | (CPH) | 10% | ≈ 0% (CALIOP**)<br>1% (MODIS) |
| Liquid Water Path | (LWP) | 10 g $m^{-2}$ | 6.17 g $m^{-2}$ (UWisc)<br>2.05 g $m^{-2}$ (MODIS) |
| Ice Water Path | (IWP) | 20 g $m^{-2}$ | -5.11 g $m^{-2}$ (MODIS) |
| Joint Cloud Histogram | (JCH) | n/a | n/a |

**Table 1-2:** Summary of CLAAS-2 validation results compared to target **precision** requirements for each cloud product. Consistency checks are marked in **blue**. * = ICOT>0 applied for CALIOP filtering; ** = ICOT>0.2 applied for CALIOP filtering.

| Product | | Precision requirement<br>bc-RMS/POD/FAR | Achieved precisions |
|---|---|---|---|
| Cloud Fractional Cover | (CFC) | L2 $POD_{cld}$ > 90%<br>L2 $FAR_{cld}$ < 15% | 87.5% (CALIOP*)<br>16.9% (CALIOP*) |
| | | L3 bc-rms < 20% | 10.0 % (SYNOP)<br>7.2 % (MODIS) |
| Cloud Top Height | (CTH) | L2 bc-rms < 2500 m | 2398 m (CALIOP**) |
| | | L3 bc-rms < 1500 m | 949 m (MODIS) |
| Cloud Top Pressure | (CTP) | L2 bc-rms < 110 hPa | 134.1 hPa (CALIOP**) |
| | | L3 bc-rms < 70 hPa | 62.7 hPa (MODIS) |
| Cloud Phase | (CPH) | L2 $POD_{liq}$ > 80%<br>L2 $FAR_{liq}$ < 20%<br>L2 $POD_{ice}$ > 80%<br>L2 $FAR_{ice}$ < 20% | 85.5 % (CALIOP**)<br>10% (CALIOP**)<br>88.9% (CALIOP**)<br>16% (CALIOP**) |
| | | L3 bc-rms < 20 % | 8.7 % (MODIS) |
| Liquid Water Path | (LWP) | L2 bc-rms < 50 g $m^{-2}$ | 34 g $m^{-2}$ (AMSR-E) |
| | | L3 bc-rms < 20 g $m^{-2}$ | 11.63 g $m^{-2}$ (UWisc)<br>6.50 g $m^{-2}$ (MODIS) |
| Ice Water Path | (IWP) | L2 bc-rms < 100 g $m^{-2}$ | - |
| | | L3 bc-rms < 40 g $m^{-2}$ | 14.82 g $m^{-2}$ (MODIS) |
| Joint Cloud Histogram | (JCH) | n/a | n/a |

- **Joint Cloud property Histograms (JCH)**
  - This product is excluded from specific requirement testing because it is composed of three already evaluated products (CPH, COT and CTP). Nevertheless, a demonstration of the product in inter-comparisons with MODIS and ISCCP products shows that it provides added value to the products by giving important

clues on the statistical distribution of the involved parameters. It is believed that the access to this product representation will greatly enhance the usefulness of CLAAS-2 for some applications.

All evaluation results included in this report demonstrate the high quality of the products, and indeed show an overall improvement compared to CLAAS edition 1 [RD 6]. The quality of the data record builds on state-of-the-art retrievals systems, which were developed at Météo France and KNMI, on well characterized IR radiances and VIS reflectances and on a carefully implemented reprocessing system and final product generation, which was done at DWD. Further guidance on how to use the products is given in the product user manual [RD 1]. The mentioned accuracy requirements are reported in detail in the product requirements document [AD 1], which have been reviewed at the Requirements Review 2.4 [AD 2]. The algorithm theoretical basis documents describe the individual parameter algorithms [RD 2–RD 5].

# 3 Introduction to the SEVIRI measurements

The CLAAS-2 data record is based on 12 years of SEVIRI measurements. SEVIRI is a passive visible and infrared imager mounted on the Meteosat Second Generation satellites 1, 2 and 3. MSG1-3 are geostationary satellites which, by their rotation, support an SEVIRI imaging repeat cycle of 15 minutes. SEVIRI itself is an optical imaging radiometer with 12 spectral channels ranging from the visible (approx. 0.6 µm) to the infrared of about 13.4 µm. The respective MSGs in operational mode are centred near 0°/0° latitude/longitude, where a full earth disk image includes Europe, Africa, the Middle East and the Atlantic Ocean. The actual satellite positions are shown in Figure 3-1. Level 2 products were generated on the native SEVIRI grid, whose spatial resolution is 3 x 3 km² at nadir and increases towards the edge of the disc (see Figure 3-2). In contrast to the CLAAS-1 data record (Stengel et al., 2014), CLAAS-2 now features the original 15-minute resolution of the sensor. The complete data record covers the time-span 2004-2015 where measurements of the actual operational MSG satellite were processed: MSG1 from 2004-01-19 to 2007-04-11, MSG2 from 2007-04-11 to 2013-01-21 and MSG3 from 2013-01-21 to 2015-12-31. Data gaps (e.g. due to sensor decontamination) were filled using data from the backup satellite, if available (see Figure 3-1).

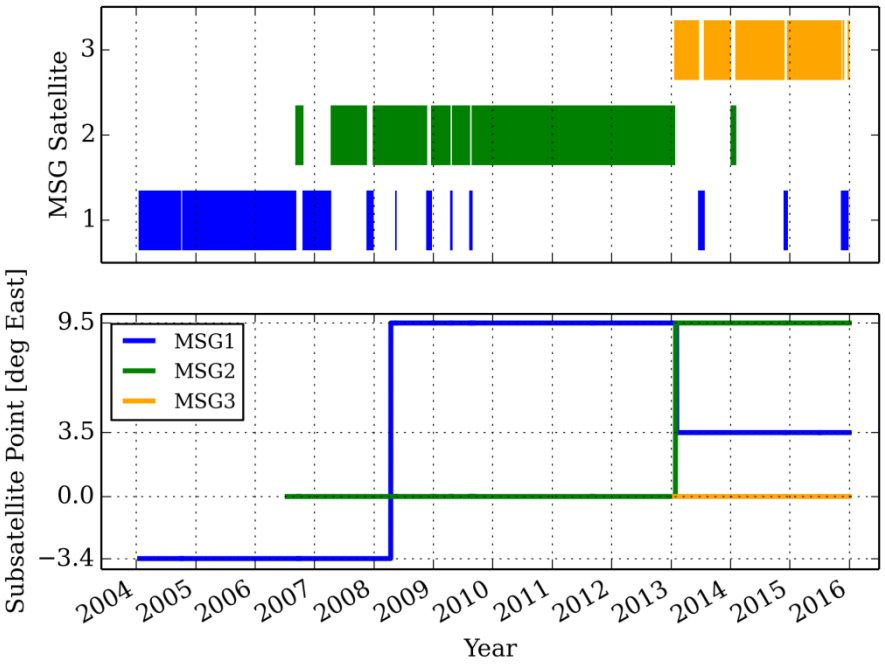


**Figure 3-1:** Overview of SEVIRI measurements record used as basis for the generation of CLAAS-2. Data gaps are shown enlarged by a factor 5 for better visibility.

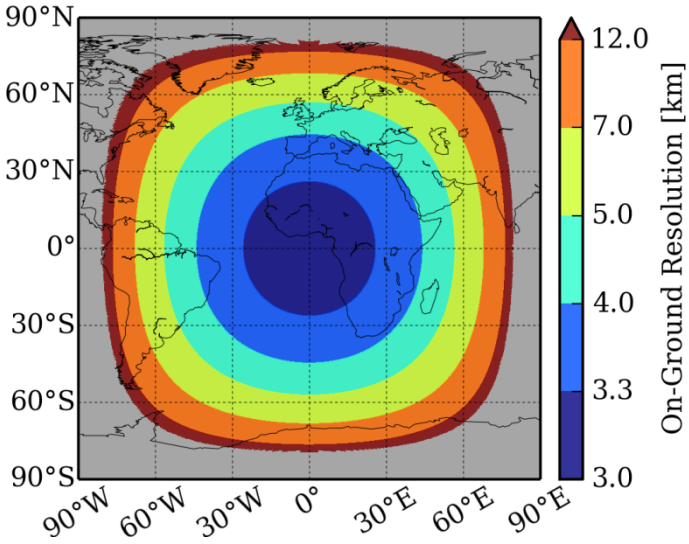


**Figure 3-2** SEVIRI on-ground resolution expressed as the edge length of a square having the same area as the SEVIRI grid cell.

The SEVIRI data record was processed using the following strategy: All timeslots within a day were processed sequentially, starting at midnight. This enables temporal cloud detection for all timeslots except 00:00 UTC (Derrien and Le Gléau, 2010). Up to 90 days were processed in parallel and isolated from each other to generate the data record in a reasonable time.

The time series of SEVIRI reflectances was carefully calibrated against the Moderate Resolution Imaging Spectroradiometer (MODIS), which improved especially the retrieval of microphysical parameters. The calibration method is outlined in Meirink et al. (2013). Because the same MODIS instrument (on the Aqua satellite) was used to calibrate all MSG satellites, the calibration also ensured homogenisation between the SEVIRI instruments. The IR radiances of SEVIRI were used as provided by EUMETSAT, relying on the on-board black-body calibration.

For a more detailed instrument specification and description of the calibration the reader is referred to the SEVIRI Algorithm Theoretical Baseline Document RD 2 and the SEVIRI Product User Manual RD 1.

# 4 Cloud products and validation strategy

In this report the following six cloud products derived from MSG SEVIRI data (with formal product IDs and abbreviations according to [AD 1] given to the right) are evaluated:

| | | |
|---|---|---|
| Fractional Cloud Cover | CM-21011 | (CFC) |
| Joint Cloud property Histogram | CM-21021 | (JCH) |
| Cloud Top level | CM-21031 | (CTO) |
| Cloud Phase | CM-21041 | (CPH) |
| Liquid Water Path | CM-21051 | (LWP) |
| Ice Water Path | CM-21061 | (IWP) |

These products are derived using the SAFNWC software MSG v2012 for level-2 CFC and CTO [RD 3], and the Cloud Physical Properties (CPP) scheme [RD 4] for level 2 of COT, CPH, LWP and IWP. JCH contains combinations of COT and CTP in histogram form and is composed in the post-processing.

The purpose of the validation effort is to characterize the cloud products in terms of accuracy and precision, thus give a guidance for applicability of the product. Furthermore, the products are confronted with the product requirements stated in [AD 1] and their compliance is reported. These requirements are summarised in Table 4-2.

For geophysical quantities at level-2, such as cloud top height, and aggregated (level-3) products, we use the bias, i.e. mean difference between CLAAS and reference data as the metric for accuracy. In addition, the bias corrected root mean squared error (BC-RMSE) is used to express the precision of CLAAS compared to a reference dataset. In case of discrete level-2 variables with only two possible events, e.g. cloud mask (*clear* or *cloudy*) and cloud phase (*liquid* or *ice*), we use the following scores which can be derived from the contingency

These scores can be viewed as a measure of precision.Table 4-1:

- Probabilities of detection (POD) for event 1, 2: $\frac{n_{11}}{n_{11}+n_{21}}$ , $\frac{n_{22}}{n_{22}+n_{12}}$
- False alarm ratios (FAR) for event 1, 2: $\frac{n_{12}}{n_{11}+n_{12}}$ , $\frac{n_{21}}{n_{22}+n_{21}}$
- Hit rate: $\frac{n_{11}+n_{22}}{n_{11}+n_{12}+n_{21}+n_{22}}$
- Hanssen-Kuipers Skill Score (KSS): $\frac{n_{11}n_{22}-n_{21}n_{12}}{(n_{11}+n_{21})(n_{12}+n_{22})} \in [-1,1]$

These scores can be viewed as a measure of precision.

**Table 4-1** Contingency table for the 2x2 problem. $n_{ij}$ is the number of cases where CLAAS reports event i and the reference reports event j. For example event 1 may be clear and event 2 may be cloudy.

| | Reference reports 1 | Reference reports 2 |
|---|---|---|
| CLAAS reports 1 | $n_{11}$ | $n_{12}$ |
| CLAAS reports 2 | $n_{21}$ | $n_{22}$ |

Table 4-2 gives the target requirements for all CLAAS-2 cloud products. Observe that two versions for the Cloud Top Level product (CM-21031) are listed: cloud top height and cloud top pressure. In addition, there are no specific requirements given for the JCH product since it is composed of individual products COT and CTP, which are validated independently. Table 4-2 only lists the target requirements for the accuracy and precision parameters. Compliance with more relaxed threshold requirements and more demanding optimal requirements (as defined in [AD 1]) are also discussed further in Sections 6 and 7.

**Table 4-2:** CM SAF CLAAS-2 products and their respective target requirements (defined in [AD 1]) for accuracy and precision. L2 requirements refer to the pixel level, L3 requirements to monthly means. The requirements are applicable to the SEVIRI disc.

| Product | | Accuracy requirement | Precision requirement |
|---|---|---|---|
| **Cloud Fractional Cover** | **(CFC)** | **L3: bias < 10 % (absolute)** | **L3: bc-rmse < 20 % (absolute)**<br>**L2: $POD_{cld}$ > 90%**<br>**$FAR_{cld}$ < 15%** |
| **Cloud Top Height** | **(CTH)** | **L2/L3: bias < 800 m** | **L3: bc-rmse < 1500 m**<br>**L2: bc-rmse < 2500 m** |
| **Cloud Top Pressure** | **(CTP)** | **L2/L3: bias < 45 hPa** | **L3: bc-rmse < 70 hPa**<br>**L2: bc-rmse < 110 hPa** |
| **Cloud Phase** | **(CPH)** | **L3: bias < 10% (liquid cloud fraction, absolute)** | **L3: bias < 20 % (liquid cloud fraction, absolute)**<br>**L2: $POD_{liq}$ > 80%**<br>**$FAR_{liq}$ < 20%**<br>**$POD_{ice}$ > 80%**<br>**$FAR_{ice}$ < 20%** |
| **Liquid Water Path** | **(LWP)** | **L2/L3: bias < 10 g $m^{-2}$** | **L3: bc-rmse < 20 g $m^{-2}$** |

| | | | |
|---|---|---|---|
| | | | **L2: bc-rmse < 50 g m$^{-2}$** |
| **Ice Water Path** | **(IWP)** | **L2/L3: bias < 20 g m$^{-2}$** | **L3: bc-rmse < 40 g m$^{-2}$** |
| | | | **L2: bc-rmse < 100 g m$^{-2}$** |
| **Joint Cloud Histogram** | **(JCH)** | **n/a** | **n/a** |

The requirement values listed in Table 4-2 are defined after taking into account requirements from different users and user groups. The most well-established reference here is the recommendations issued by the Global Climate Observation System - GCOS – community, see GCOS, 2011). However, values are also influenced by requirements from users working with regional climate monitoring and regional climate modelling applications (often having even stricter requirements than GCOS). More background on how the current requirements were established can be found in [AD 2].

The CM SAF MSG SEVIRI data record consists of instantaneous data (Level 2), and daily and monthly mean (Level 3) products for the period 2004-2015. Furthermore, monthly mean diurnal cycles are composed as well as monthly single- and multi-parameter histograms. The validation task comprises evaluation of the Level 2 and Level 3 products, with the latter done if reference measurements were available. However, inter-comparisons with Level 3 products from other sources are often more difficult to interpret than comparisons with instantaneous and simultaneous observations (i.e., the classical Level 2 validation process). The reason is that Level 3 products not only depend on the quality of Level 2 products but also on the method of compiling Level 3 products (i.e., in terms of the applied temporal and spatial sampling, criteria for including or excluding a measurement, averaging method, etc.). This means that Level 3 product differences do not always reflect true product differences in the same way as monitored by standard Level 2 validation activities. For practical reasons Level 2 studies have been limited in time and space compared to the task of evaluating the full CLAAS-2 data record. We believe that the mix of Level 2 (instantaneous) and Level 3 (monthly mean) studies provide enough information about the expected quality of daily Level 3 products, which were not separately evaluated. The evaluation in this report is done with respect to ‘best practice’, based on the accessibility to high quality and homogeneous observations, which can be considered close to the truth and being independent, and based on well-established and highly utilized products.

The chosen validation references may be subdivided into two groups:

- **independent observations**, which are generally considered to be true references, i.e. of superior quality. We have used the following observations:
  - Cloud amount from surface stations (SYNOP), 2004-2015
  - Cloud amount and cloud top level from space-based lidar CALIOP: 2006-2015
  - Cloud phase and ice water path from space-based lidar+radar DARDAR: January 2008
  - Liquid water path from passive microwave sensors: 2004-2012
- **similar satellite datasets** based on passive VIS-IR measurements, which are used for inter-comparisons rather than pure validation
  - All cloud properties from MODIS: 2004-2015

The first group of observations is the most important group since it fulfils the condition that the observation reference must be independent. Thus, results achieved from comparisons with

this group of observations will be given highest credibility. However, this type of reference observation is not available for all considered parameters. It also has to be realized that none of these independent observation types is perfect, and they all have their uncertainties related to, for example, representativeness, sensitivity, and aggregation.

The reference datasets, including associated uncertainties, are described in Section 5, level-2 evaluation results are presented in Section 6, and level-3 evaluation is documented in Section 7.

# 5 Datasets for comparison with MSG SEVIRI

## 5.1 SYNOP: manual cloud observations from surface stations

Observations of total cloud cover made at meteorological surface stations (i.e. synoptic observations – hereafter called SYNOP) constitute one of the datasets used to evaluate the cloud fractional coverage estimates. At manned stations the total cloud cover is visually estimated by human observers. In contrast, ceilometers are used for that purpose at automatic stations. However, for data quality and consistency reasons, only those SYNOP reports provided by manned airport stations were taken into account (~1800 stations globally).

SYNOP cloud cover observations are used for the evaluation of the level-3 CFC product.

Manual cloud observations are affected by many sources of error. We list some of the most important ones in the following:

- The observation is subjective in nature, i.e., despite clear instructions on how to make an observation, differences will appear because of different interpretations from person to person. This introduces a random noise in global cloud amount observations but may also lead to geographical biases (reflecting some systematic behaviour related to the way people have been educated/trained).
- The human eye has a detection limit for when a cloud can be clearly discernible against a cloud-free sky. This limit is somewhere in the cloud optical thickness range of 0.5-1.0 (with some dependence on solar zenith angle, on which viewing angles clouds are observed and the degree of aerosol load or haze in the troposphere). Thus, many satellite sensors have a higher sensitivity to e.g. cirrus detection than SYNOP observations.
- At night, the random error in the observations increases. This is natural since the observer does not have a clear sky background against which a cloud can be observed (i.e., clouds are as dark as the cloud-free sky). However, accuracies improve in the presence of moonlight. Nevertheless, the overall effect is normally a negative bias (underestimated cloud amounts) since the observer is tempted to report cloud free conditions as soon as stars becomes visible, thus neglecting that large fractions of thin cirrus and other cloud types may still be present.
- A well-known deficiency of SYNOP observations is the scenery effect, i.e. overestimation of convective cloud towers at a slanted view (Karlsson, 2003). This effect is most pronounced in the summer season and for low to moderate cloud amounts when the overestimation easily can reach values of 20-30 % (1-2 octas).
- It is important to consider that most SYNOP stations are located at land stations and with higher density in developed countries. Thus, global averages tend to be biased towards land conditions in densely populated countries.

Since no rigorous study has been able to cover all those aspects in a quantitative manner (mainly because of lack of an absolute truth as reference) we can only make a very general statement about the overall quality. We would suggest that the accuracy of SYNOP observations vary between approximately +10 % (some overestimation) at daytime conditions changing to -10 % or worse (some underestimation) at nighttime. However, the variability (precision) probably reaches higher absolute values and it is largest during night conditions. This may lead to a strong seasonal variation in quality with the worst accuracy and precision

features during the winter season (at least at middle and high latitudes including the Polar Regions).

It is worth noting that the increasing trend to replace manual cloud observations with automatic observations from ceilometers will change the accuracy and precision of cloud observations in several ways. This may possibly lead to improved accuracies at nighttime but there is also a considerable risk that the precision figures degrades, mainly as an effect of that ceilometers only observer a very small fraction of the sky.

Despite their subjective character and varying quality, SYNOP observations still provide a useful reference data set suitable for monitoring and validating space-based estimations of cloud coverage, particularly due to their long-term availability.

## 5.2 CALIPSO-CALIOP

Measurements from space-born active instruments (radar + lidar) provide probably the most accurate information we can get about cloud presence in the atmosphere. The reason is the fact that the measured reflected radiation comes almost exclusively from cloud and precipitation particles and is therefore not “contaminated” by radiation from other surfaces or atmospheric constituents as is the case for measurements from most passive radiometers. In this validation study we have decided to utilise measurements from the CALIOP lidar instrument carried by the CALIPSO satellite (included in the A-Train series of satellites - Figure 5-1).

The Cloud-Aerosol Lidar and Infrared Pathfinder Satellite Observation (CALIPSO) satellite was launched in April 2006 together with CloudSat. The satellite carries the Cloud-Aerosol Lidar with Orthogonal Polarization (CALIOP) and the first data became available in August 2006. CALIOP provides detailed profile information about cloud and aerosol particles and corresponding physical parameters.

CALIOP measures the backscatter intensity at 1064 nm while two other channels measure the orthogonally polarized components of the backscattered signal at 532 nm. In practice the instrument can only probe the full geometrical depth of a cloud if the total optical thickness is not larger than a certain threshold (somewhere in the range 3-5). For optically thicker clouds only the upper portion of the cloud will be sensed. The horizontal resolution of each single measurement is 333 m and the vertical resolution is 30-60 m.

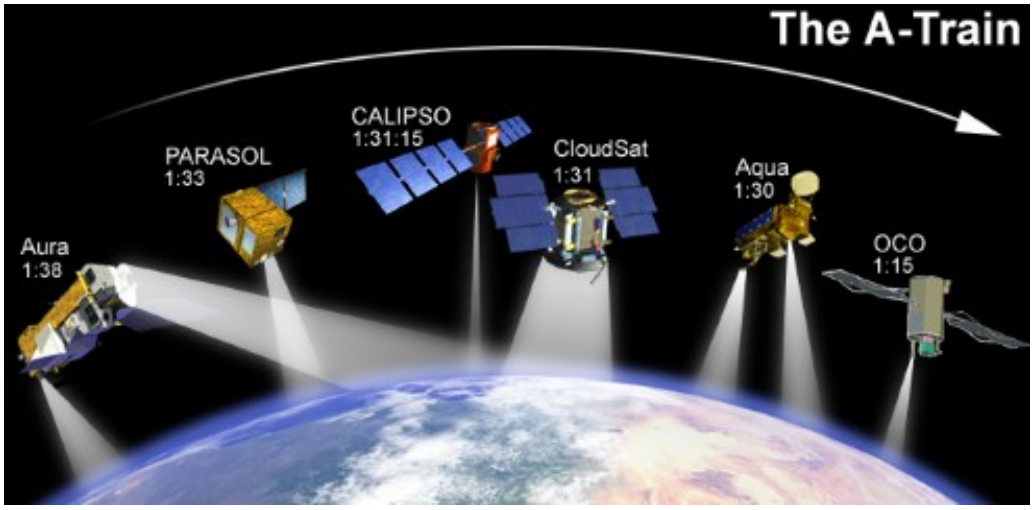


**Figure 5-1:** The Aqua-Train satellites. (Image credit: NASA)

The CALIOP products are available in five different versions with respect to the along-track resolution ranging from 333 m (resolution based on the spacing between consecutive footprints of 70 m), 1 km, 5 km, 20 km and 80 km. The four latter resolutions are consequently constructed from several original footprints/FOVs. This allows a higher confidence in the detection and identification of cloud and aerosol layers compared to the original footprint resolution. For example, the identification of very thin Cirrus clouds is more reliable in the 5 km dataset than in the 1 km dataset since signal-to-noise levels can be raised by using a combined dataset of several original profiles.

We used the CALIOP Level-2 5km cloud layer dataset versions 3-01, 3-02 and 3-30 (CALIPSO Science Team, 2015) for validation purpose since this resolution is closest to the nominal SEVIRI resolution and because of the advantages described above. It reports up to 10 cloud layers per column and provides information about cloud phase and cloud type of each layer as well as the pressure, height and temperature at each layer's top.

The CALIOP dataset classifies cloud layers into cloud types according to Table 5-1. To be noticed here is that the ISCCP cloud type method has been used in the sense that the vertical separation of Low (categories 0-3), Medium (categories 4-5) and High (categories 6-7) clouds is defined by use of vertical pressure levels of 680 hPa and 440 hPa. However, the separation of thin and thick clouds is made using the information on whether the surface or lower layers below the current layer can be seen by CALIOP.

**Table 5-1:** Cloud type categories according to the CALIOP Vertical Feature Mask product.

| | |
|---|---|
| Category 0 | Low, overcast, thin (transparent St, StCu, and fog) |
| Category 1 | Low, overcast, thick (opaque St, StCu, and fog) |
| Category 2 | Transition stratocumulus |
| Category 3 | Low, broken (trade Cu and shallow Cu) |
| Category 4 | Altocumulus ( transparent) |
| Category 5 | Altostratus (opaque, As, Ns, Ac) |
| Category 6 | Cirrus (transparent) |
| Category 7 | Deep convective (opaque As, Cb, Ns) |

CALIOP data is used for Level 2 validation of the CFC, CTH and CPH products. It has the following uncertainties and error sources.

It should be emphasized that the CALIOP measurement is probing the atmosphere very efficiently in the along-track direction since it is a nadir pointing instrument. Here, cloud dimensions down to the original FOV resolution (333 m) will be detected. However, it should be made clear that the across-track extension of the observation is still limited to 70 m, the individual footprint of the lidar beam. Thus, to compare CALIOP-derived results with the results of 3 km SEVIRI pixel data is not entirely consistent (i.e., CALIOP is only capable of covering the SEVIRI pixel properly in one direction and not in the perpendicular direction). However, we believe that this deficiency is of marginal importance. Most cloud systems on the SEVIRI scale will be detected, e.g., it is very unlikely to imagine elongated clouds with size and shapes below 0.3x4 km that might risk remaining undetected within a SEVIRI pixel that coincides with a CALIOP measurement. Most clouds will have aspect ratios for the two horizontal directions that guarantee detection by CALIOP.

It is important to consider that the CALIOP lidar instrument is much more sensitive to cloud particles than the measurement from a passively imaging instrument. It means that a significant fraction of all CALIOP-detected clouds will not be detected by imagers. This sensitivity difference also propagates into CPH and CTH, which will typically be sensed at a lower cloud layer by passive instruments compared to CALIOP (see e.g., Hamann et al., 2014). Thus, to get reasonable and justified results (i.e., saying something on the performance of the applied cloud detection method for clouds that should be theoretically detectable) one should consider filtering out the contributions from the very thinnest clouds. We have tested this approach in this validation study, both in the study of cloud amount (CFC), cloud phase (CPH) and cloud top height (CTH).

The cloud detection efficiency with CALIOP is slightly different day and night because of the additional noise from reflected solar radiation at daytime that can contaminate lidar backscatter measurements. However, Chepfer *et al.* (2010) reports that this can introduce an artificial difference of not more than 1 % when comparing night time and daytime data.

In the CLAAS-2 validation context we have used the 5 km CALIOP dataset since this resolution is closest to the nominal SEVIRI resolution. However, the results in different datasets from CALIPSO, related to different horizontal resolutions (with the five options 333 m, 1 km, 5 km, 20 km and 80 km) are unfortunately not entirely consistent (e.g., Karlsson and Johansson, 2013). It means that some of the thick (opaque) boundary layer clouds that are reported in fine resolution (333 m and 1 km) datasets are not reported in the higher resolution (5 km or higher) datasets. This has to do with the methodology to do averaging at the longer scales (5 km or higher) where contributions from strongly reflecting boundary layer clouds are removed from the original signal to facilitate detection of very thin cloud layers and aerosols.

In conclusion: despite the fact that the CALIPSO cloud observations most likely are the best available cloud reference dataset being released so far, we might still see a negative bias of a few percent in the CALIOP-derived cloud cover when using the 5 km dataset. Other errors, e.g. due to mis-interpretation of heavy aerosol loads as clouds, are in this respect of minor importance when judging the effect on accumulated results based on a large number of full global orbits. This also concerns problems with reduced signal-to-noise ratios due to solar contamination during daytime.

## 5.3 DARDAR

To complement the picture drawn by the CALIOP lidar also CPR onboard CloudSat is considered. CPR is a nadir-looking cloud profiling radar in principle working like MIRA (see

section 5.2) but sensing the atmosphere from above at 94 GHz. The instruments sensitivity is defined by a minimum detectable reflectivity factor of -30 dBZ and calibration accuracy of 1.5 dB. The minimum detectable reflectivity factor requirement was reduced to -26 dBZ when the mission was changed to put CloudSat into a higher orbit for formation flying in A-train.

The DARDAR dataset (Delanoë and Hogan, 2008) provides the result from a synergistic retrieval method combining the measurements from the CALIOP lidar, the CLOUDSAT radar and the MODIS imager, all three elements of the A-Train satellite constellation. By combining these different measurements, consistent profiles of microphysical properties are retrieved based on the specific particle size (instrumental) wavelength sensitivities. The lidar signals for instance are sensitive to the particle surfaces in the line of sight (~radius$^2$ ), which is dominated by the smaller particles in a particle size distribution (PSD) whereas the radar signals are sensitive to the square of the particle volume which is dominated by the larger particles in the PSD. When both signals are available the combined PSD sensitivities provide the best guess of extinction, effective particle radius and IWC. When only one of the signals is available, i.e. when the lidar is fully attenuated or when the particles are too small to be detected by radar, the DARDAR retrievals are based on the single instrument parameterizations. The optimal estimation framework used for this retrieval ensures a smooth transition from these different regimes. The DARDAR product has the vertical resolution of CALIOP (30/60 m) and a horizontal resolution given by the radar footprint (700m). This is in contrast to the comparison to the CALIOP data (Section 5.2) which has been averaged to 5 km wide layers before being compared to the CLAAS-2 data records. The DARDAR data for the current evaluation has been downloaded from the ICARE site: http://www.icare.univ-lille1.fr/projects/dardar/overview_dardar_cloud.

DARDAR data is used for level-2 evaluation of CPH and IWP (including ice COT and ice particle effective radius). Comparisons with this dataset are affected by the same issues related to high ice clouds as discussed for CALIOP, i.e. DARDAR is much more sensitive to thin ice cloud than passive imagers.

In the lower part of the atmosphere, the reflectance of the surface affects the backscattered radar signal, so clouds may not be properly detected below 1 km distance to the surface.

## 5.4 MODIS

MODIS (or Moderate Resolution Imaging Spectroradiometer) is an advanced imaging instrument onboard the Terra (EOS AM) and Aqua (EOS PM) polar satellites (see http://modis-atmos.gsfc.nasa.gov/index.html). Terra's orbit around the Earth is sun synchronous and timed so that it passes from north to south across the equator in the morning (local solar time 10:30), while Aqua passes south to north over the equator in the afternoon (local solar time 13:30). Terra MODIS and Aqua MODIS are viewing the entire Earth's surface every 1 to 2 days, acquiring data in 36 spectral bands or groups of wavelengths.

Because the MODIS instruments are among the most advanced passive imagers in space, have proven to be very stable over time, and have been flying during the complete MSG time frame, the cloud products from MODIS (Platnick et al., 2003) are used here as a reference.

We have used the level-3 MODIS gridded atmosphere monthly global products - MOD08_M3 (Terra) and MYD08_M3 (Aqua). They contain monthly 1 × 1 degree grid average values of atmospheric parameters related to atmospheric aerosol particle properties, total ozone burden, atmospheric water vapour, cloud optical and physical properties, and atmospheric stability indices. Statistics are sorted into 1 × 1 degree cells on an equal-angle

grid that spans a (calendar) monthly interval and then summarized over the globe. For this particular study we have used data from Terra and Aqua Collection 6.

MODIS data is used for Level 3 inter-comparisons of all cloud products as well as for sample level-2 comparisons. Uncertainties are expected to be somewhat smaller than what can be obtained with SEVIRI retrievals, because MODIS has a wider variety of channels, for example: multiple $CO_2$ channels allow a more accurate cloud-top height determination, additional shortwave channels allow better discrimination of (thin) cirrus and a more reliable retrieval of cloud optical properties over very bright surfaces. Otherwise, uncertainties should lie in the same ballpark as for CLAAS-2. Therefore, the inter-comparisons have to be viewed as an evaluation rather than pure validation, allowing to judge the overall consistency of the dataset.

## 5.5 Microwave imagers

Passive microwave imagers, such as the Special Sensor Microwave/Imager (SSM/I) series, can be used to retrieve column-integrated liquid water along with water vapour and surface wind speed. Because the microwave (MW) channels fully penetrate clouds, they provide a direct measurement of the total liquid (but not solid) cloud condensate amount. For precipitating clouds an estimate of the rain water path has to be made and subtracted from the total liquid water path to retrieve the cloud liquid water path.

Microwave imagers are used both for level-2 and level-3 validation of LWP. For level-2 comparisons data from the Advanced Microwave Scanning Radiometer – EOS (AMSR-E) is used. AMSR-E is a dual-polarization conical-scanning passive microwave radiometer with 12 channels ranging from 6.9 to 89 GHz. This instrument was designed to measure cloud properties, sea surface temperature and surface water, ice and snow. Here we utilize exactly the same AMSR-E data as in Stengel et al. (2013), which is from the Version 06 Level 2B Ocean product suite (see Wentz and Meissner (2000) for more information on the algorithm). The data was collected from the EOS Data Pool at NSIDC (http://nsidc.org/). AMSR-E LWP products are derived primarily from the liquid sensitive 37 GHz channel measurement, which has a spatial footprint of 10 × 14 km. A list of all parameters included in this product can be found at http://nsidc.org/data/docs/daac/ae_ocean_products.gd.html. This page also indicates a root mean square error of 17 g/m$^2$ as preliminary error estimate for LWP retrievals.

For level-3 comparisons, the University of Wisconsin (UWisc) MW-based LWP climatology (O'Dell et al., 2008) was chosen as an independent reference dataset. The LWP climatology is based on retrievals from various microwave radiometer instruments, including the SSM/I series, the Tropical Rainfall Measurement Mission Microwave Imager (TMI), and the AMSR-E. The most recent version of the dataset that was used for the evaluation (version 4) spans the years 1988 – 2012. Liquid water path estimates are reported to have an accuracy of 15% to 30% (O'Dell et al., 2008).

Two remarks have to be made regarding the validation. First, the MW LWP measurements are only possible over ocean, so the validation is restricted to marine clouds. Second, since the MW measurements are not sensitive to ice, care has to be taken to select for the validation only those grid cells with a sufficiently low monthly mean ice cloud fraction. In the SEVIRI disk these requirements lead to selection of the South-Atlantic area off the Namibian coast with persistent marine stratocumulus (Sc). Specifically, the region from 20º – 10ºS and 0º – 10ºE was used for LWP evaluation.

# 6 Evaluation of SEVIRI instantaneous (level-2) cloud parameters

This section covers the evaluation of CLAAS-2 level-2 products and is organized according to Table 6-1.

**Table 6-1** Overview of reference datasets used for the evaluation of CLAAS-2 level-2 parameters.

| Section | Reference observations | Parameters |
|---|---|---|
| 6.1 | Calipso | CFC, CPH, CTH |
| 6.2 | DARDAR (Cloudsat-Calipso) | CPH, IWP, (ice COT, ice REFF) |
| 6.3 | AMSR-E | LWP |
| 6.4 | MODIS | CTH, LWP, IWP, (COT, REFF) |

## 6.1 Validation with CALIOP

The validation against CALIOP on CALIPSO requires the spatial and temporal matching of observations from SEVIRI and CALIOP. Collocations were computed using spatial nearest neighbour search and scanline-based time matching: For each CALIOP measurement, the nearest neighbour in the SEVIRI grid is determined yielding its line number in the image. The matching SEVIRI scan is given by the scan where the acquisition time of this particular scanline is closest to the timestamp of the CALIOP measurement. An example matchup is shown in Figure 6-1. Maximum collocation distances are 5 km and 7.5 minutes in space and time.

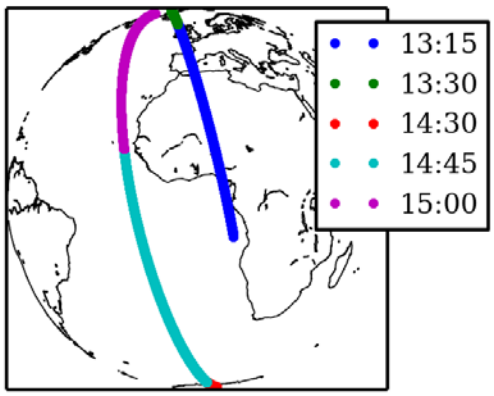


**Figure 6-1** Exemplary matchup of CALIOP track and SEVIRI scan. The labels display the nominal timestamp of the SEVIRI scan that was matched to the identically coloured ground track segment.

Due to the advanced lidar technique, CALIOP is much more sensitive to high and optically thin clouds than SEVIRI. Therefore, we do not only compare CLAAS-2 against the uppermost cloud layer detected by CALIOP, but also compare against CALIOP data which was filtered by means of the cloud optical thickness (COT). The latter can tell us more about how accurate CLAAS-2 products are relative to the potential of the SEVIRI sensor.

In the following validation sections, we excluded measurements known to be of reduced quality:

- Absolute value of latitude/longitude > 80 degrees.
- SEVIRI satellite zenith angles > 75 degrees.
- CLAAS-2 cloud top information where the SAFNWC algorithm did not converge and cloud top information was reconstructed using nearest neighbour interpolation to ensure consistency with the cloud mask.
- CALIOP phase information flagged as *bad quality*.

### 6.1.1 Cloud Mask and Cloud Phase

We derived a binary CALIOP cloud mask by interpreting all CALIOP measurements with total column COT > 0 as cloudy. The CLAAS-2 cloud mask, which consists of four values *clear, cloud contaminated, cloudy* and *snow/ice*, was converted to a binary cloud mask, by setting all *cloud contaminated* pixels to *cloudy* and excluding *snow/ice* values. This is required to allow for a comparison against the CALIOP binary cloud mask. For sensitivity analysis we include comparisons against CALIOP cloud masks which were derived using total column COT thresholds larger than zero.
In contrast to the cloud mask, cloud phase from CLAAS-2 and CALIOP are directly comparable. For sensitivity analysis we include comparisons against the CALIOP layer, where the top-to-bottom integrated cloud optical thickness (ICOT) exceeds a certain threshold.

Figure 6-2 shows a timeseries of cloud fraction and ice cloud fraction from CLAAS-2 and CALIOP at all collected collocations in 2006-2015. As one can see, CLAAS-2 slightly overestimates the cloud fraction and reports significantly less ice clouds compared to CALIOP. While the latter finding is expected since CALIOP is more sensitive to thin ice clouds, the former finding may appear surprising. There are several possible reasons that can explain this (see also Reuter et al., 2009). Firstly, the CALIOP 5 km product omits some of the clouds detected at the 1 km scale (Karlsson and Johansson, 2013). Secondly, SEVIRI has a relatively coarse resolution on which broken clouds will typically be classified as (fully) cloudy. Thirdly, passive imager cloud retrievals have a well known tendency to overestimate cloud cover at large viewing angles (e.g. Maddux et al., 2010), which make up a considerable part of the SEVIRI disc.

When excluding the uppermost optically thinnest CALIOP layers, i.e. applying COT > 0.2 as cloud criterion (upper panel) and taking the CALIOP phase from the layer where ICOT exceeds 0.2 (lower panel), the ice cloud fraction agrees very well, whereas the CALIOP cloud fraction diverges even more from its CLAAS-2 counterpart.

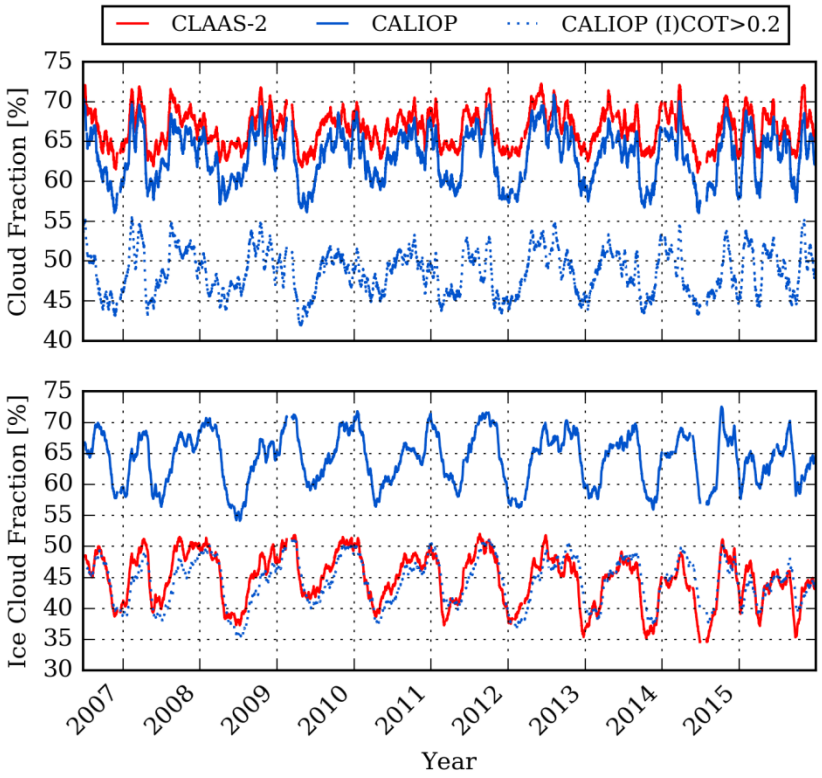


**Figure 6-2** 10-day moving average of cloud mask (yielding a cloud fraction, top) and cloud phase (bottom, yielding an ice cloud fraction) from CLAAS-2 and CALIOP. Dashed lines show COT filtered CALIOP data.

Overall cloud and phase scores are listed in Table 6-2 for the complete disc and timeseries (column *All*), as well as a variety of temporal and spatial subsets. The overall cloud POD is 87.5%, the overall cloud FAR is 16.9%. The cloud hit rate reaches 80.9%. The cloud POD is significantly higher over sea than over land, whereas there are only small differences between day and night. Both cloud POD and FAR meet the threshold requirement. Filtering high, thin CALIOP clouds raises the POD into the optimal region, but it causes the FAR to exceed the threshold requirement. In these cases we obviously exclude clouds already detected by CLAAS-2.

The overall liquid POD (91.6%) meets the optimal requirement, but the corresponding FAR (29.8%) only meets the threshold requirement. The overall ice POD (74.9%) only reaches the threshold requirement, but with an optimal FAR of 6.7%. The phase hit rate reaches 81.4%.

Like for the cloud POD, liquid POD is higher over sea than over land. The liquid FAR over land is rather high and misses the threshold requirement. When excluding high, thin CALIOP clouds, phase PODs and FARs are more balanced and collectively meet the target requirement.

**Table 6-2:** Summary of validation results for CLAAS-2 cloud mask and cloud phase. Abbreviations: clr = clear, cld = cloud, liq = liquid, Thr. = Threshold-Requirement, Targ. = Target-Requirement, Opt. = Optimal-Requirement. Dark green cells meet the optimal-, light green cells the target- and gray cells the threshold-requirement. Red cells miss the threshold-requirement. All values in percent.

| | | | | | CALIOP (I)COT > 0.0 | | | | | CALIOP (I)COT > 0.2 | | | | |
|---|---|---|---|---|---|---|---|---|---|---|---|---|---|---|
| | | Thr. | Targ. | Opt. | All | Day | Night | Sea | Land | All | Day | Night | Sea | Land |
| Cloud Mask | POD clr | | | | 69.4 | 67.1 | 71.9 | 58 | 88 | 61.4 | 58.3 | 64.9 | 49.6 | 80.6 |
| | FAR clr | | | | 23.6 | 20.7 | 26.4 | 18.6 | 28.2 | 5.5 | 3.4 | 7.5 | 2.9 | 7.9 |
| | POD cld | >85 | >90 | >95 | 87.5 | 88.7 | 86.5 | 93.1 | 75.2 | 96.2 | 97.5 | 95.2 | 98.6 | 90.3 |
| | FAR cld | <20 | <15 | <10 | 16.9 | 19.3 | 14.6 | 19.1 | 10.2 | 29.8 | 34.3 | 25.3 | 31.9 | 23.1 |
| | Hit rate | | | | 80.9 | 80.3 | 81.5 | 81.1 | 80.6 | 78.3 | 75.9 | 80.7 | 75.1 | 84.6 |
| | KSS | | | | 56.9 | 55.9 | 58.4 | 51.1 | 63.2 | 57.6 | 55.8 | 60.1 | 48.3 | 70.9 |
| Cloud Phase | POD liq | >70 | >80 | >90 | 91.6 | 89.3 | 93.7 | 92.9 | 84.7 | 85.5 | 83.7 | 87 | 88 | 74.8 |
| | FAR liq | <35 | <20 | <10 | 29.8 | 27.3 | 31.9 | 25.2 | 48.2 | 10 | 9.8 | 10.2 | 7.6 | 20.1 |
| | POD ice | >60 | >80 | >90 | 74.9 | 77.9 | 72.3 | 73.6 | 77.3 | 88.9 | 90.1 | 87.7 | 89.1 | 88.4 |
| | FAR ice | <35 | <20 | <10 | 6.7 | 8.3 | 5.2 | 7.5 | 5.4 | 16 | 16.4 | 15.6 | 16.7 | 14.9 |
| | Hit rate | | | | 81.4 | 82.4 | 80.6 | 82.4 | 79 | 87 | 86.8 | 87.3 | 88.5 | 83.2 |
| | KSS | | | | 66.5 | 67.2 | 66 | 66.5 | 62 | 74.4 | 73.8 | 74.7 | 77.2 | 63.2 |

We also analysed the impact of removing CALIOP measurements with total column COT smaller than a certain threshold and found that SEVIRI is indeed less sensitive to optically thin clouds. One can see that in the left panel of Figure 6-3, where the probability of detection increases with the COT threshold used to distinguish clear and cloudy CALIOP measurements. However, it does not imply that optically clouds thinner than, say COT=1.0, can generally not be detected by SEVIRI, because the false alarm ratio also increases with the COT threshold. One could rather say that it is more likely to miss a cloud with SEVIRI, if it is optically thin. Thus there are two effects happening simultaneously when increasing the COT threshold (left panel of Figure 6-3):

- Optically thin CALIOP clouds not detected by SEVIRI are reset to cloud-free, hence the cloud POD increases.
- Optically thin CALIOP clouds detected by SEVIRI are reset to cloud-free, leading to an increased False Alarm Ratio.

The coupling of these effects causes the Hit rate and KSS to peak already at COT≈0.05.

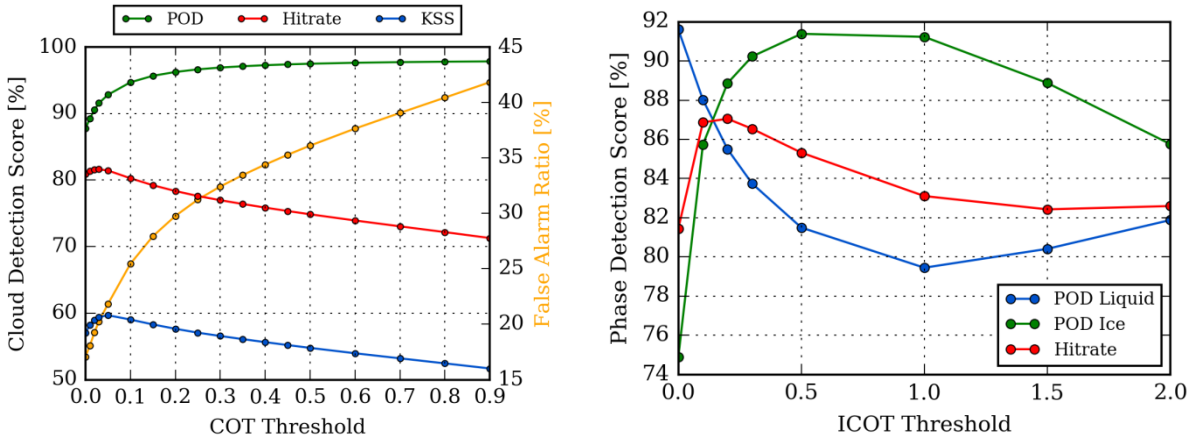


**Figure 6-3** Left: CLAAS-2 cloud scores as a function of the COT threshold used to discriminate clear and cloudy CALIOP observations. KSS denotes the Hanssen-Kuiper-Skill-Score. Right: CLAAS-2 phase scores as a function of the ICOT threshold, which determines the reference CALIOP cloud layer. (Figure taken from Benas et al., 2016)

How does the cloud type distribution change, if we do not compare against the uppermost CALIOP cloud layer, but against the layer where the ICOT exceeds a certain threshold? This is shown in Figure 6-4. As intended, mostly Cirrus clouds are affected. From ICOT=0 to ICOT=0.1, about half of the drop in Cirrus clouds is compensated by an increase of liquid clouds. Here we obviously exclude the optically thinnest Cirrus clouds over optically thicker liquid clouds. The other half of the excluded Cirrus clouds just disappears, because there is no further cloud layer below. At ICOT=2.0, nearly all Cirrus clouds have been excluded.
In the following, we will include sensitivity comparisons against (I)COT=0.2, because using this threshold has a significant influence on the scores and biases, but does not exclude too many Cirrus clouds.

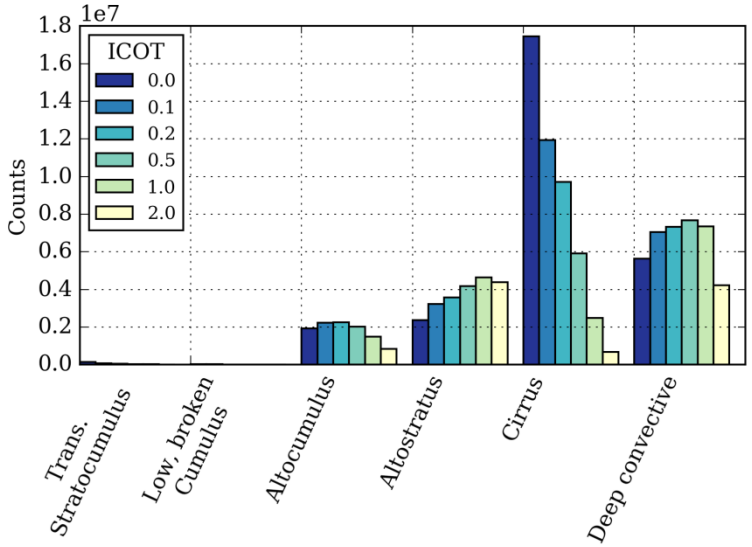


**Figure 6-4** CALIOP cloud type distribution at the layers where ICOT exceeds a certain threshold. Only matchups with valid CLAAS-2 phase are shown.

The influence of not using the phase of the uppermost CALIOP cloud layer as reference, but the phase at the layer where the ICOT exceeds a certain threshold, is shown in the right panel of Figure 6-3. As mentioned above, applying an ICOT threshold mostly affects the thinnest ice clouds. If there is no cloud layer below, the thin ice cloud just disappears. If there is a layer below, it is most often a liquid cloud layer so that we compare more and more against liquid clouds as the ICOT threshold increases. This has the following effects:

1. Excluding undetected ice clouds increases the ice POD. This can be seen in the right panel of Figure 6-3.
2. Excluding a thin ice cloud and instead comparing against a liquid cloud located below will
    a) Increase the liquid POD if the thin ice cloud was incorrectly reported as liquid by CLAAS-2 (purple line in Figure 6-5).
    b) Decrease the liquid POD if the thin ice cloud was correctly reported as ice by CLAAS-2 (orange line in Figure 6-5).

    It depends on the ratio of occurrences of cases a) and b) whether the liquid POD finally decreases or increases. In this study, case b) increases approx. 3 times stronger with ICOT than case a) resulting in the decrease of liquid POD seen in Figure 6-3.

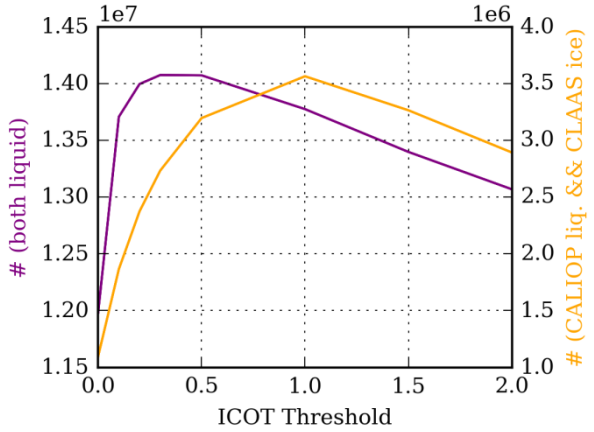


**Figure 6-5** Counts required to compute the liquid POD as a function of the ICOT threshold. Liquid POD = #(both liq) / (#(CALIOP liq && CLAAS ice) + #(both liq)).

The contribution of different CALIOP cloud types to the probabilities of cloud and phase detection are shown in Figure 6-6. Please note that all cloud analyses with respect to the CALIOP cloud type have a very strong ice cloud bias. We found that CALIOP provides a cloud type classification for 98% of the ice clouds, but only for 30% of the liquid clouds. The latter value may be even lower in certain regions, for example in the south Atlantic stratocumulus region (0-10°E, 10-20°S) a cloud type is provided only for 6% of the liquid clouds.

Altostratus and deep convective clouds are detected with almost 100% probability, whereas the PODs for Transition-, and Alto-Cumulus as well as Cirrus clouds closely miss the threshold specification. However, when ignoring CALIOP measurements with total column COT < 0.2, Altocumulus & Cirrus meet the target and Transition Cumulus the threshold requirement. Only approximately 50% of low, broken Cumulus clouds are detected. Yet this CALIOP cloud type is reported two orders of magnitude less often than for example Cirrus clouds.

The liquid/ice POD meets the threshold requirements in all cases and, when excluding CALIOP cloud layers with ICOT < 0.2, also the target requirements. Note that the decrease of liquid POD seen in Figure 6-3 does not occur here, because we only show the ice POD for Cirrus clouds.

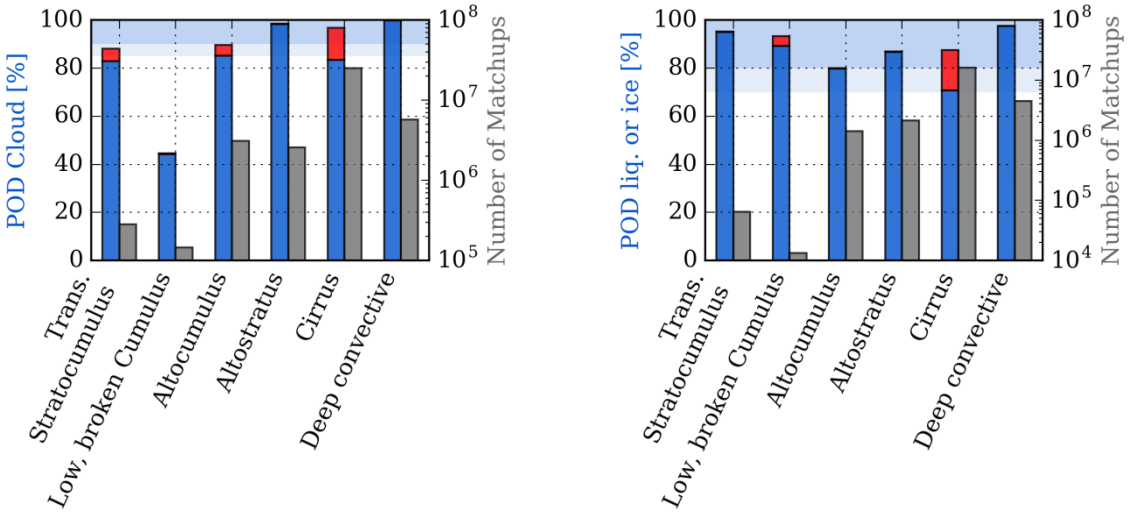


**Figure 6-6** Probability of detection for CLAAS-2 cloud mask and phase, resolved by cloud type of the uppermost CALIOP cloud layer. Left: Blue bars were computed by interpreting all CALIOP measurements with total column COT > 0 as cloudy. Red bars were derived using COT > 0.2 as cloud criterion. Darker and lighter blue shadings indicate the target and threshold requirements, respectively. Right: Bars for Cirrus and Deep Convective clouds represent ice POD, the rest is liquid POD. Blue bars were derived using the uppermost CALIOP cloud layer as reference. Red bars refer to the CALIOP cloud layer where ICOT exceeds 0.2. Darker and lighter blue shadings indicate the target and threshold requirements for liquid POD. Requirements for ice POD are not shown, because they are less strict.

In order to investigate the spatial characteristics, all collected cloud mask & phase matchups were remapped to a regular 1.5x1.5 degree grid and averaged within each grid box (see Figure 6-8). The large scale patterns of both cloud fraction and cloud phase are very similar in CLAAS-2 and CALIOP. However, CLAAS-2 overestimates the cloud fraction over the northern and southern Atlantic as well as over the Indian Ocean. On the other hand, cloud fraction in the tropics is underestimated, which can be explained by the large percentage of Cirrus clouds in this region, which are more likely to be missed by SEVIRI. The phase agreement is really remarkable. Only over Africa and the central Atlantic slightly less ice clouds are reported by CLAAS-2. The spatial distribution of the collected matchups is very homogeneous.

The cloud POD exceeds 90% in large regions, especially over the northern and southern Atlantic as well as the Indian Ocean. Over the central Atlantic and over land the POD is considerably lower, especially in the Sahara, where cloud detection is difficult due to the high surface albedo. This is also reflected by the cloud POD minimum near 20 degrees north in Figure 6-7, top. On the other hand, the cloud FAR is very low over land and larger over sea, especially over the north- and south-eastern Atlantic and the Indian Ocean, which can also be seen by the two cloud FAR maxima in the zonal plot. The low cloud POD over the central Atlantic and over Africa is caused by missing high, optically thin clouds, as can be seen in the

top panel of Figure 6-7: When filtering clouds with total column COT < 0.2, the POD is significantly increased in that region.
The phase of liquid Stratocumulus clouds over the southern Atlantic is correctly detected with a very high probability > 94% when applying ICOT > 0.2. However, liquid clouds in the ITCZ are incorrectly classified as ice in about 60% of the matchups, which causes a distinct minimum in the zonal plot (Figure 6-7, mid). Simultaneously, the liquid FAR has a distinct maximum in the same zonal band, which is caused by classifying thin ice clouds over liquid clouds as liquid: If high, optically thin CALIOP cloud layers are excluded, the liquid FAR is significantly reduced.
The phase of ice clouds is detected correctly with 88% probability and beyond in very large regions when applying ICOT > 0.2. Only over the south-eastern Atlantic and the Sahara considerably lower ice PODs are observed. The zonal variability is quite low (Figure 6-7, bottom).

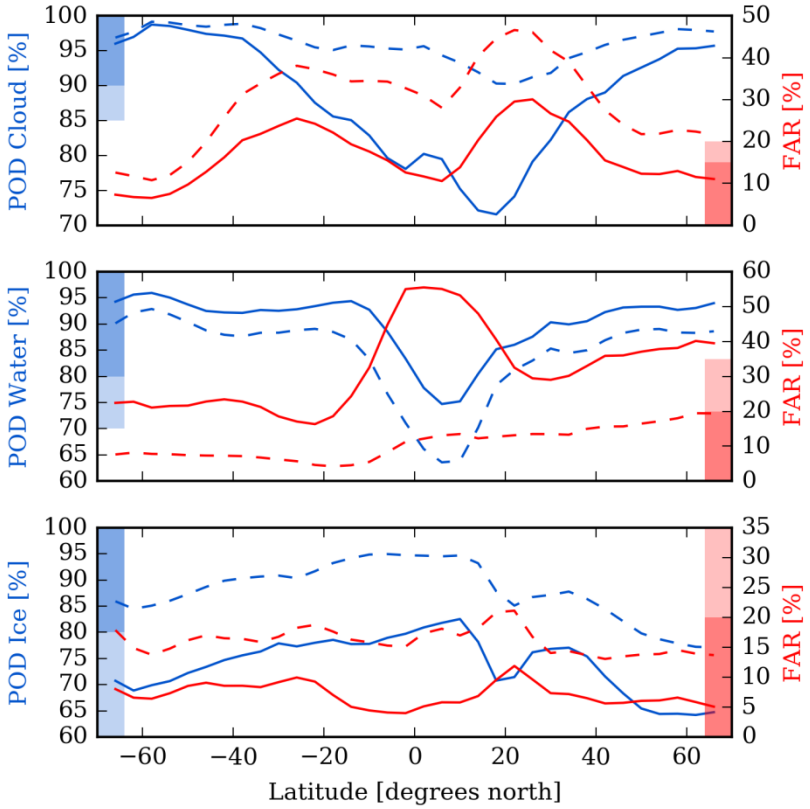


**Figure 6-7** CLAAS-2 cloud mask and phase scores in 4-degree latitude bands. Darker and lighter blue/red shadings indicate the target and threshold POD/FAR requirements, respectively. Top: Solid/dashed lines were calculated using total column COT > 0/0.2 as cloud criterion. Mid & Bottom: Solid lines refer to the uppermost CALIOP cloud layer, dashed lines refer to the CALIOP cloud layer where ICOT exceeds the 0.2 threshold.

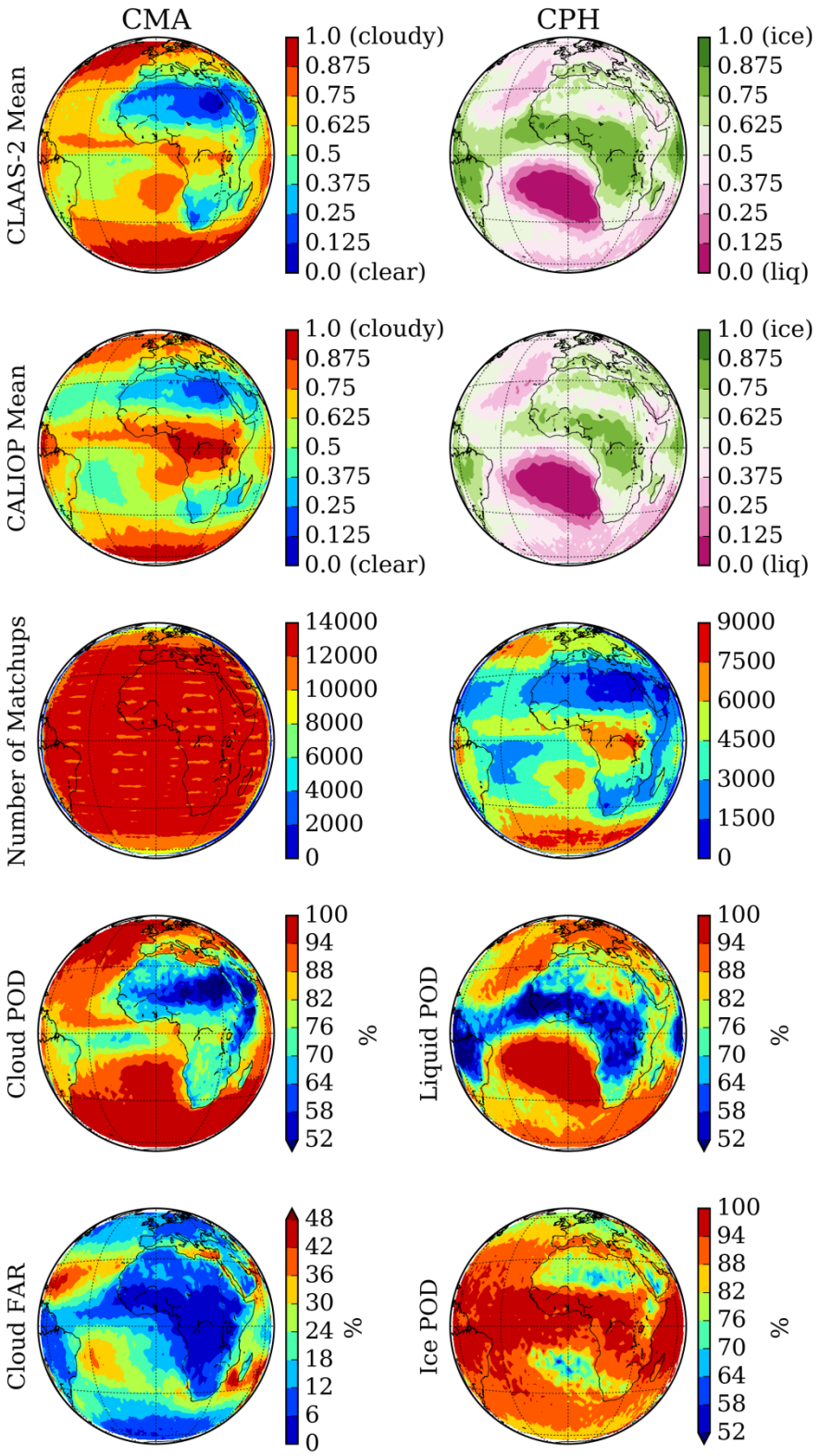


**Figure 6-8** Left column: Spatial distribution of cloud fraction as seen by CLAAS-2 and CALIOP as well as cloud scores. CALIOP cloud criterion is total column COT > 0. Right column: Spatial distribution of the fraction of ice clouds as seen by CLAAS-2 and CALIOP as well as phase scores. CALIOP phase is taken from the layer where ICOT exceeds 0.2. (Upper four panels taken from Benas et al., 2016)

Finally, we compared the relation of cloud top temperature and cloud phase, where the CALIOP cloud top temperature was taken as a reference. The results are shown in Figure 6-9. As you can see, there is an excellent agreement in the phase histograms of both liquid and ice clouds (left panel) when taking the CALIOP phase and temperature from the layer where ICOT exceeds 0.2 The transition from ice to liquid clouds (right panel) also matches very well, although it is less sharp in CLAAS-2 due to the broader distribution of liquid and ice clouds. Note that the occurrence of CLAAS-2 liquid phase below -42 C and ice clouds above -8 C is explained by the fact that the x-axis refers to CALIOP CTT. If CLAAS-2 CTT were used on the x-axis, such cases would not exist because the phase algorithm does not allow this (see [RD 3]).

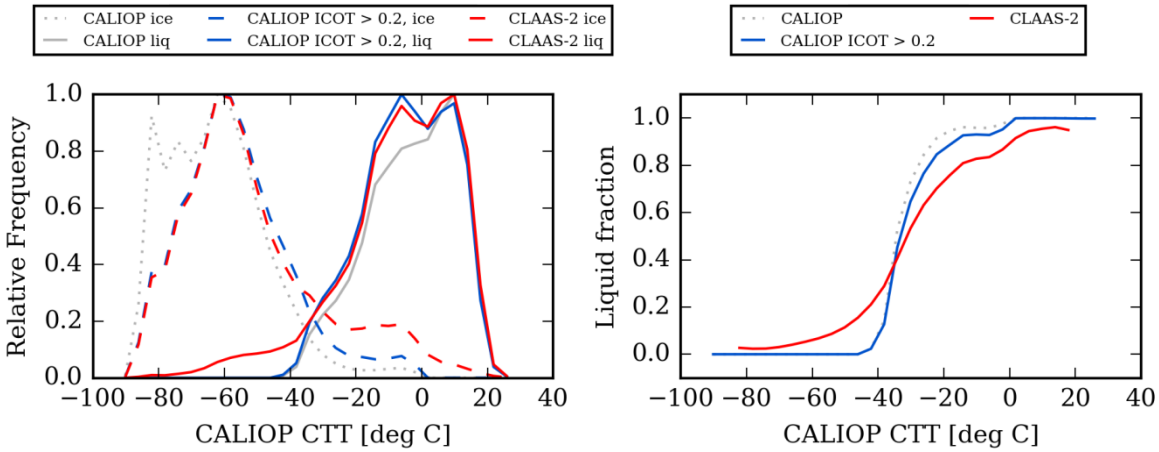


**Figure 6-9** Phase histograms (left) and fraction of liquid clouds (right) as a function of CALIOP cloud top temperature. For the red and blue line, binning is based on the CALIOP CTT taken from the layer where ICOT exceeds 0.2. For the gray line, phase and temperature of the uppermost CALIOP cloud layer were used. CLAAS-2 liquid fraction was only computed, if both ice and liquid histogram values were > 1E-3 in order to avoid artifacts at very small numbers. Bin size is 4 degrees C. (Left panel taken from Benas et al., 2016)

### 6.1.2 Cloud Top Products

CLAAS-2 cloud top pressure, height and temperature are directly comparable to the pressure, height and temperature of the uppermost cloud layer detected by CALIOP. For sensitivity analysis we also include comparisons against the CALIOP layer where ICOT exceeds a certain threshold.

A timeseries of cloud top products from CLAAS-2 and CALIOP between 2006 and 2015 is shown in Figure 6-10. When comparing against the uppermost CALIOP layer (left panel), CLAAS-2 significantly underestimates cloud top height (CTH) and consequently overestimates cloud top temperature (CTT) and cloud top pressure (CTP). As one can see in the right panel of Figure 6-10, this discrepancy can again be affiliated to high optically thin clouds. If CALIOP cloud layers with ICOT < 0.2 are excluded, the bias is significantly reduced and the target requirements are met by both CTH and CTP throughout the timeseries. See Table 6-3 for the overall mean bias and BC-RMSE. Note that while CLAAS-2 and CALIOP CTP almost exactly match when filtered for ICOT < 0.2, there is still a bias for CTH. This may appear inconsistent, but can be explained by the averaging of low and high clouds. Suppose the CTP for a low cloud is underestimated by 25 hPa, while the CTP for a

high cloud is overestimated by 25 hPa. Then the CTP bias is zero, but the CTH difference will be small (overestimation) for the low cloud and large (underestimation) for the high cloud, leading to a negative bias in CTH.

Furthermore one can recognize a slight negative CTH trend and positive CTP/CTT trend beginning in 2012 in both datasets as well as a slight jump in 2013 in the bias (Figure 6-11). The jump might be related to the CALIOP version change from V3-02 to V3-30 in March 2013: due to a change in the tropopause height used by CALIOP, some stratospheric features now appear as additional very high clouds leading to an even larger underestimation of CTH and overestimation of CTP & CTT in CLAAS-2 (Tackett, 2013). The described trend should be object of further analysis in the future.

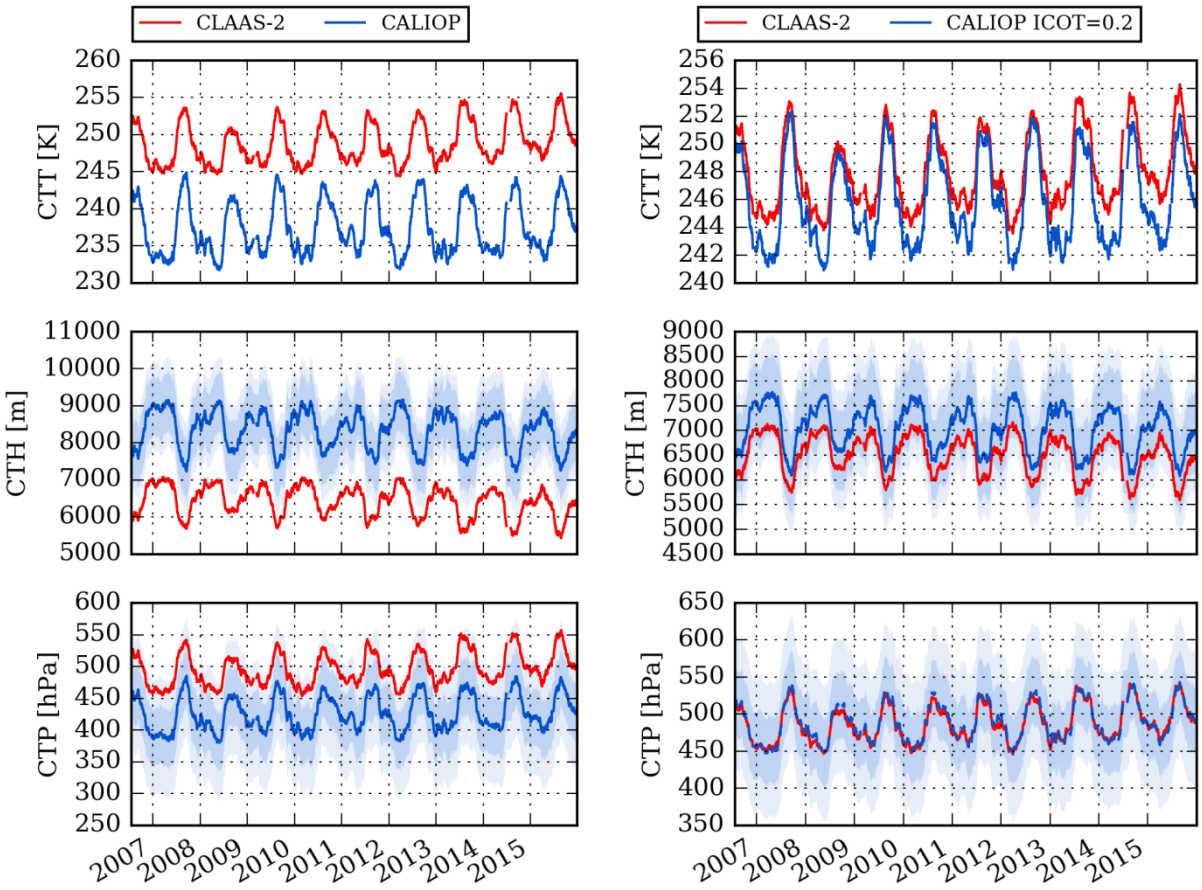


**Figure 6-10** Ten-day moving average of cloud top products. In the left panel we compare against the uppermost CALIOP cloud layer, in the right panel we compare against the CALIOP cloud layer where ICOT exceeds the 0.2 threshold. The red curve is identical in both plots. Darker and lighter blue shadings indicate the target and threshold requirements, respectively. For better visibility, only every 100th matchup is plotted here.

**Table 6-3** Overall validation results for CLAAS-2 cloud top products. Dark green cells meet the optimal-, light green cells the target- and grey cells the threshold-requirement. Red cells miss the threshold-requirement.

| | | Threshold | Target | Optimal | Uppermost Layer | Layer where ICOT exceeds 0.2 |
|---|---|---|---|---|---|---|
| CTH [m] | Mean Bias | 1200 | 800 | 500 | -1903 | -520 |
| | BC-RMSE | 4000 | 2500 | 2000 | 3296 | 2398 |
| CTP [hPa] | Mean Bias | 90 | 45 | 30 | 69.5 | -2.2 |
| | BC-RMSE | 200 | 110 | 80 | 180.4 | 134.1 |
| CTT [K] | Mean Bias | - | - | - | 11.4 | 2.1 |
| | BC-RMSE | - | - | - | 22.2 | 16.3 |

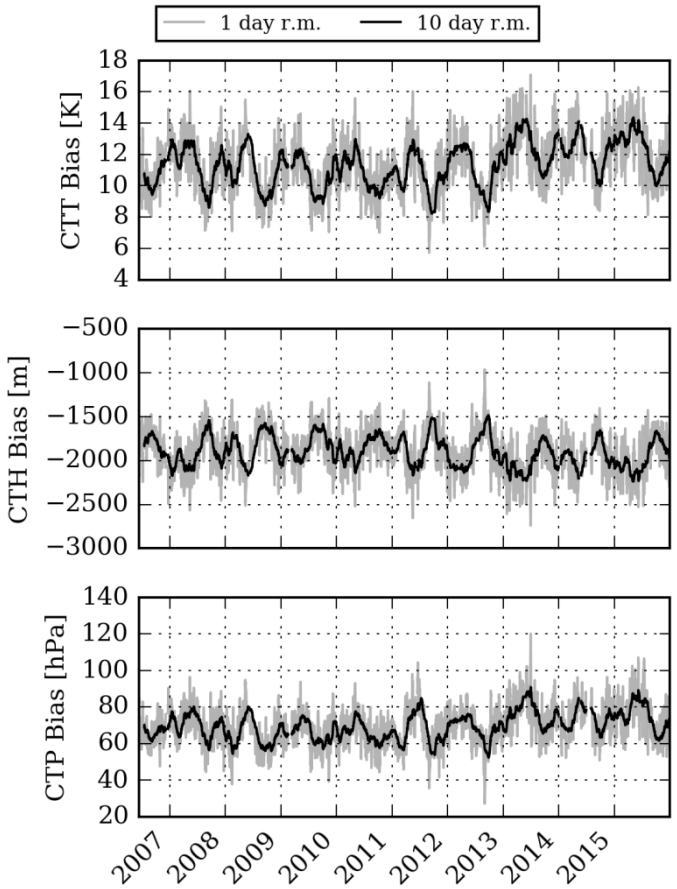


**Figure 6-11** Timeseries of cloud top bias (CLAAS2 – CALIOP) using two different temporal averaging windows. For better visibility, only every 100th matchup is plotted here.

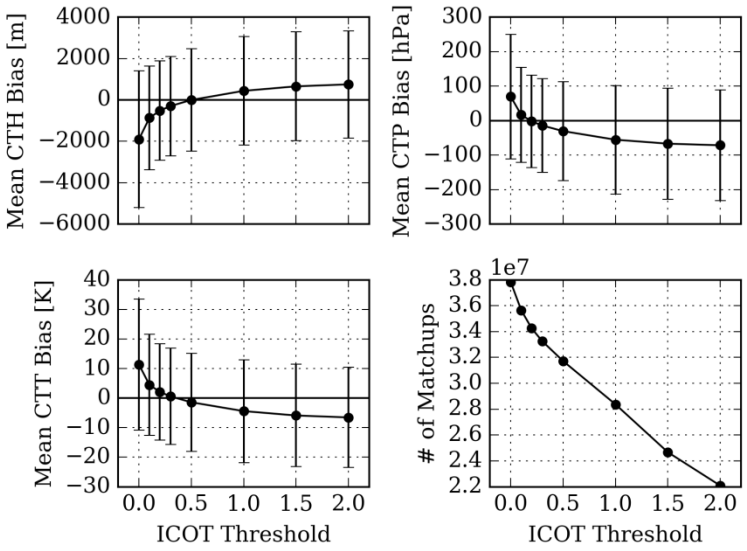


**Figure 6-12** Mean cloud top bias (CLAAS2 – CALIOP) compared against the CALIOP cloud layer where ICOT exceeds a certain threshold. Errorbars represent the BC-RMSE. (Figure taken from Benas et al., 2016)

Additionally, we analyzed the impact of excluding high CALIOP cloud layers with low COT on the accuracy of the cloud top products. As can be seen in Figure 6-13, the largest contribution to the bias of cloud top products comes from Cirrus clouds. Excluding the high, thin CALIOP layers, strongly influences the bias: The underestimation of CTH and overestimation of CTP/CTT at ICOT=0 turn into an overestimation of CTH and underestimation of CTP/CTT at ICOT=2.0 with lower absolute value of the bias (Figure 6-12). Note that the number of Cirrus clouds almost vanishes at ICOT=2.0, see Figure 6-4. At ICOT=0.2, the target requirement for CTH and CTP are met in all cloud categories, except low broken Cumulus.
Regarding all analyses with respect to the CALIOP cloud type, please remember the strong ice cloud bias of the cloud type classification explained in the previous section.

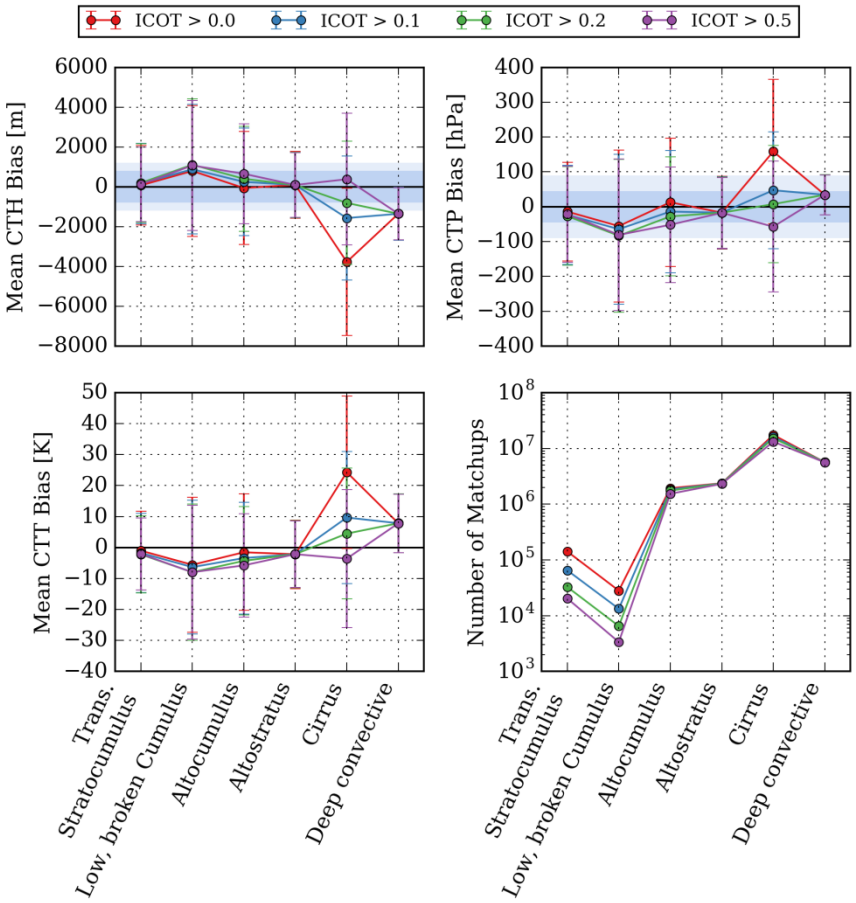


**Figure 6-13** Bias (CLAAS2 - CALIOP) of cloud top products computed using multiple ICOT thresholds and resolved by CALIOP cloud type. Error bars represent the BC-RMSE. Darker and lighter blue shadings indicate the target and threshold requirements, respectively. Note that the cloud type binning always refers to the uppermost CALIOP cloud layer, so that clouds do not change the cloud type *bin.*

The zonal characteristics of cloud top products from both CLAAS-2 and CALIOP are shown in Figure 6-14. The underestimation of CTH and overestimation of CTP/CTT described above is largest in the tropics and decreases towards high latitudes. This is consistent with the previous findings, because Cirrus clouds prevail in that region. As seen in the timeseries, the bias is significantly reduced by excluding high, thin CALIOP layers, so that CTH meets the threshold and CTP the target requirement in nearly all zonal bands.

Finally, all collected cloud top matchups were remapped to a 1.5x1.5 degree grid and averaged within each grid cell in order to compare the spatial features of both datasets (Figure 6-15, row 1-3). The agreement is excellent, especially in the northern and southern Atlantic. Yet CALIOP still reports higher clouds with lower CTP and CTT, mostly over Africa.

The overall correlation between cloud top products from CLAAS-2 and CALIOP is quite strong with Pearson correlation coefficients between 0.84 and 0.88 (Figure 6-15, row 4). The scatter plots also reflect the underestimation in height and overestimation in temperature and pressure of high clouds.

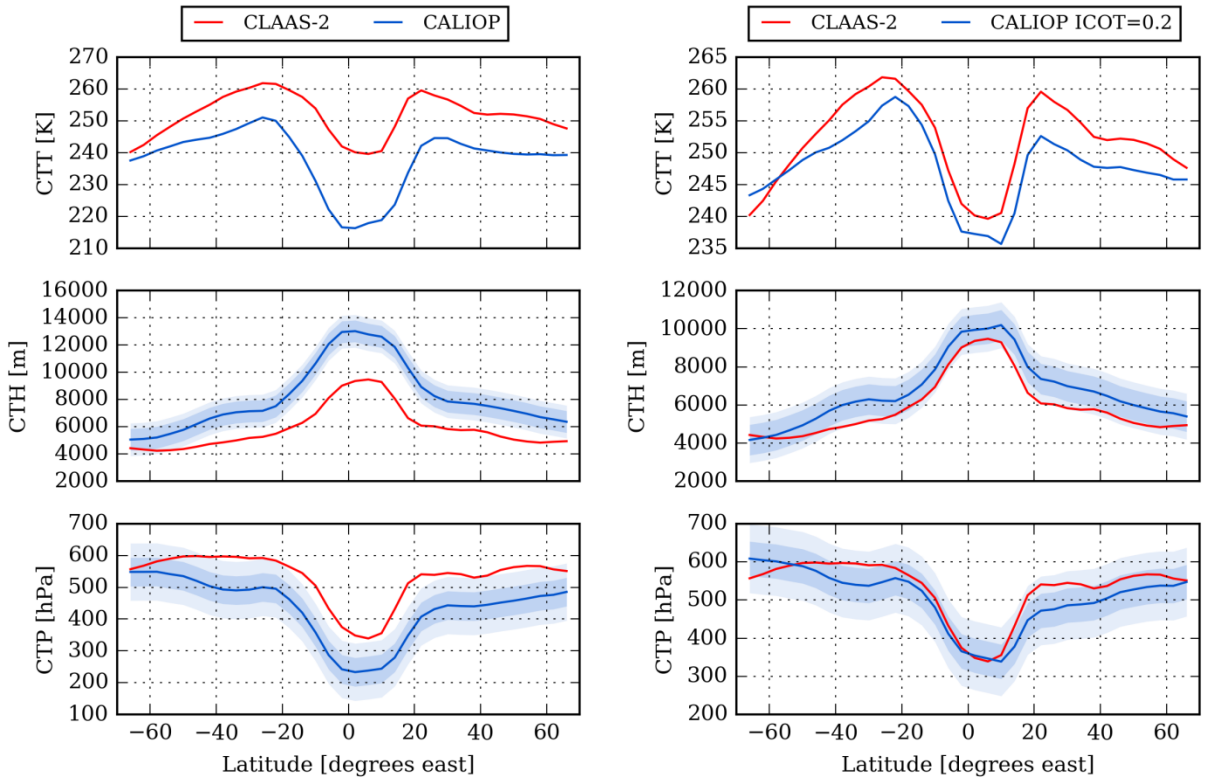


**Figure 6-14** Averages of cloud top products in 4-degree latitude bands. In the left panel we compare against the uppermost CALIOP cloud layer, in the right panel we compare against the CALIOP cloud layer where ICOT exceeds the 0.2 threshold. The red curve is identical in both plots. Darker and lighter blue shadings indicate the target and threshold requirements, respectively.

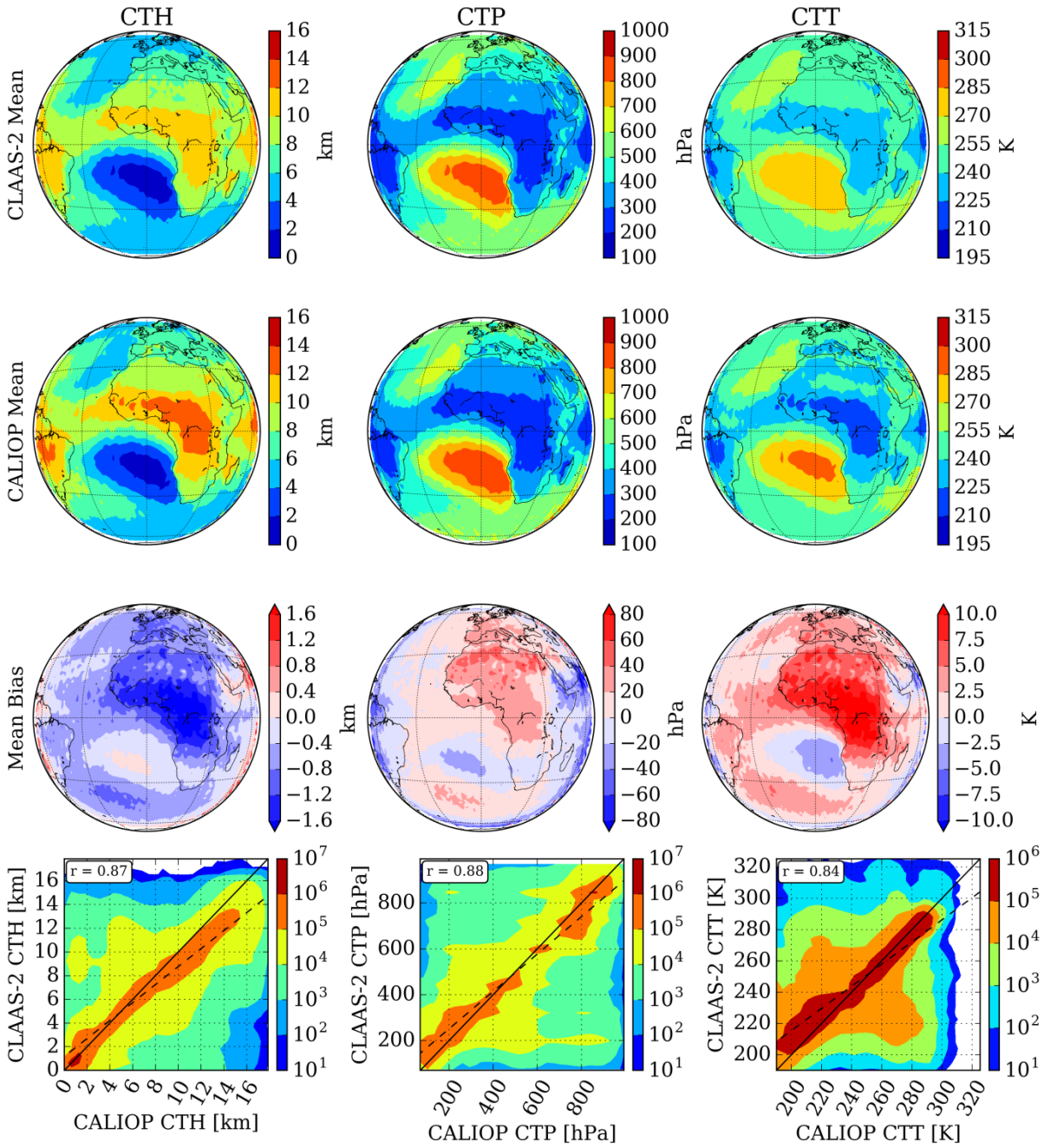


**Figure 6-15** Row 1-3: Spatial distribution of cloud top products from CLAAS-2 and CALIOP. Row 4: Correlation of cloud top products between CLAAS-2 and CALIOP. The diagonal is marked by a solid line; dashed lines show the result of a least squares linear fit. The textbox in the upper left corner displays the Pearson correlation coefficient. p-values are practically zero because of the very large number of matchups. Note: CALIOP values were taken from the layer where ICOT exceeds 0.2 in all plots. (The three bottom panels taken from Benas et al., 2016)

## 6.2 Validation with DARDAR

For this evaluation all DARDAR overpasses though the SEVIRI disk for the month of January 2008 have been combined. Since the interest at this point is the evaluation of ice cloud microphysics, first all DARDAR profiles were checked for the number of different

cloud phases within the profile. Only those profiles which consist of a single cloud phase (either liquid or ice) have been taken into account. Since multiple DARDAR profiles are available within a single SEVIRI pixel the choice has been made to include a single profile per SEVIRI pixel only when all profiles within this pixel at that specific observation time have a consistent cloud phase. The resulting phase detection scores for the month of data, ensuring that only single phase profiles are compared, is shown in Figure 6-16.

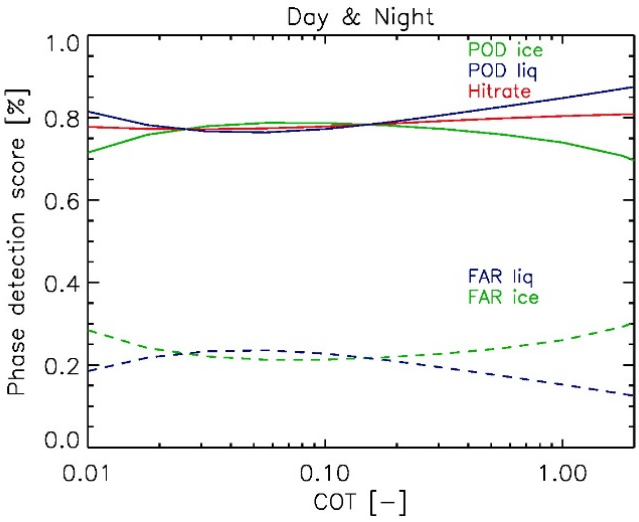


**Figure 6-16:** The cloud phase hit rate, probability of detections and false alarm ratios for both liquid and ice layers as a function of the integrated optical thickness from the top of the cloud. Only single cloud phase DARDAR columns were used in these statistics and both day & night observations were taken into account.

The probabilities of detection are smaller in comparison to the results presented in Figure 6-3 which is most likely representing the difference in approach between using the individual profile information and the layer averaged values in the 5-km CALIOP product.

In Figure 6-17 the CLAAS-2 vs. DARDAR single layer ice cloud optical depth comparison is depicted. For the comparison of the optical properties, only solar zenith angles < 75 degrees have been taken into account. The distribution contours show the number of points enclosed, i.e. the black area shows the top 20% of the number of points. The distribution is clearly correlated and lies along the one-to-one line. However, the remaining 25% of the observations are so much scattered in parameter space that the total correlation remains weak (0.33). The CLAAS-2 retrievals become very sensitive at low optical depth, below a DARDAR optical depth of ~0.3, resulting in a region with hardly any retrieval skill (no correlation).

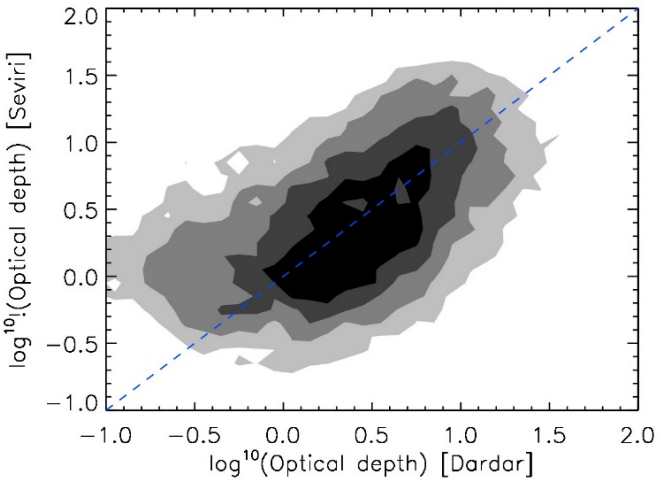


**Figure 6-17:** Ice cloud optical thickness distribution comparing the DARDAR and CLAAS-2 retrieved collocated values. The blue dashed line shows the 1-1 line with the greyscales indicating the regions enclosing 20, 40, 60 and 75% of all data points. (Figure taken from Benas et al., 2016)

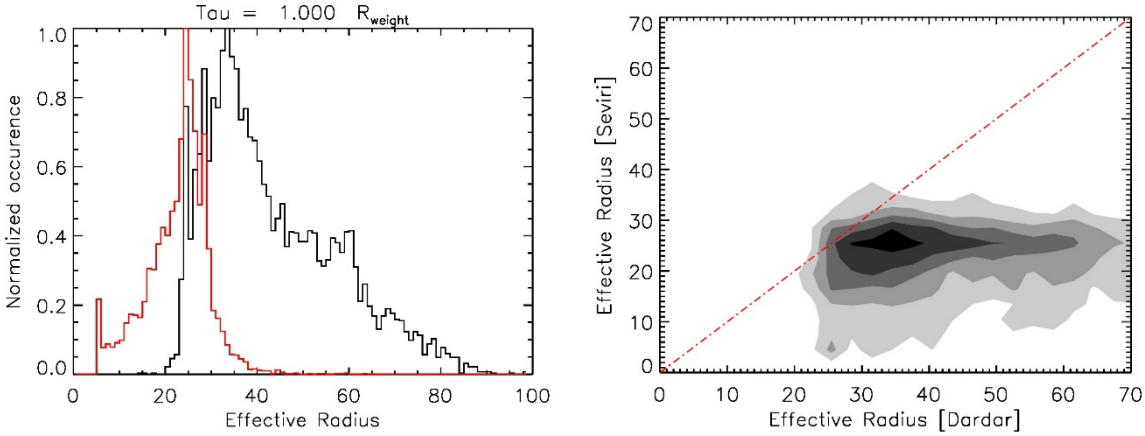


**Figure 6-18** Comparison of CLAAS-2 ice effective radius and DARDAR weighted effective radius from cloud top to an optical depth of 1 (or to cloud base if the total optical depth is smaller than 1). The left plot shows 1D-histograms with CLAAS-2 indicated in red and DARDAR in black; on the right a scatter density plot is shown. The dynamic range of the DARDAR retrievals is a lot larger resulting in no correlation between the two distributions.

The second direct retrieval from the CPP algorithm used to calculate the CLAAS-2 results is the effective radius. The retrieval uses the Nakajima and King (1990) approach, calculating both optical depth and effective radius simultaneously using pre-calculated lookup tables (LUTs). These LUTs have been calculated assuming microphysical radiative properties that are different from the assumptions used in the lidar-radar retrievals. This especially shows up in the comparison of the effective radii, which show very different distributions (Figure 6-18; left panel), even though both retrievals are radiatively consistent within their individual assumptions. Next to this the DARDAR product provides the effective radius profile and not the radiative layer effective radius observed by the SEVIRI imager. To enable the comparison, the layer averaged effective radius was calculated in three ways: (i) the local effective radius with respect to optical depth, (ii) the mean profile radius seen from cloud top

(optical depth dependent), and (iii) the weighted effective radius taking into account the local extinction and transmission up to the local optical depth ($\tau$)

$$R_{eff}(\tau) = \frac{\int R_{eff}(z)\,\alpha(z)\,e^{-\tau(z)}\,dz}{\int \alpha(z)\,e^{-\tau(z)}\,dz}$$

In Figure 6-18 the results are shown for all ice clouds up to an optical depth of 1. This procedure weighs the Reff towards cloud top and high extinction regions, resulting in a slightly lower Reff value in comparison to the averaged Reff and a lot smaller in comparison to the local effective radius at an optical depth of 1. Even with this focus on the upper part of the ice clouds the resulting distribution is a lot wider (between 20 and 80 microns). When looking deeper into the cloud (tau > 1), the DARDAR Reff distribution moves to larger sizes and vice versa. The CLAAS-2 effective radius distribution in contrast is very narrow and peaks between 20 and 30 microns, resulting in the end in no correlation between the two distributions. In Figure 6-18 a pronounced peak around Reff = 25 micron is visible. This is related to the weighting with a climatological effective radius for thin clouds (see [RD 3]). Figure 6-19 shows that for thick clouds only the histogram has a much less pronounced peak, which also moves to somewhat lower effective radii. Thus, differences between CLAAS-2 and DARDAR cannot be explained by thin cloud artifacts.

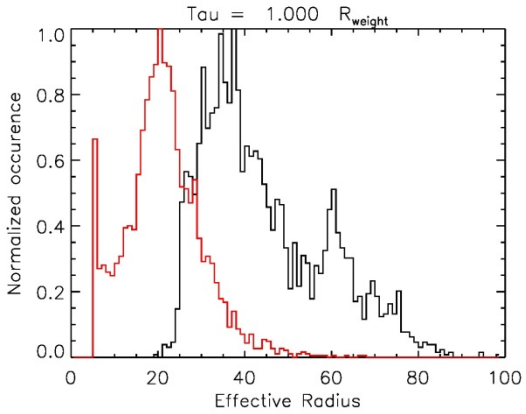


**Figure 6-19** Same as the left panel of Figure 6-18 but for clouds with CLAAS-2 optical thickness larger than 4.

The ice water path (IWP) is proportional to the product of the two retrievals discussed above. Due to the differences seen in the effective radius distributions the overlay along the 1-1 line for the optical depth data is converted into a curved 2D-occurrence distribution (Figure 6-20; left panel). The occurrence distributions, dynamic range, for each of the individual data sets however is very similar (right panel).

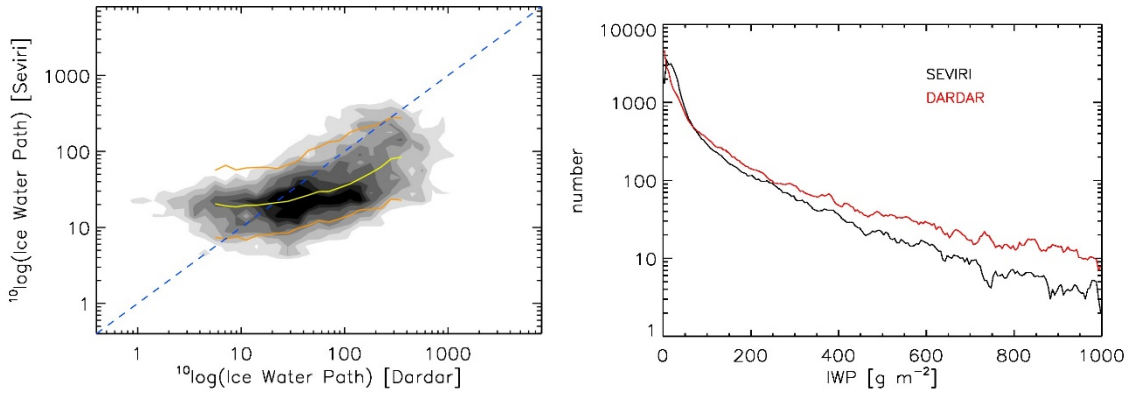


**Figure 6-20** Left panel: CLAAS-2 IWP vs. DARDAR IWP. The yellow line depicts the median and orange the 16th/84th percentiles of the CLAAS-2 distribution at the local DARDAR IWP. Right panel: 1D-histogram of DARDAR and CLAAS-2 LWP for the same collocations. (Figure taken from Benas et al., 2016)

The distributions look similar to the ones presented in Eliasson et al. (2013), with the curve for low IWP values as seen in their Figure 6 for MODIS and PATMOS-X. The results once more show that an evaluation of passive versus active instruments is difficult due to the different microphysical assumptions, the difference between profile information vs. column averaged (but weighted to the top of the cloud) measurements and the viewing and solar angles vs the near nadir view of the active instruments. All three points have an influence on what the effective cloud depth is from where most of the information comes from. What is clear is that the CLAAS-2 retrieved effective radius is on the small side, even though it is radiatively internally consistent with the CLAAS-2 microphysical assumptions.

It will be considered to alter the microphysical assumptions for CLAAS-3 to a more general aggregate habit mode, e.g., Baum et al (2012) or Baran et al. (2005), instead of the roughened randomly oriented hexagons used in CLAAS-2. This should enable the retrieval of a more consistent IWP with respect to the active instruments in a future data record.

## 6.3 Validation with AMSR-E

A limited validation with AMSR-E level-2 data was performed. This concerns one orbit of AMSR-E data in March 2008, which was also used in Stengel et al. (2013). CLAAS-2 SEVIRI pixels were collocated in space and time with the AMSR-E footprints. Furthermore, the following requirements were applied for data to be included:

- AMSRE-E:
  1. Ocean_products_quality_flag = 0.
  2. LWP smaller than 180 g/m$^2$.
- SEVIRI:
  1. LWP smaller than 300 g/m$^2$.
  2. No ice pixels in AMSR-E footprint.
  3. Clear-sky pixels within the AMSR-E footprint were included as 0s in the average.

Results are shown in Figure 6-21. From the spatial maps (panels a and b) it is clear that the AMSR-E data coverage is much larger. This is because for CLAAS-2 only liquid-phase pixels are shown. The additional AMSR-E coverage consists of scenes with liquid water in the

column but likely ice near the top, so that CLAAS-2 retrieves ice phase. For the fully liquid pixels satisfying the above-listed criteria, there is a clear correlation between CLAAS-2 and AMSR-E LWP (panel c). The bias is 3.4 g/m$^2$, which is within the optimal requirement. The bc-rms error is around 34 g/m$^2$, which fulfils the target requirement. A striking difference is that SEVIRI has many more clouds with low (less than 10 g/m$^2$) LWP (panel d). This is likely related to a clear-sky bias in the AMSR-E data (e.g., Seethala and Horvath, 2010).

Overall, the agreement between CLAAS-2 and AMSR-E for this single orbit is favourable.

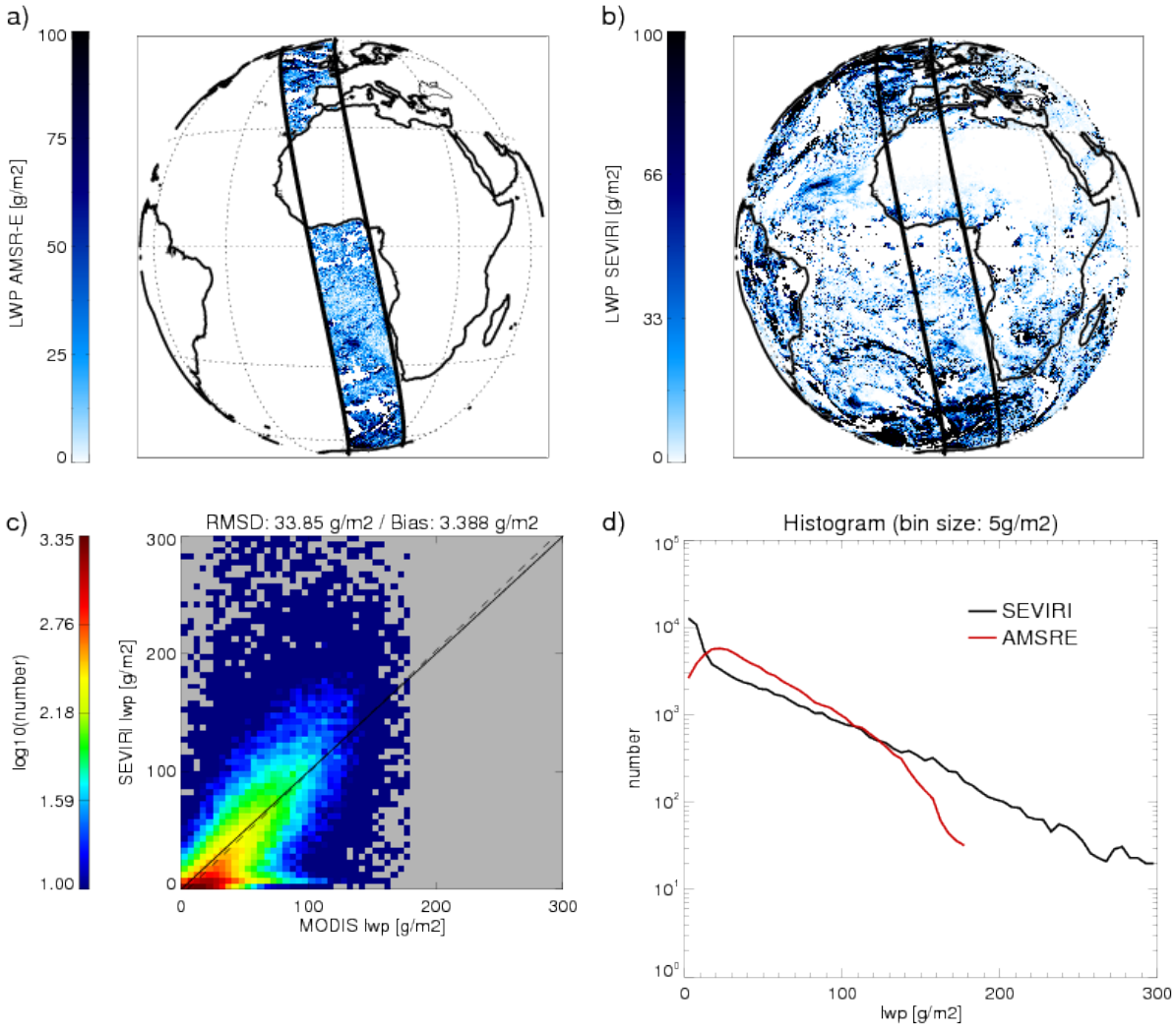


**Figure 6-21:** Validation of CLAAS-2 LWP with AMSR-E: (a) AMSR-E LWP in g/m2 of an afternoon orbit on 2008-03-20. (b) CLAAS-2 LWP for pixels with liquid clouds taken from the temporally closest SEVIRI slot. (c) 2D-histogram of spatiotemporal matches between AMSRE-E and SEVIRI for the AMSRE-E orbit shown. (d) 1D-histogram of AMSRE-E and CLAAS-2 LWP for the same collocations.

## 6.4 Comparison with MODIS

The evaluations with MODIS focus on level-3 inter-comparisons covering the full CLAAS-2 time range. However, limited evaluation of level-2 products with MODIS was also performed. Based on a number of criteria, including a balanced mix between low/high, liquid/ice, and thin/thick clouds as well as sufficiently low solar zenith angles and little time difference with the nearest SEVIRI slot, a MODIS granule on 20 June 2008 from 10:50 to 10:55 UTC was selected. This granule was collocated (nearest neighbour) with SEVIRI data from the 10:45 UTC image, which covered Europe around 10:50 UTC.

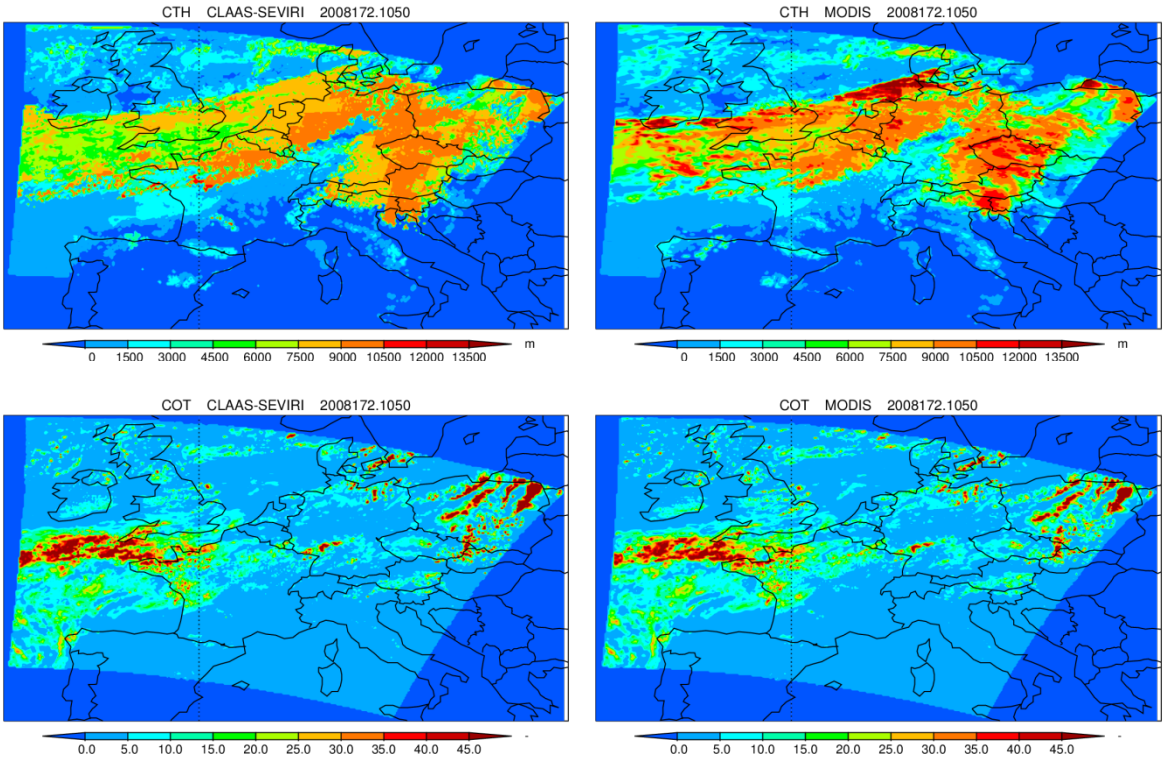


**Figure 6-22:** Maps of cloud top height (top) and cloud optical thickness (bottom) for the selected MODIS granule on 20 June 2008. Left: CLAAS-2; right: MODIS.

Figure 6-22 shows spatial distributions of CTH and COT for the granule. For CTH differences for high clouds are clearly visible, with MODIS placing these at a higher level. The COT images are hardly discernible. Scatter plots in Figure 6-23 confirm that the MODIS high cloud top heights are about 1 km higher than for CLAAS-2. Also, many more clouds with tops higher than 12 km are retrieved by MODIS. On the other hand, low clouds are placed somewhat higher in the atmosphere by CLAAS. COT agrees very well between the datasets, as does the effective radius of liquid water clouds. In contrast, the ice particle effective radius from CLAAS-2 is much lower than that from MODIS. The ice effective radii are correlated but with a slope far below unity.

1D-histograms of CTH, presented in Figure 6-24, suggest that the differences for low clouds are not that large. However, the high cloud bias is again confirmed. Also, CLAAS-2 has a small peak for mid-level clouds around 6 km that is not observed in the MODIS data. Finally,

1D-histograms of COT, REFF, and CWP are shown in Figure 6-25 separately for liquid and ice clouds. COT is plotted on a log scale, again illustrating the very good agreement between the two products. Note however the local peak of about 1% in CLAAS-2 COT at the maximum retrievable value of 100, which does not occur for MODIS. The CLAAS-2 effective radius for liquid clouds agrees well with the MODIS 1.6 µm REFF (which is the channel used by CLAAS-2), but even much better with the MODIS 2.1 µm REFF. The latter is a remarkable finding, which we cannot currently explain. For ice clouds the differences in REFF are large with overall much lower values in the CLAAS-2 data record. The cloud water path (LWP/IWP) is proportional to the product of COT and REFF and thus shows their combined features, resulting in very good agreement for liquid clouds but much poorer agreement for ice clouds.

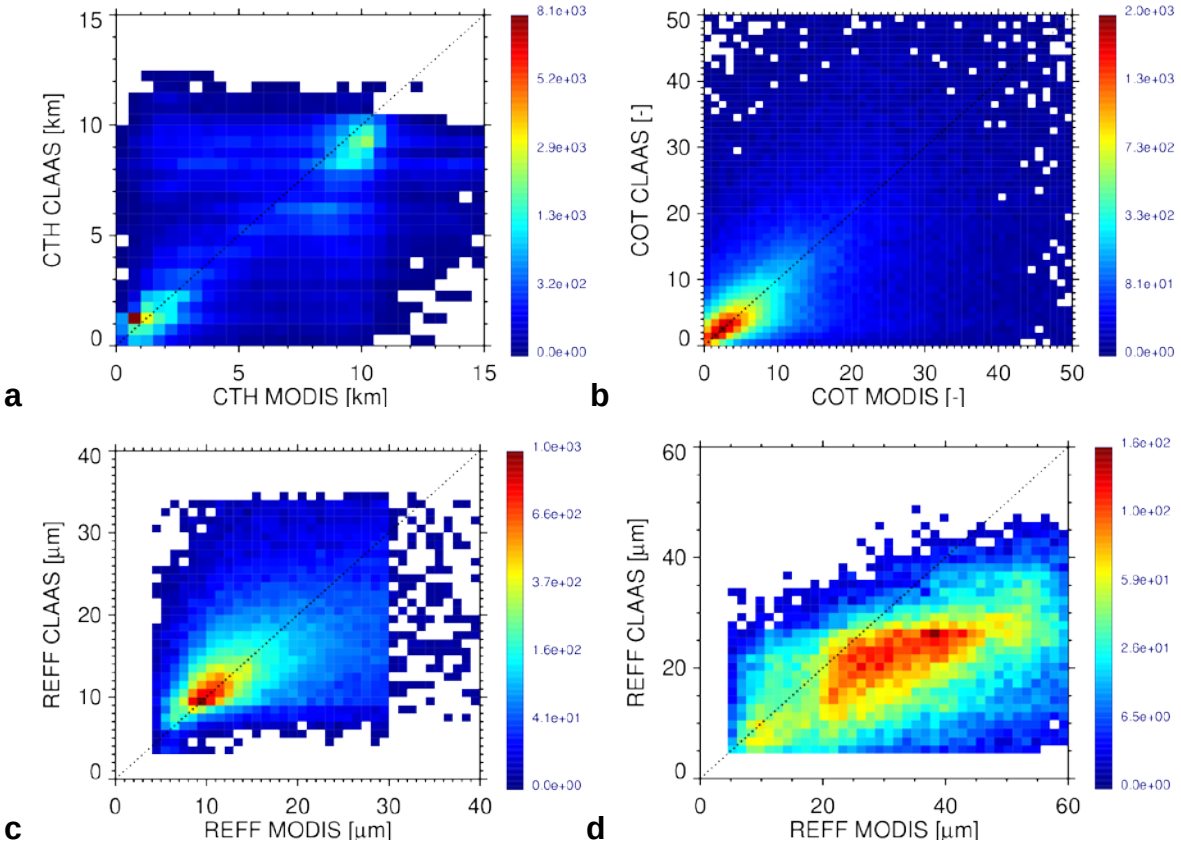


**Figure 6-23:** Joint histograms of CLAAS-2 and MODIS cloud properties for the MODIS granule on 20 June 2008: (a) cloud top height, (b) cloud optical thickness, (c) liquid water droplet effective radius, and (d) ice particle effective radius. For MODIS the 1.6 micron based effective radii have been plotted.

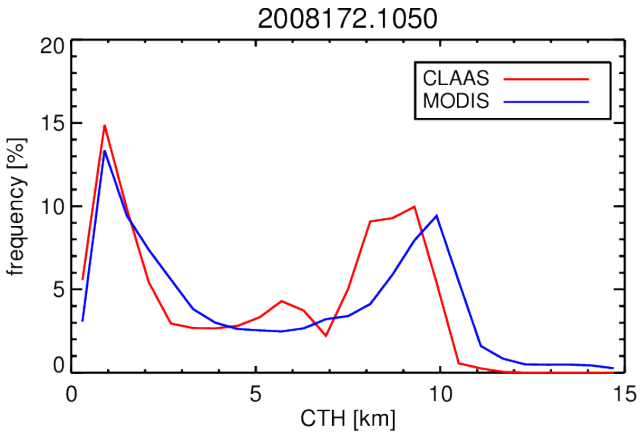


**Figure 6-24:** Histograms of CLAAS-2 and MODIS cloud top height for the selected MODIS granule on 20 June 2008.

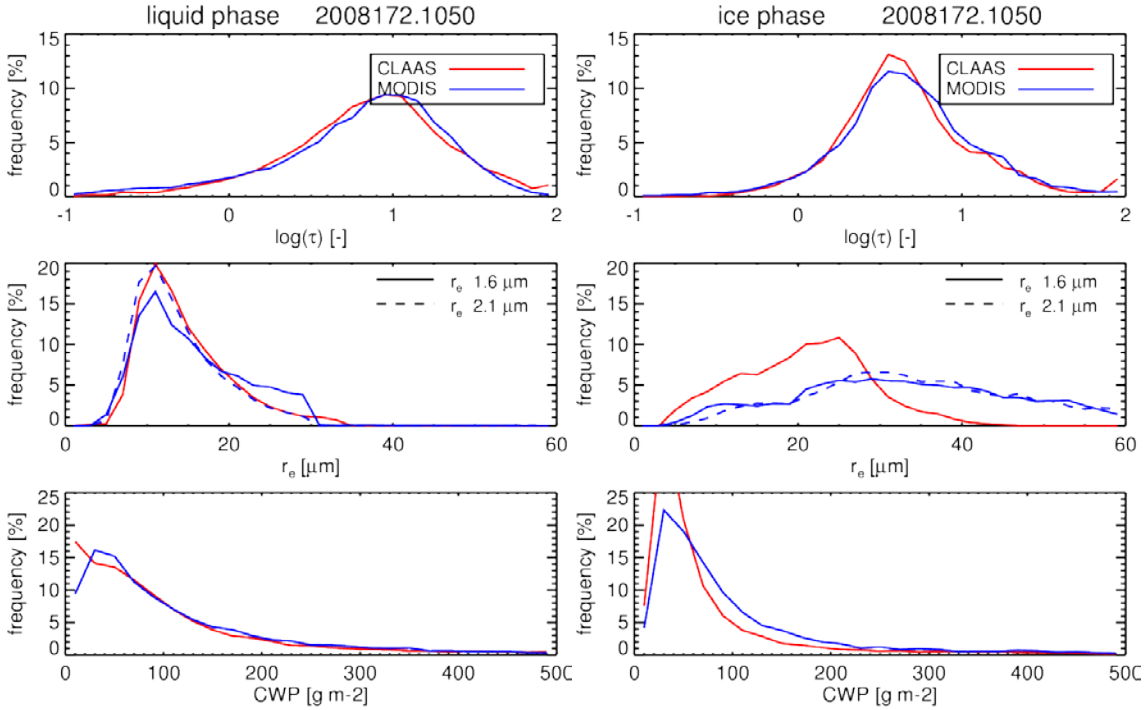


**Figure 6-25:** Histograms of CLAAS-2 and MODIS cloud optical thickness (top), effective radius (middle), and cloud water path (bottom) for the selected MODIS granule on 20 June 2008. Left: liquid clouds; right: ice clouds. Only pixels for which both products agree on the phase are included. (Figure taken from Benas et al., 2016)

The analysis of this granule has given insight into some retrieval agreements and differences between CLAAS-2 and MODIS. Statistics of a single granule are not meaningful in relation to the requirements compliance evaluation, and are therefore not provided.

# 7 Evaluation of SEVIRI aggregated (level-3) cloud parameters

This section covers the evaluation of CLAAS-2 level-3 products. These consist of daily and monthly aggregations as well as monthly mean diurnal cycles. The evaluation is organized according to Table 7-1.

**Table 7-1** Overview of reference datasets used for the evaluation of CLAAS-2 level-3 parameters.

| Section | Reference observations | Parameters |
|---|---|---|
| 7.1 | SYNOP | CFC |
| 7.2 | UWisc | LWP |
| 7.3 | MODIS | CFC, CTH, CTP, CPH, LWP, IWP, JCH |

## 7.1 Validation with SYNOP

In this section, the monthly mean cloud fractional cover derived from SEVIRI measurements is compared against SYNOP data. The complete time-span from 2004-2015 is validated.

All available SYNOP reports in the geographical domain covered by the Meteosat full disk field of view were taken into account, nevertheless the weather station records from the SYNOP data base had to be preselected as described in section 5.1. Further, observations with very high SEVIRI viewing zenith angles (VZA) are omitted, as described above, and only those stations that are within 75° VZA of SEVIRI are used here. Daily mean cloud fraction is derived based on all available 15 minute time slots of SEVIRI cloud mask. These are then averaged to the monthly mean, if at least 20 daily means are available. The following constraints had to be applied on station record basis: For a daily mean at least 6 measurements had to be found and for a monthly mean at least 20 daily means were needed.

First, the complete time series is considered, which is shown in Figure 7-1: After the monthly mean averaging and collocation procedures of SYNOP and SEVIRI data all results were aggregated over the entire domain.

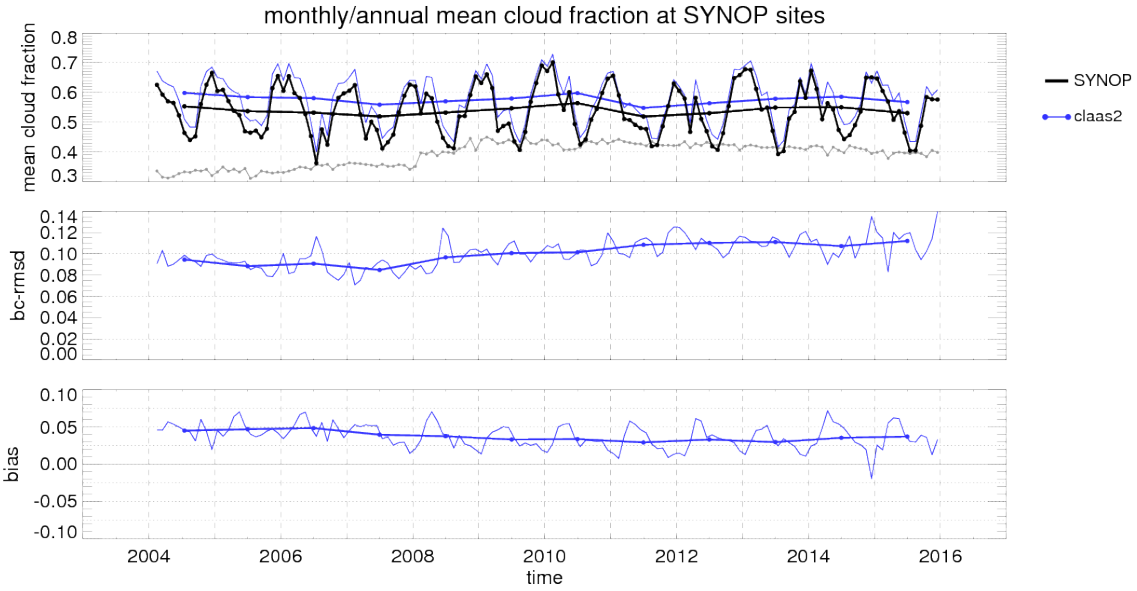


**Figure 7-1** CFC monthly mean from SEVIRI and dedicated SYNOP measurements, each averaged over all available stations in a month. Top panel: CFC; central panel: standard deviation; bottom panel: bias. The grey dotted line is the scaled number of stations.

As can be seen, both time series show a seasonal cycle with maximum cloud cover in winter and minimum cover during summer. This is due to the fact that the majority of SYNOP stations is located in the northern hemisphere on land, e.g. in Central Europe. So the course of the time series is mainly determined by the seasonal cycle of cloudiness in the northern hemisphere.

Both time series show a good overall agreement, while SEVIRI 's average cloud cover is slightly higher than SYNOP throughout the entire period. In the central and bottom panel the bias and the bias corrected root mean square deviation (BC RMSD) are shown. For the complete data record the target requirements are met, the bias does not exceed 7.5 % and the BC RMSD lies generally below 15 %.

The BC RMSD shows a small increasing trend. The increase in BC RMSD is well in line with the increase in SYNOP stations. In particular, several stations were added over the central African continent with very low viewing zenith angles. These, as shown later in Figure 7-2, are viewing conditions with an increased BC RMSD. Summarized, this confirms that the calibration efforts were successful in a sense that no artificial trends in cloud cover were introduced into the SEVIRI data record by changing between MSG 1, 2, and 3 or by sensor degradation.

The overall bias is positive for the complete time-series. Plausible reasons for this bias can be the geographical location of the SYNOP stations in connection with the well-known overestimation of cloudiness by geostationary satellites at high viewing zenith angles (VZA).

As stated earlier, also the SYNOP measurements can be inaccurate for the same reason with a more small scale geometry. The so-called scenery effect leads to the overestimation of cloudiness by SYNOP due to the obscuring of cloud-free spaces by convective clouds with high vertical extent. In some regions, for example Scandinavia this effect shows a seasonal cycle. (Karlsson, 2003). On the other hand, cloud cover is often underestimated in synoptical measurements at night-time because of difficulties in observing semi-transparent cirrus

clouds. In the monthly mean time-series all these effects are averaged. But, no further conclusions can be drawn on that subject within this report. A temporally and spatially higher resolved study, possibly separated for the different cloud types would be needed to investigate the individual effects more closely.

For a more detailed analysis of the SEVIRI viewing geometry effect, the dependency of the CFC bias on the viewing angle was investigated.

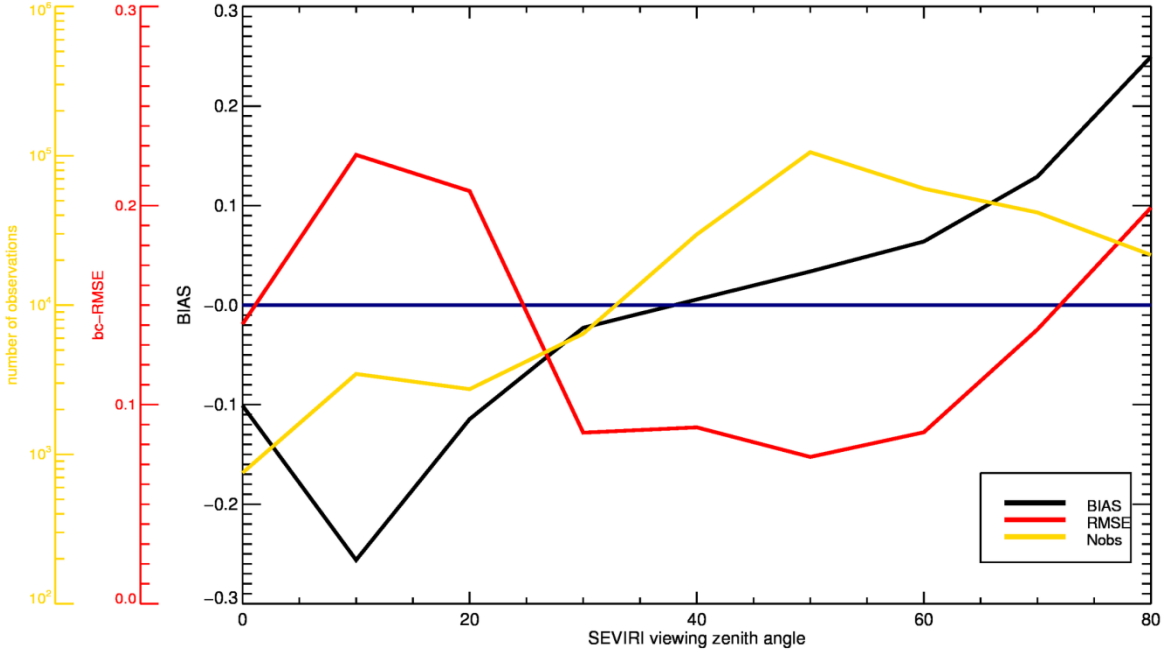


**Figure 7-2** Dependency of CFC bias (SEVIRI - SYNOP) on SEVIRI viewing zenith angle. (Figure taken from Benas et al., 2016)

This dependency can be found in Figure 7-2, where all bias values in steps of 10° viewing zenith angle of SEVIRI were averaged. The black line shows the bias, it is negative for VZA < 40° and positive for larger angles. The corresponding bias corrected root mean square deviation, indicated in red in the same plot, is highest around VZA=15° and VZA>80°. According to this figure, the best accuracy and precision of SEVIRI CFC data can be found for VZA being between 25 and 75°. This part of the data is dominated by northern mid-latitudes (.i.e. Europe). As can be seen from the yellow line, also in that region the greatest number of observations can be found, making corresponding bias and rmsd results very mature, in contrast to the rest of the data range. Especially for small SZA the number of observations might not be sufficient.

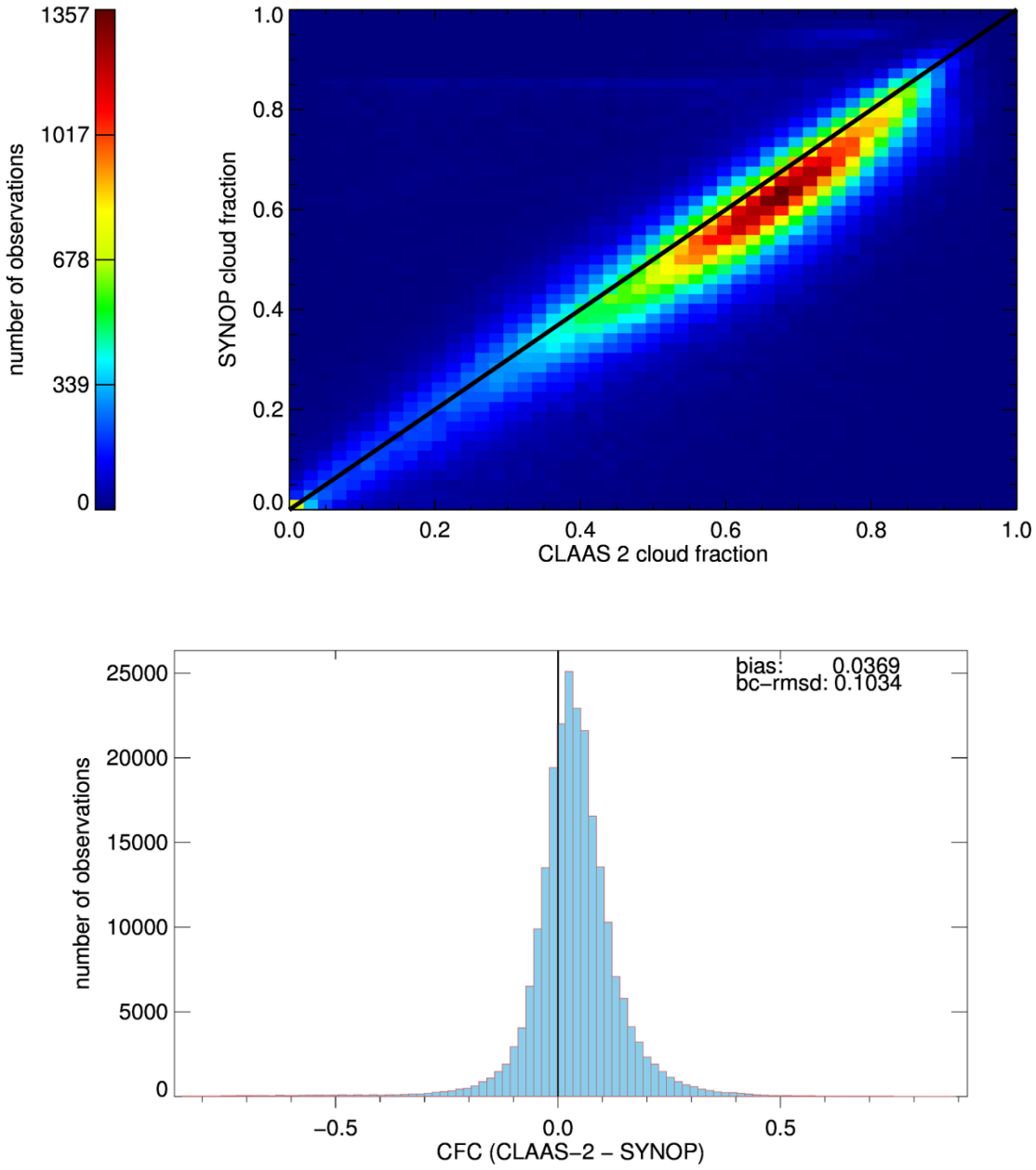


**Figure 7-3** Validation of monthly mean CFC from SEVIRI with SYNOP: scatter plot [top] and frequency distribution of deviation [bottom].

In Figure 7-3 more statistical aspects of the validation results are presented. The top plot shows the monthly mean CFC values for SEVIRI and SYNOP as a scatter plot. Here becomes clear that CFC is overestimated by SEVIRI mainly at high average cloud cover between 50 to 80 %. For lower averaged cloud cover the bias is close to zero.

This difference can be caused by the geometry of cloud fields, assuming that high cloud cover is also connected with spatially large extended cloud fields whereas small cloud fields often denotes cumuli fields. The first have naturally a larger detection error in geostationary satellites at high viewing zenith angles, i.e. clouds that are already horizontally extended will appear even larger when seen at high viewing zenith angles.

No further analysis could be made whether this effect is caused by the detection algorithm, which distinguishes between different opacity states of a cloud.

The synoptical records do not give hints to the type of cloud concerning its radiative properties, but refer more to the form and approximate height of a cloud (e.g. altocumulus or stratus) which makes a comparison of averaged values complex.

The overall bias of the complete time series is 3.7 %. In the lower box the frequency distribution of the difference SYNOP-SEVIRI shows that the differences are slightly shifted to positive values. There is additionally a declination to the right observable causing the generally positive bias.

The results of this section can be summarized as follows:

- SEVIRI CFC products are well within target requirements. The compliances with requirements are summarized in Table 7-2.
- Monthly mean SEVIRI CFC values show only a slight positive bias of 3.7% on average over the entire disk. SEVIRI disk mean standard deviations of CFC MM lies around 10%.
- Good stability, although bias and bc-rmsd show impact of new SYNOP stations over central Africa. Considering that, no artificial trends were introduced by the transition between MSG 1, 2, and 3.
- Dependence on viewing zenith angle (VZA): negative biases for VZA < 40° and positive biases for large viewing angles. Underestimation is most significant for tropical regions in Africa. In these regions the statistics however are not mature due to the small number of observations. Significant overestimation at the SEVIRI disk edges if found, which is most likely due to viewing geometry effects.

**Table 7-2** Compliance matrix of found CFC monthly mean product characteristics with respect to the defined product requirements for accuracy and precision. Comparisons were made against SYNOP observations. Remark: The anticipated error of SYNOP observations is probably of the order of 10 %, i.e., close to the Target requirement.

| % | CFC product requirements Level 3 (MM) | | | SYNOP Level 3 (2004 - 2015) |
|---|---|---|---|---|
| | Threshold | Target | Optimal | |
| Bias | 20 | 10 | 5 | 3.8 % |
| Bc-RMS | 40 | 20 | 10 | 10 % |

## 7.2 Validation with UWisc

The UWisc LWP dataset (see Section 5.5) comprises monthly mean all-sky LWP in 1° × 1° grid boxes that is based on all available data for a specific month. In addition, for each month and each grid box over the 1988-2012 period the mean diurnal cycle of LWP is available. In order to obtain the monthly mean all-sky LWP from UWisc in 1-hour time steps, to compare it

with corresponding diurnal CLAAS-2 data, the mean diurnal cycle parameters, available in the UWisc dataset, were used to adjust the monthly mean grid box values, based on the equation:

$$\langle LWP(Y,t)\rangle = \langle LWP(Y)\rangle + A_1 cos\omega(t - T_1) + A_2 cos2\omega(t - T_2)$$

where $\langle LWP(Y)\rangle$ represents the uncorrected monthly mean LWP for year $Y$, $t$ is the time (h), $\omega$ the radial frequency that corresponds to a 24-hour period, and $A_1(T_1)$ and $A_2(T_2)$ are the amplitudes (phases) of the first and second harmonics of the diurnal cycle, respectively (see also O'Dell et al. 2008).

As described in Section 5.5, the marine stratocumulus region in the south Atlantic off the Namibia coast was selected for this validation (Figure 7-4). Monthly mean diurnal results were computed as spatial averages from this region and span the 02/2004-12/2012 period, when both CLAAS-2 and UWisc data records are available.

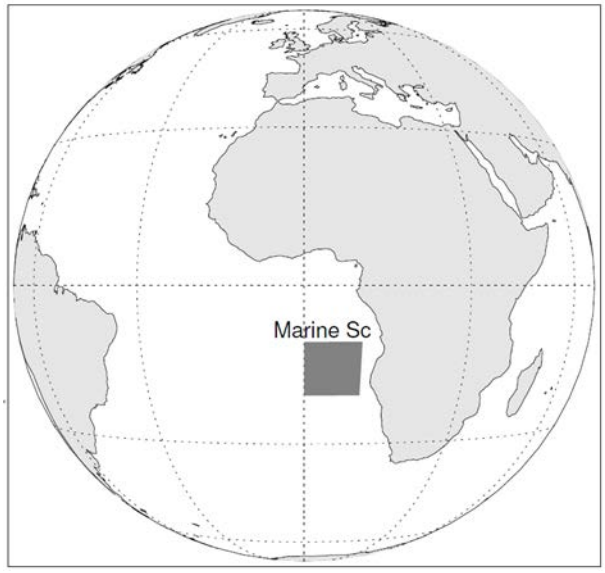


**Figure 7-4:** The marine stratocumulus region off the Namibia coast (0-10°E, 10-20°S), selected for the validation of CLAAS-2 all-sky LWP monthly mean diurnal cycle against corresponding UWisc data.

Figure 7-5 shows a typical time series plot of the monthly mean all-sky LWP at 12:00 UTC from CLAAS-2 and UWisc, along with their bias and bc-RMS. The two data records exhibit similar seasonal characteristics and the bias fluctuates in the -20 to 20 g $m^{-2}$ zone, which defines the threshold accuracy for CLAAS-2 all-sky LWP. Bias maxima and minima occur due to higher CLAAS-2 values in winter and lower in autumn, while the best agreement, lying in the optimal accuracy zone, occurs during summer. The bc-RMS is usually lower than 10 g $m^{-2}$, which is the optimal threshold.

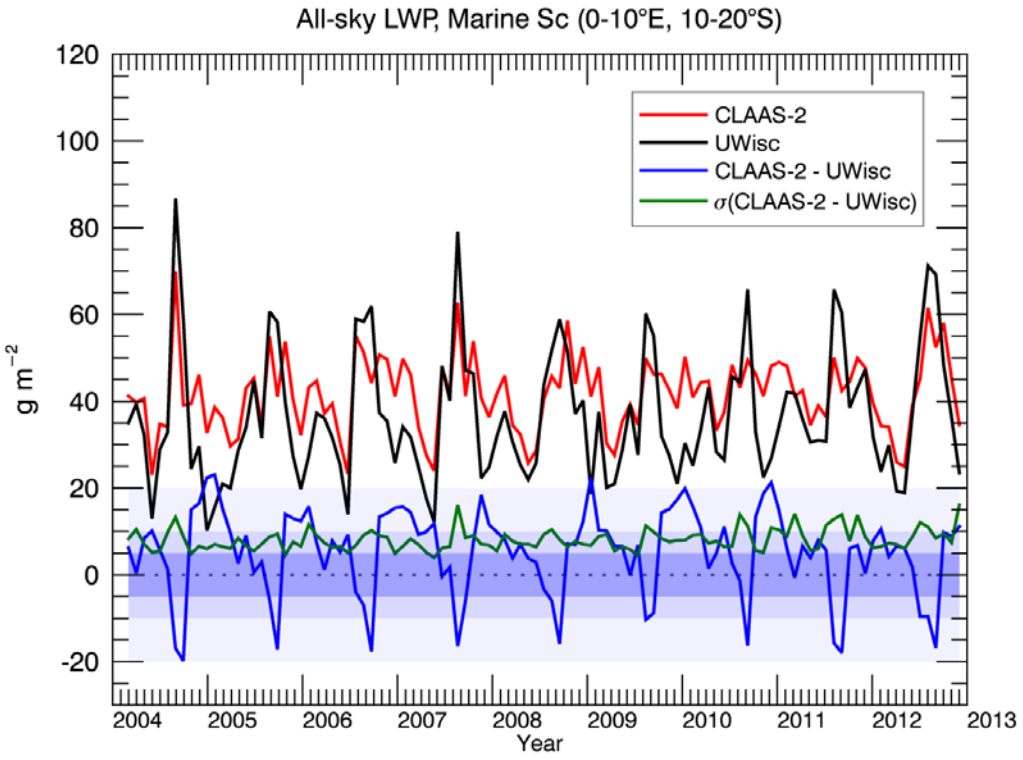


**Figure 7-5:** Time series of the spatially averaged all-sky LWP at the marine Sc region (0-10°S, 10-20°E) at 12:00 UTC from CLAAS-2 and UWisc data. The difference between these data sets (bias) and corresponding standard deviation (bc-RMS) are also shown. Shaded areas (darker to lighter) correspond to optimal, target and threshold accuracy for bias. The optimal bc-RMS accuracy is 10 g m-2. (Figure taken from Benas et al., 2016)

The diurnal monthly mean all-sky LWP from CLAAS-2 and UWisc is shown in Figure 7-6. In order to ensure the representativeness of the results on the marine Sc region, spatial averages were computed when at least 50% of the pixels had valid LWP values. Due to this threshold, night time hours as well as hours early in the morning and late in the afternoon are excluded from this analysis. In general the 10-hour part of the diurnal cycle in CLAAS-2 and UWisc, depicted in Figure 7-6, is very similar, showing the reduction in all-sky LWP throughout the day. The UWisc diurnal cycle is clearly smoother than CLAAS-2, since the former is the result of fits to data from satellites at various overpass times. Another apparent feature is the slightly increased CLAAS-2 LWP in the first two hours after sunrise and the last two hours before sunset. This is not observed in the UWisc data, and may be a retrieval artefact related to the illumination geometry (high solar zenith angles). Nevertheless, in most cases the bias fulfills the optimal and target requirements, while the bc-RMS is constantly close to the 10 g $m^{-2}$ optimal threshold.

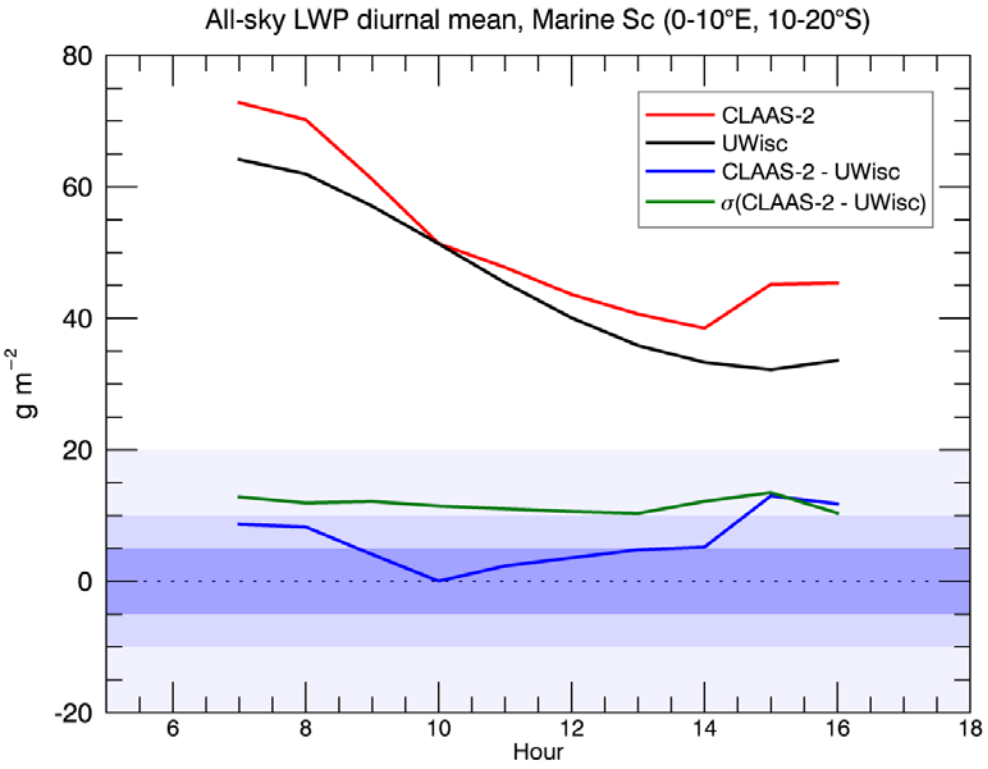


**Figure 7-6:** Monthly mean diurnal average of all-sky LWP from CLAAS-2 and UWisc, spatially averaged at the marine Sc region (0-10°S, 10-20°E), along with their bias and bc-RMS. Shaded areas (darker to lighter) correspond to optimal, target and threshold accuracy for bias. The optimal bc-RMS threshold is 10 g m-2. (Figure taken from Benas et al., 2016)

Table 7-3 summarizes the overall validation results for CLAAS-2 all-sky LWP in terms of the bias and bc-RMS with respect to the corresponding UWisc product. Results are shown separately for the 45° W-E, S-N area, and the full SEVIRI disk (90°). It is found that in both the bias and bc-RMS cases, the product fulfills the target requirements, with values lying close to the optimal threshold.

**Table 7-3** Overall requirement compliance of the CLAAS-2 all-sky LWP product with respect to the Mean Error and the bias-corrected RMS (bc-RMS), calculated over the marine stratocumulus region (10°-20° S, 0°-10°E) for validation with UWisc data. Units are g m-2.

| Mean Error (g $m^{-2}$) | Fulfilling Threshold requirements (20) | Fulfilling Target Requirements (10) | Fulfilling Optimal Requirements(5) |
|---|---|---|---|
| 6.17 | YES | YES | NO |
| bc-RMS | Fulfilling Threshold requirements (40) | Fulfilling Target Requirements (20) | Fulfilling Optimal Requirements (10) |
| 11.63 | YES | YES | NO |

## 7.3 Comparison with MODIS

The MODIS Level 3 Collection 6 monthly mean data set (data type names: MOD08_M3 and MYD08_M3 for Terra and Aqua, respectively), available at 1° × 1° spatial resolution, has been used as the main reference for the cloud properties evaluation. Three aspects are important to mention here:

1) As the MODIS products, the CLAAS-2 data records contain cloudy sky monthly averages of liquid/ice water paths and corresponding optical thickness. These averages have been compiled in the same way (effectively directly from the Level 2 data), which is essential for the products to be compared. The MODIS standard parameters have been used, where the retrieval algorithm applies clear-sky restoral, which means that optical properties are not available for pixels containing cloud edges or broken clouds. Although the MODIS Collection 6 product contains data sets of cloud optical properties for these partially cloudy cases, their quality is not ensured and they were not used here. As a result, the CLAAS-2 cloudy-sky LWP, IWP and COT will be higher. Therefore, to enable a fair comparison, all-sky properties were evaluated for these properties, calculated by multiplying average cloud-sky properties with corresponding cloud fraction. Cloud thermodynamic phase was evaluated in terms of the fraction of liquid clouds relative to the total cloud fraction.

2) CLAAS-2 optical property monthly means are an average of all daytime SEVIRI time slots (SZA < 75 degrees). On the other hand, there are two MODIS instruments with equatorial overpass times at 10:30 and 13:30. Monthly means from these two instruments were averaged in order to best mimic the CLAAS-2 averaging. In the cases of CFC and CPH, however, only Aqua MODIS data were used. This was due to the Terra MODIS band 29 (8.6 μm) radiometric calibration drift issue; this band is used in the cloud fraction and phase retrieval algorithms (Baum et al. 2012), and causes significant biases in the monthly time series, extending back to earlier than 2010.

3) Cloud optical properties retrievals rely on measurements of reflected sunlight. This implies that retrievals have to be discontinued if the solar zenith angle reaches a certain threshold. This threshold is set to 75 degrees for CLAAS-2 daytime level-3 products, but has a different value for MODIS. Similarly, CLAAS-2 Level 3 data records are computed only for SEVIRI viewing zenith angles up to 75 degrees. Therefore, to enable a meaningful comparison of time series, spatial aggregation was not performed over the full SEVIRI disk, but over a subset of the disc, in which valid SEVIRI retrievals are available for all seasons and during the whole record. This restriction determined the choice of an aggregation area bounded by 45 degrees West-East and South-North. However, in the requirements compliance tables also full disc values are presented.

### 7.3.1 Cloud Fractional Cover (CFC)

CFC is available in CLAAS-2 separately for day and night, as well as for the full 24-hour period. These three monthly mean parameters were compared with corresponding MODIS Level 3 data sets, created by counting the lowest two clear sky confidence levels in Level 2 Cloud Mask (cloudy and probably cloudy), and averaging the daily means. Since these MODIS data are based on the cloud mask product, they are affected by the Terra calibration drift issue, allowing an intercomparison only with Aqua MODIS data, as mentioned before.

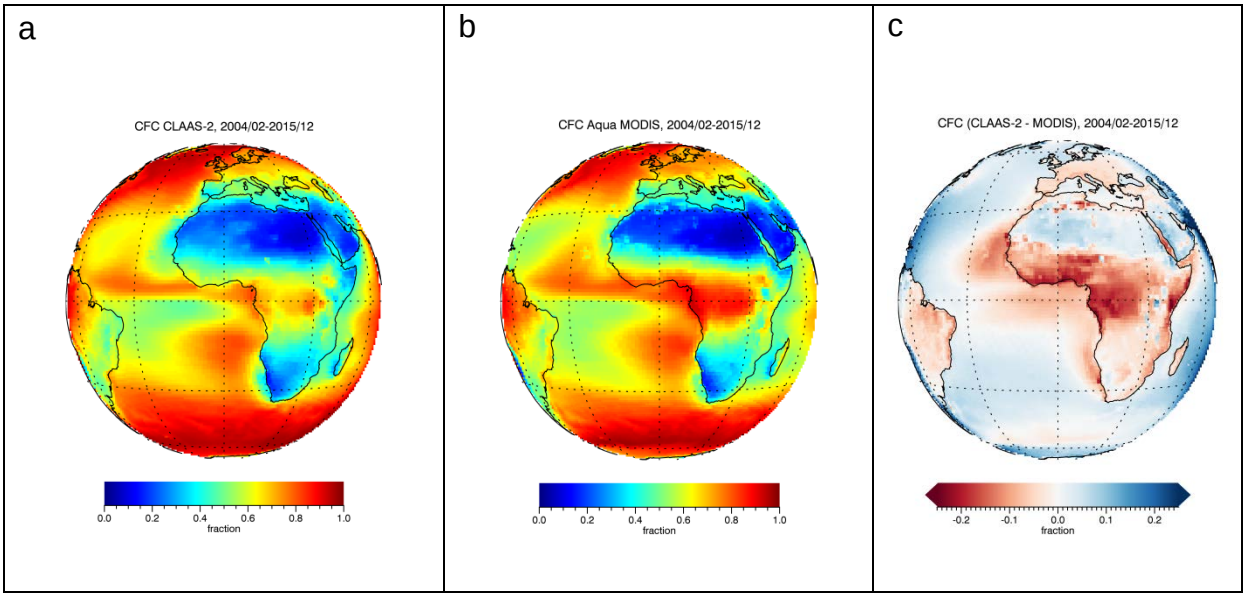


Figure 7-7 shows the time series averages of CLAAS-2 and Aqua MODIS 24-hour CFC, estimated from their common period (02/2004-12/2015), along with their differences. While spatial patterns between the two data sets are very similar, differences tend to be located in specific regions, with the highest ones occurring over central and western Africa, where CLAAS-2 CFC values are lower than the Aqua MODIS CFC. This feature should be attributed to the small viewing angles in the area around the Meteosat nadir, which lead to reduced cloud cover retrieval, compared to the MODIS typical range of viewing angles. Other possible reasons of differences include the CFC diurnal variability, which is pronounced in many regions and cannot be captured by MODIS, as well as differences in cloud mask definitions and spatial averaging for the creation of Level 3 data sets. It should also be noted that results from daytime and nighttime CFC are not presented here due to their similarity with the 24-hour CFC characteristics shown in Figure 7-7

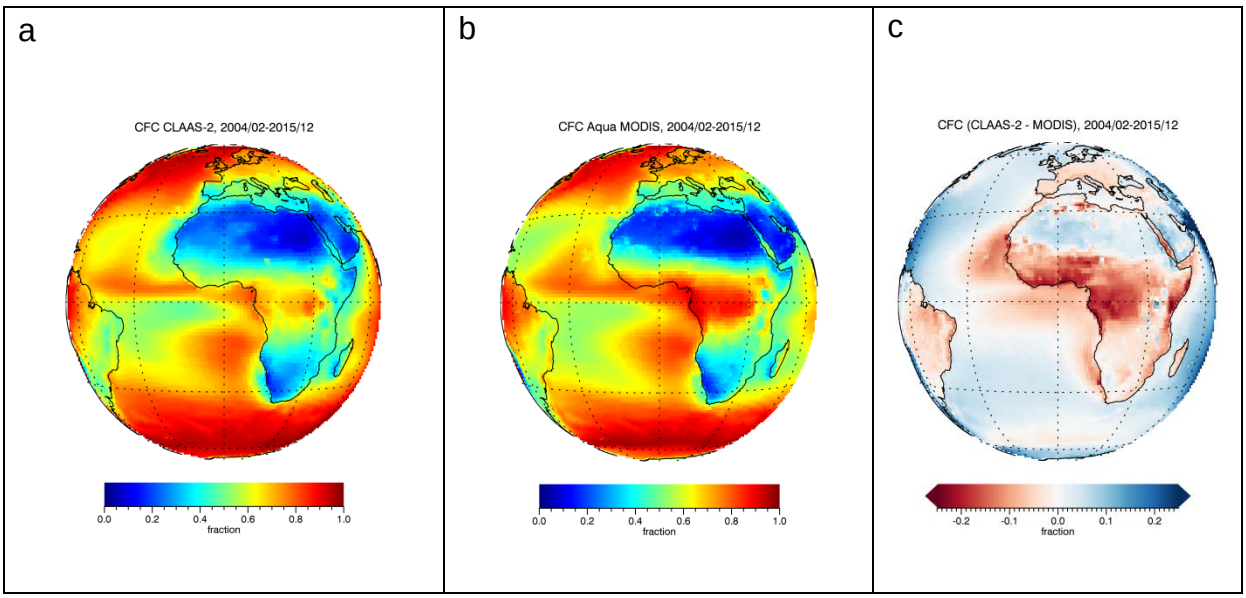


**Figure 7-7:** Spatial distribution of the cloud fractional cover averaged from February 2004 until December 2015 based on CLAAS-2 (a) and Aqua MODIS (b) data. The absolute difference between these data sets is shown in (c). (Panels a and b taken from Benas et al., 2016)

The time series of CLAAS-2 and Aqua MODIS CFC (averaged over the 45° S-N, W-E area) is displayed in Figure 7-8, along with their bias and bc-RMS. The agreement between the two sensors is very good in terms of both seasonal cycle and amplitude depictions, also considering the differences in temporal sampling. The bias is close to zero (-0.011 on average), and always inside the optimal accuracy zone (defined by the [-0.05, 0.05] interval), while the bc-RMS also fulfils the optimal requirement of values lower than 0.1. The time series also show a very stable behavior in CFC, without any significant trend within the 12-year period examined.

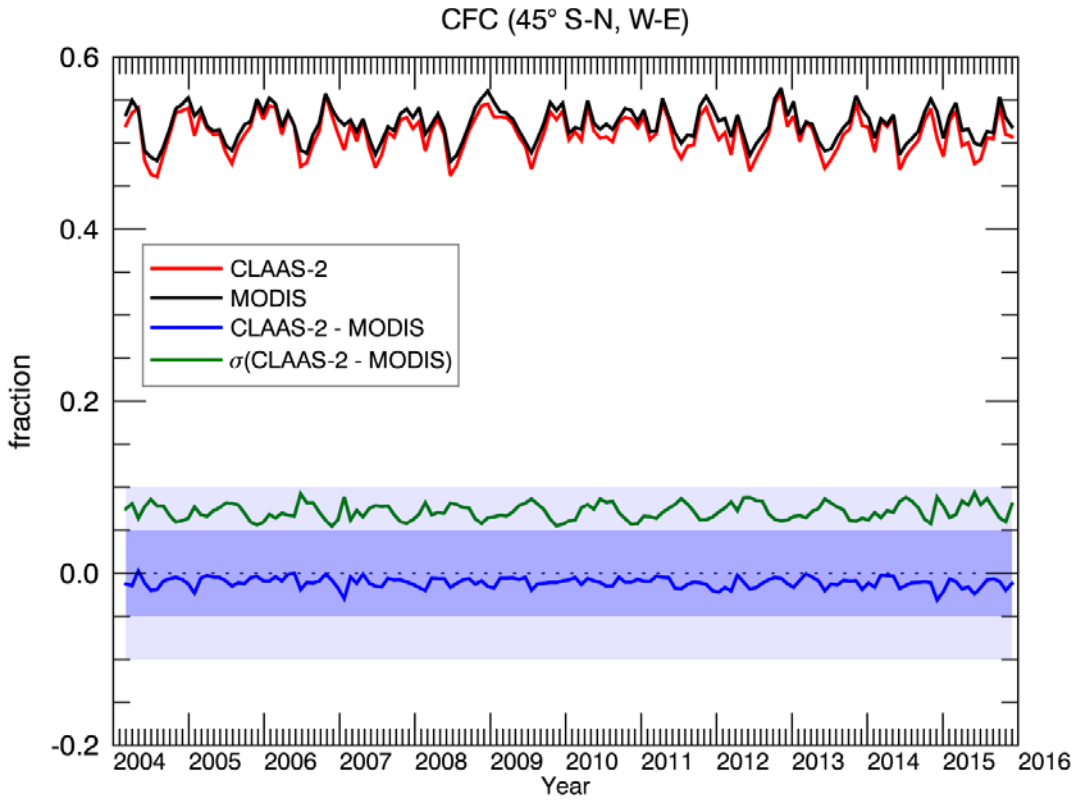


**Figure 7-8:** Time series of the 45° W-E and S-N area-averaged cloud fractional cover from CLAAS-2 and Aqua MODIS, their biases and the corresponding standard deviations. Optimal and target bias zones are indicated by dark and pale shading, respectively. The optimal standard deviation of the bias is 0.1. . (Figure taken from Benas et al., 2016)

Table 7-4 summarizes the results of the analysis of all three data sets (CFC. CFC Day and CFC Night) in terms of their average bias and bc-RMS, when compared with corresponding Aqua MODIS data. The analysis was performed for both the 45° S-N, W-E area and the full SEVIRI disk (90°). It is found that, as in the CFC case, CFC day and night also fulfill the optimal accuracy requirements for bias and bc-RMS in both cases examined.

**Table 7-4** Overall requirement compliance of the CLAAS-2 CFC, CFC day and CFC night products, with respect to the Mean Error and the bias-corrected RMS (bc-RMS), calculated separately for the 45° S-N, W-E area and the full disk (90°). Units are fraction.

| | **Mean Error 45°/90°** | **Fulfilling Threshold requirements (0.20)** | **Fulfilling Target Requirements (0.10)** | **Fulfilling Optimal Requirements (0.05)** |
|---|---|---|---|---|
| CFC | -0.011/0.023 | YES/YES | YES/YES | YES/YES |
| CFC Day | 0.014/0.043 | YES/YES | YES/YES | YES/YES |
| CFC Night | -0.050/-0.006 | YES/YES | YES/YES | YES/YES |
| | bc-RMS | Fulfilling Threshold requirements (0.40) | Fulfilling Target Requirements (0.20) | Fulfilling Optimal Requirements (0.10) |
| CFC | 0.072/0.083 | YES/YES | YES/YES | YES/YES |
| CFC Day | 0.085/0.095 | YES/YES | YES/YES | YES/YES |
| CFC Night | 0.084/0.089 | YES/YES | YES/YES | YES/YES |

### 7.3.2 Cloud Top Properties

Cloud top properties, namely cloud top pressure and height, were evaluated against corresponding MODIS data. Cloud top temperature is not included in this analysis, since it represents the same information in different units. In the cloud top properties case, average values from Aqua and Terra MODIS data were used, since the Terra degradation issue does not affect the cloud top retrieval algorithm. Figure 7-9 shows the spatial distribution of cloud top height and pressure from CLAAS-2 and MODIS, along with their differences. As expected, cloud top height and pressure are anti-correlated. While the spatial features of both data sets are quite similar with higher clouds appearing in central Africa and the ITCZ, and lower in the marine Sc region of south Atlantic, CLAAS-2 generally tends to estimate higher cloud top heights Figure 7-9c), leading to lower cloud top pressures (Figure 7-9f). This tendency reverses over central Africa and the Sahara, where MODIS estimates higher clouds.

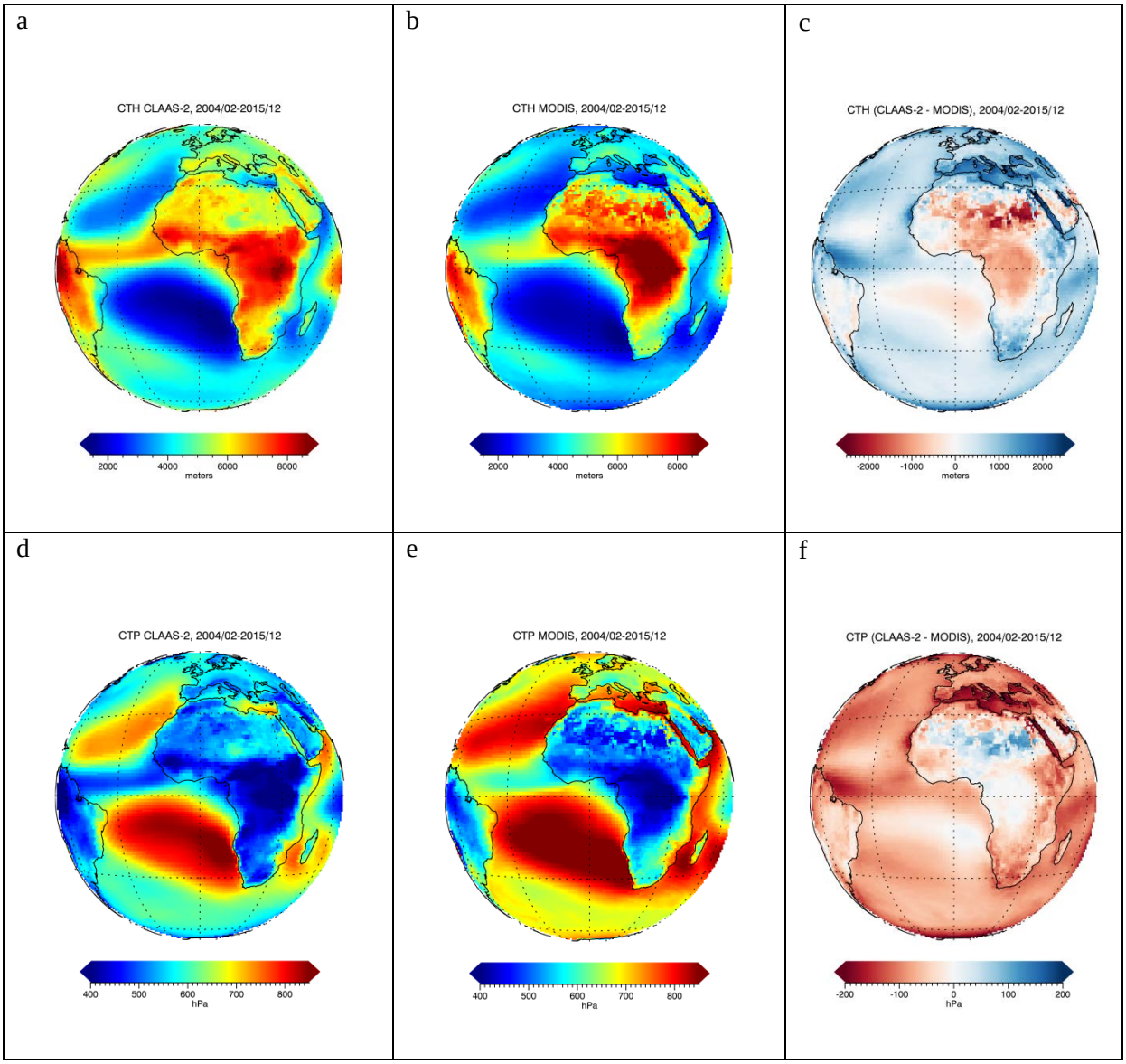


**Figure 7-9:** Spatial distribution of the cloud top height averaged from February 2004 until December 2015 based on CLAAS-2 (a), MODIS (b) data, and their absolute difference (c). Corresponding results for cloud top pressure are shown in (d), (e) and (f). (Panels a, b and c taken from Benas et al., 2016)

These differences between CLAAS-2 and MODIS are also depicted in the spatially averaged time series results (Figure 7-10). It is worth noting that the agreement between the two data sets improves after 2013, due to a slight decrease (increase) in CLAAS-2 CTH (CTP). The optimal bias requirement is achieved most of the times in CTH, while CTP fulfills the threshold requirement, also reaching target bias values towards the last years of the time series. The bc-RMS fluctuates around its optimal threshold in CTH (1000 m) and between optimal and target thresholds in the case of CTP (50-70 hPa).

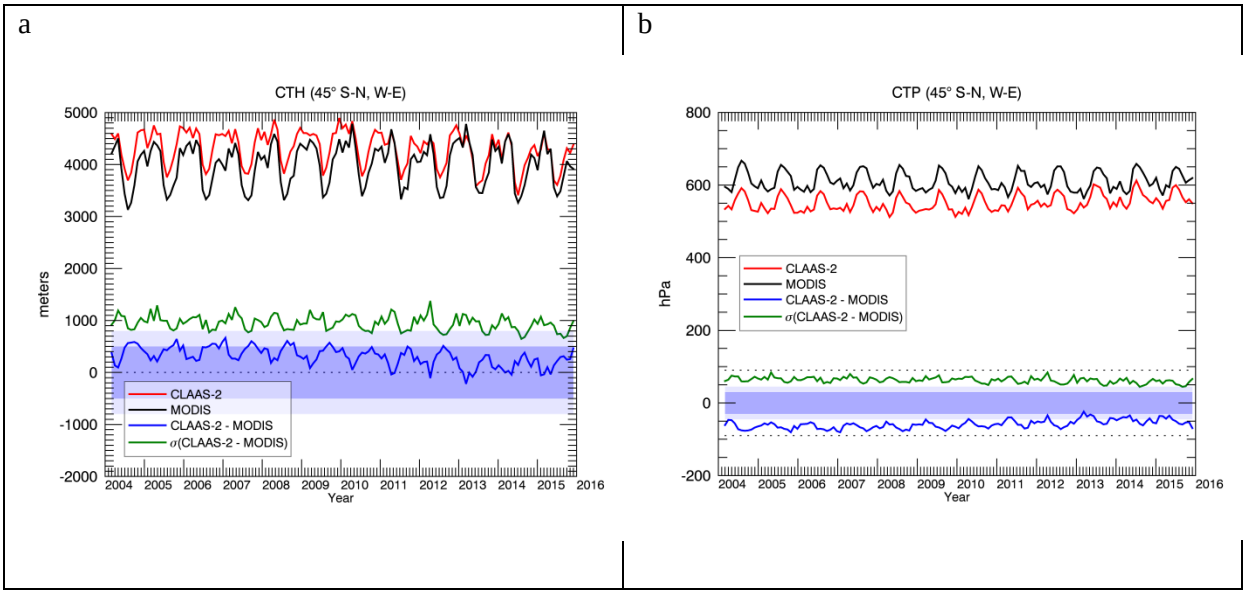


**Figure 7-10:** Time series of the 45° W-E and S-N area-averaged CTH (a) and CTP (b) from CLAAS-2 and MODIS, their biases and the corresponding standard deviations. Optimal and target bias zones are indicated by dark and pale shading, respectively. The dotted lines in (b) define the threshold bias zone. The optimal standard deviation of the bias is 1000 m for CTH and 50 hPa for CTP. (Left panel taken from Benas et al., 2016)

Table 7-5 andTable 7-6 summarize the evaluation results of CLAAS-2 CTH and CTP level 3 products in terms of the bias and bc-RMS threshold requirements, when compared with corresponding MODIS data. The analysis is performed for both the 45° S-N, W-E area and the full SEVIRI disk. Results show that CTH fulfills the optimal requirements in all cases. CTP, on the other hand, fulfills the threshold and target requirements in both areas examined, for bias and bc-RMS, respectively.

**Table 7-5** Overall requirement compliance of the CLAAS-2 CTH product with respect to the Mean Error and the bias-corrected RMS (bc-RMS), calculated separately for the 45° S-N, W-E area and the full disk (90°). Units are meters.

| Cloud Top Height | | | |
|---|---|---|---|
| Mean Error (m)<br>45°/90° | Fulfilling Threshold requirements (1200) | Fulfilling Target Requirements (800) | Fulfilling Optimal Requirements (500) |
| 307/452 | YES/YES | YES/YES | YES/YES |
| bc-RMS (m) | Fulfilling Threshold requirements (3000) | Fulfilling Target Requirements (1500) | Fulfilling Optimal Requirements (1000) |
| 949/851 | YES/YES | YES/YES | YES/YES |

**Table 7-6** Overall requirement compliance of the CLAAS-2 CTP product with respect to the Mean Error and the bias-corrected RMS (bc-RMS), calculated separately for the 45° S-N, W-E area and the full disk (90°). Units are hPa.

| Cloud Top Pressure | | | |
|---|---|---|---|
| Mean Error (hPa) 45°/90° | Fulfilling Threshold requirements (90) | Fulfilling Target Requirements (45) | Fulfilling Optimal Requirements (30) |
| -58.6/-64.1 | YES/YES | NO/NO | NO/NO |
| bc-RMS | Fulfilling Threshold requirements (120) | Fulfilling Target Requirements (70) | Fulfilling Optimal Requirements (50) |
| 62.7/56.8 | YES/YES | YES/YES | NO/NO |

### 7.3.3 Cloud Thermodynamic Phase (CPH)

There are two cloud phase algorithms included in the MODIS cloud product, one based on infrared channels and run in parallel with the cloud top properties retrievals, while the second is part of the cloud optical properties retrieval algorithm and uses information from both IR and SWIR bands. For consistency purposes, the CLAAS-2 CPH was intercompared with the IR-based MODIS cloud phase, which is also available for both day and night.

Figure 7-11 shows the spatial distributions of the multiyear averages of cloud phase separately for CLAAS-2 (first row) and Aqua MODIS (second row), both diurnally (first column) and for day-only measurements (CPH_Day, second column). These averages were computed from the entire CLAAS-2 time series, spanning the period 02/2004-12/2015. In both data sets spatial patterns are very similar, with the highest cloud phase values occurring over the southern Atlantic ocean and the lowest appearing mainly in central Africa. At the same region, CLAAS-2 exhibits lower cloud phase values compared to MODIS (Figure 7-11e, f), contrary to the large liquid cloud fraction over tropical land, reported in CLAAS-1. Opposite difference signs, compared to CLAAS-1, are also found over parts of desert areas and the southern polar region.

The time series of the 45° W-E, S-N averaged monthly cloud phase from CLAAS-2 and Aqua MODIS, along with their biases and standard deviations, are shown in Figure 1.9. The two data sets are in very good agreement, while there is a small positive bias in CLAAS-2, appearing after 2011. Nevertheless, biases are always below 0.05, which is the optimal requirement, while the bc-RMS is also very close to its optimal requirement of 0.1.

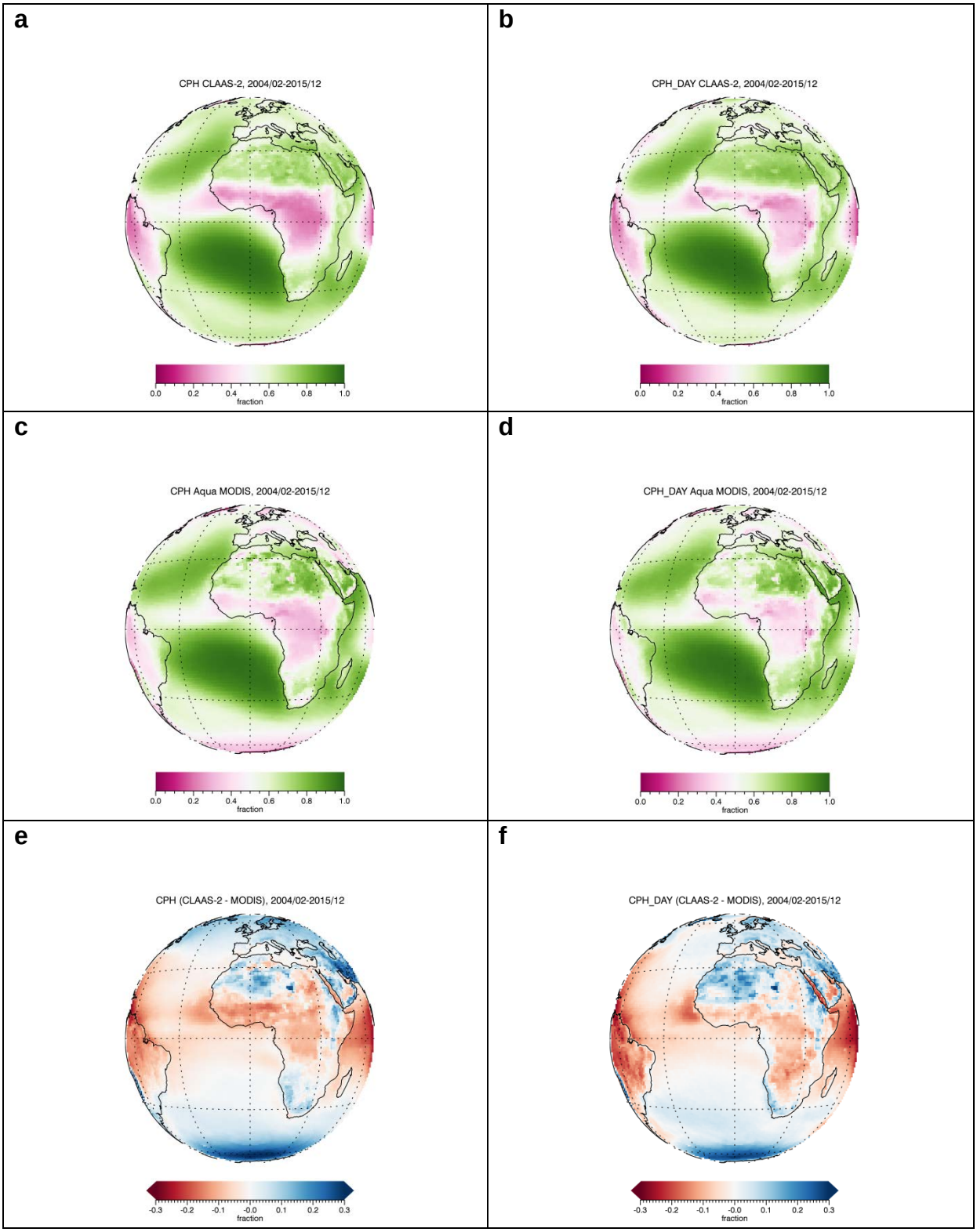


**Figure 7-11:** Spatial distribution of cloud phase (fraction of liquid clouds relative to total cloud fraction), averaged from February 2004 until December 2015: (a, b) CLAAS-2 diurnal and day-only, (c, d) Aqua MODIS day-night and day-only, (e, f) corresponding differences between CLAAS-2 and Aqua MODIS. (Panels a and c taken from Benas et al., 2016)

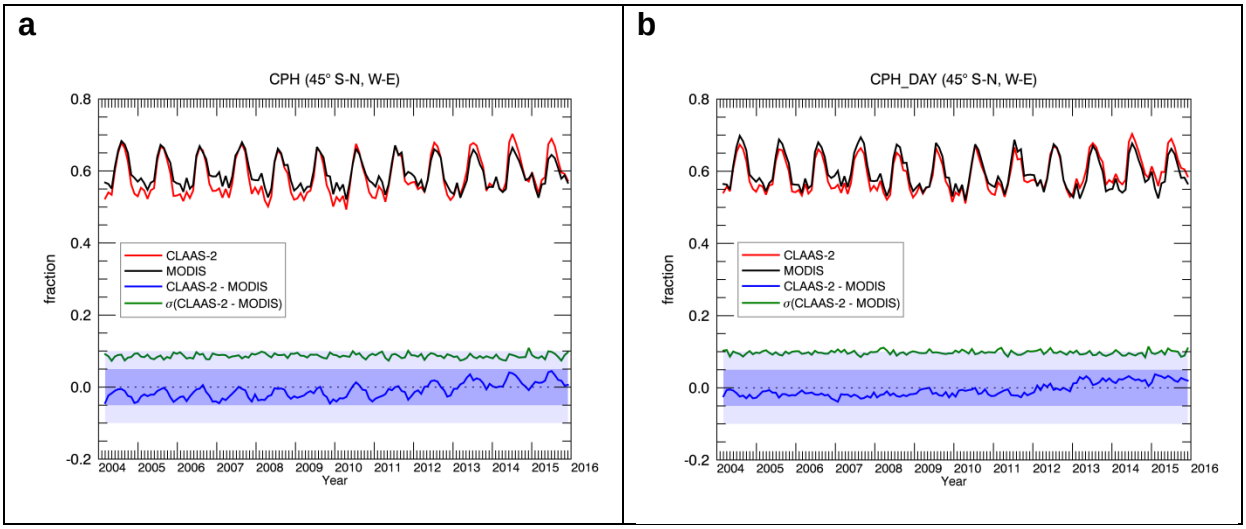


**Figure 7-12:** Time series of the 45° W-E and S-N area-averaged diurnal (a) and day-only (b) cloud phase from CLAAS-2 and Aqua MODIS, their biases and the corresponding standard deviations. Optimal and target bias zones are indicated by dark and pale shading, respectively. The optimal standard deviation of the bias is 0.1.

#### 7.3.3.1 Summary of overall results

Table 7-7 summarizes the overall evaluation results for CLAAS-2 CPH in terms of the bias and bc-RMS with respect to the corresponding Aqua MODIS product. Except for the selected 45° W-E and S-N area, averages from the full SEVIRI disk (90°) are also included. The compliance of these results against the predefined accuracy requirements is then checked. It is found that in both spatial cases, both CPH and CPH_Day fulfil the optimal requirement for bias and the target requirement for bc-RMS, although values of the latter lie very close to the optimal threshold (0.105 and 0.113, compared to 0.10).

**Table 7-7** Overall requirement compliance of the CLAAS-2 cloud phase products with respect to the Mean Error and the bias-corrected RMS (bc-RMS), calculated separately for the 45° S-N, W-E area and the full disk (90°). Units are in fraction of liquid clouds relative to the total cloud fraction.

| | Mean Error (%) 45°/90° | Fulfilling Threshold requirements (0.20) | Fulfilling Target Requirements (0.10) | Fulfilling Optimal Requirements (0.05) |
|---|---|---|---|---|
| Cloud Phase | -0.010/0.006 | YES/YES | YES/YES | YES/YES |
| Cloud Phase Day | -0.006/-0.012 | YES/YES | YES/YES | YES/YES |
| | bc-RMS | Fulfilling Threshold requirements (0.40) | Fulfilling Target Requirements (0.20) | Fulfilling Optimal Requirements (0.10) |
| Cloud Phase | 0.087/0.105 | YES/YES | YES/YES | YES/NO |
| Cloud Phase Day | 0.098/0.113 | YES/YES | YES/YES | YES/NO |

### 7.3.4 Liquid Water Path (LWP)

Figure 7-13 shows the spatial distribution of the all-sky LWP from CLAAS-2 (a) and MODIS (b, Terra and Aqua average), averaged over their common period (02/2004-12/2015). Patterns are very similar, with highest LWP values primarily over Antarctica and the southern and northern Atlantic, and secondarily over Europe. The stratocumulus region west of southern Africa is also highlighted in both images. In terms of differences, presented in both absolute values (Figure 7-13c) and percentages (Figure 7-13d), there is an overall tendency for CLAAS-2 to acquire higher values over sea and lower over land, compared to MODIS.

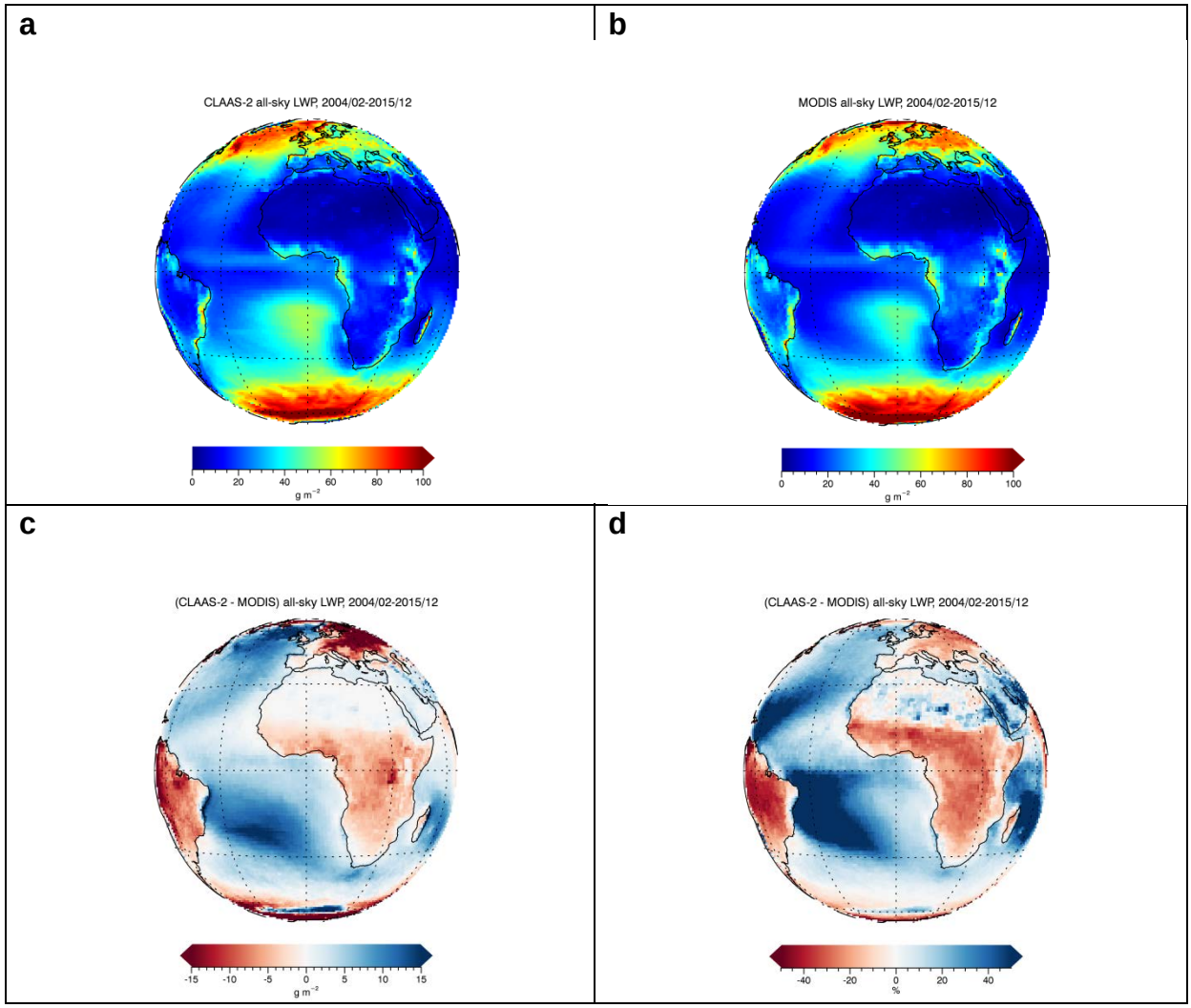


**Figure 7-13:** Spatial distribution of all-sky LWP, averaged from February 2004 until December 2015, from CLAAS-2 (a) and MODIS (b). Differences between CLAAS-2 and MODIS are also shown, in absolute values (c) and percent (d). (Panels a and b taken from Benas et al., 2016)

This CLAAS-2 tendency for higher all-sky LWP values over sea is also depicted in the time series of the 45° W-E, S-N area-weighted averages (Figure 7-14), where the difference between CLAAS-2 and MODIS is always positive. It is, however, also below the optimal accuracy requirement, set to 5 g $m^{-2}$, while the standard deviation of this bias also fulfils the

optimal requirement of 10 g $m^{-2}$. No tendency of any significant decadal change is apparent in either data set.

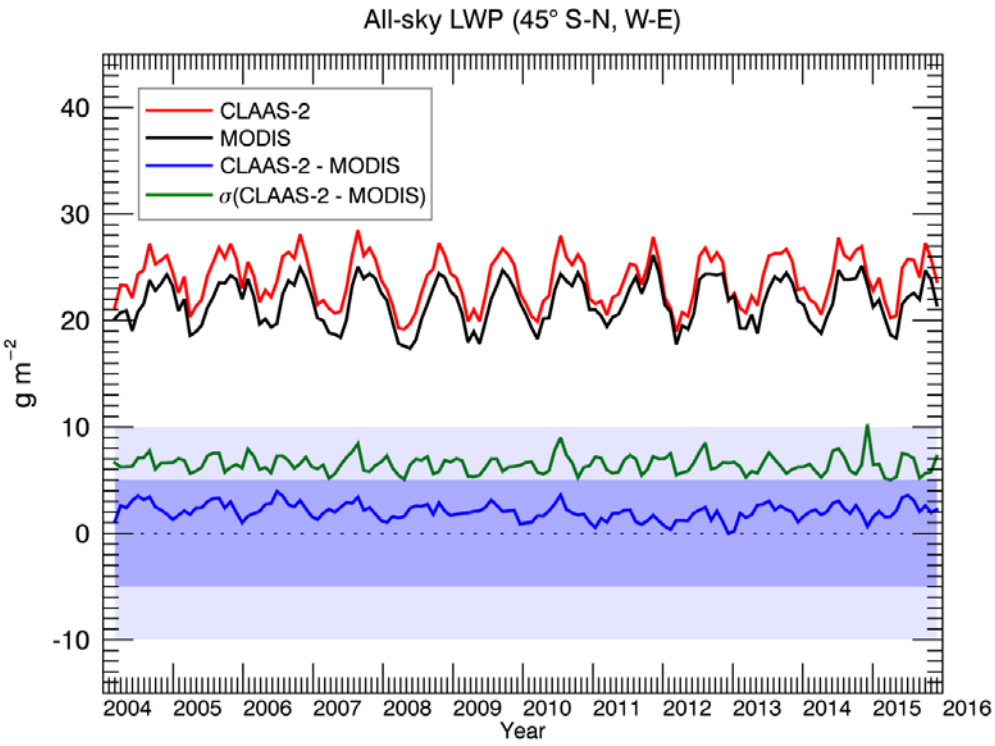


**Figure 7-14:** Time series of the 45° W-E and S-N area-averaged all-sky LWP from CLAAS-2 and MODIS, their bias and standard deviation of the bias. Optimal and target bias zones are indicated by dark and pale shading, respectively. The optimal standard deviation of the bias is 10 g m-2. (Figure taken from Benas et al., 2016)

#### 7.3.4.1 Evaluation of liquid Cloud Optical Thickness (COT) and Effective Radius (REFF)

To further investigate results of the all-sky LWP evaluation, the same analysis was repeated for the all-sky liquid COT and the liquid REFF, which are used for the computation of corresponding LWP values. Figure 7-15 shows the COT and REFF averages from CLAAS-2 and MODIS, along with corresponding differences. It is obvious that the LWP is determined primarily by COT, since the latter has very similar spatial distribution with the former in both data sets. In the case of COT, CLAAS-2 acquires higher values than MODIS over oceans and bright surfaces (e.g. the Sahara and Arabian deserts and the Alps). In the REFF case, while spatial patterns in CLAAS-2 and MODIS are similar, CLAAS-2 values are systematically lower, with the highest differences occurring over the Sahara and the Indian ocean. These features, however, do not appear to affect corresponding LWP results.

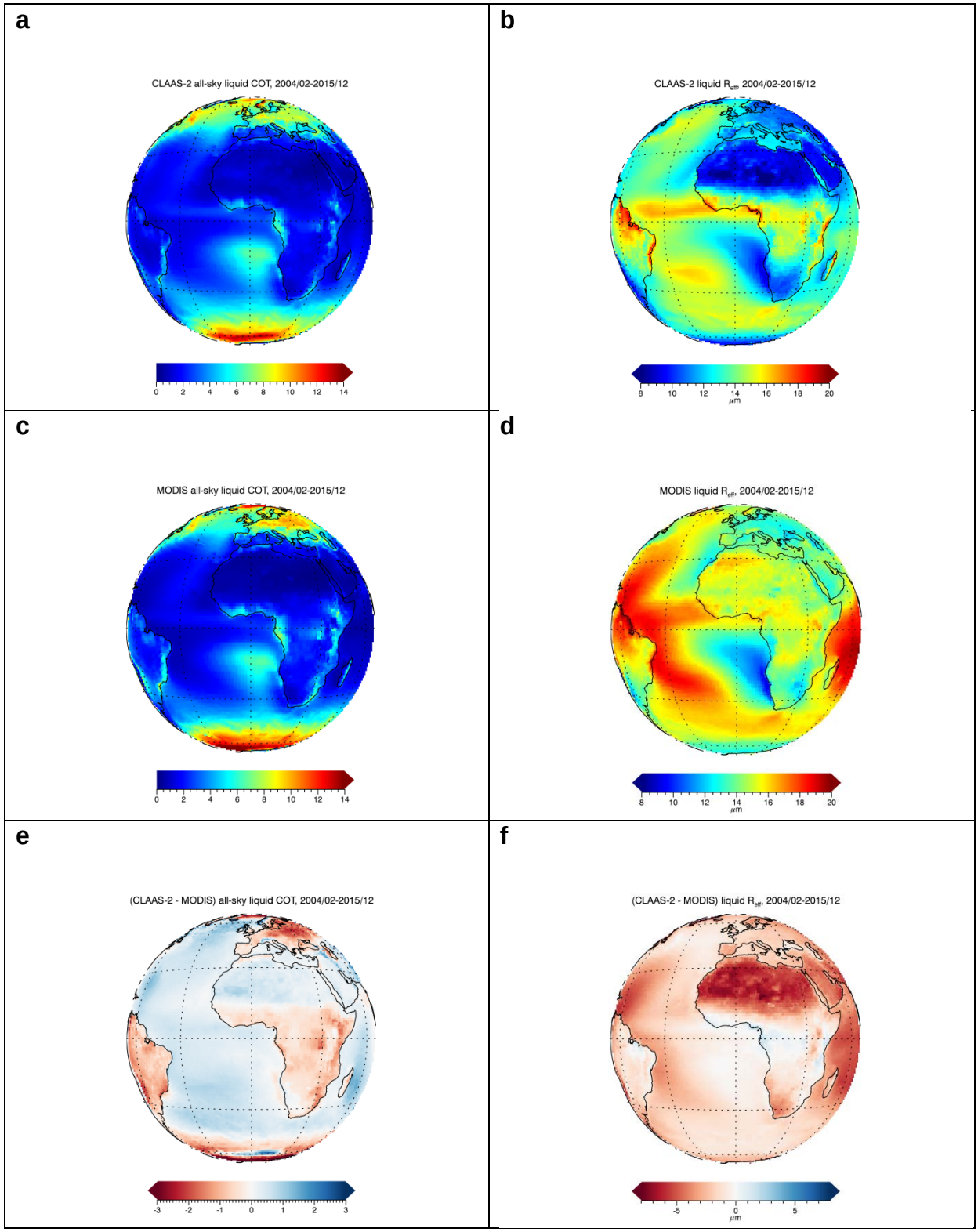


**Figure 7-15:** Spatial distribution of the all-sky liquid COT and liquid REFF, averaged from February 2004 until December 2015, from CLAAS-2 (a, b) and MODIS (c, d). Differences between CLAAS-2 and MODIS, for COT and REFF are also shown in absolute values (e and f, respectively).

#### 7.3.4.2 Summary of overall results

Table 7-8 summarizes the overall evaluation results for CLAAS-2 all-sky LWP in terms of the bias and bc-RMS with respect to the corresponding Aqua and Terra MODIS averaged product. Results are shown separately for the 45° W-E, S-N area, and the full SEVIRI disk (90°). It is found that in almost all cases, the bias and bc-RMS are within the optimal accuracy requirements. The only exception is the bc-RMS computed from the full disk, which fulfils the target requirement, being almost equal to the optimal threshold (10.10 g $m^{-2}$).

**Table 7-8** Overall requirement compliance of the CLAAS-2 all-sky LWP product with respect to the Mean Error and the bias-corrected RMS (bc-RMS), calculated separately for the 45° S-N, W-E area and the full disk (90°). Units are g m-2.

| All-sky Liquid Water Path | | | |
|---|---|---|---|
| Mean Error (g $m^{-2}$) 45°/90° | Fulfilling Threshold requirements (20) | Fulfilling Target Requirements (10) | Fulfilling Optimal Requirements (5) |
| 2.05/0.07 | YES/YES | YES/YES | YES/YES |
| bc-RMS | Fulfilling Threshold requirements (40) | Fulfilling Target Requirements (20) | Fulfilling Optimal Requirements (10) |
| 6.50/10.10 | YES/YES | YES/YES | YES/NO |

### 7.3.5 Ice Water Path (IWP)

Figure 7-16 shows the temporally averaged spatial distribution of all-sky IWP from CLAAS-2 and MODIS from their common period (02/2004-12/2015). Patterns are very similar, with high IWP values occurring over central Africa, South America and the ITCZ. As shown in Figure 7-16c and d, CLAAS-2 generally acquires lower IWP values than MODIS, leading to mostly negative biases. A significant exception is the area close to Antarctica, where CLAAS-2 IWP is very high, probably due to retrieval artefacts over sea ice.

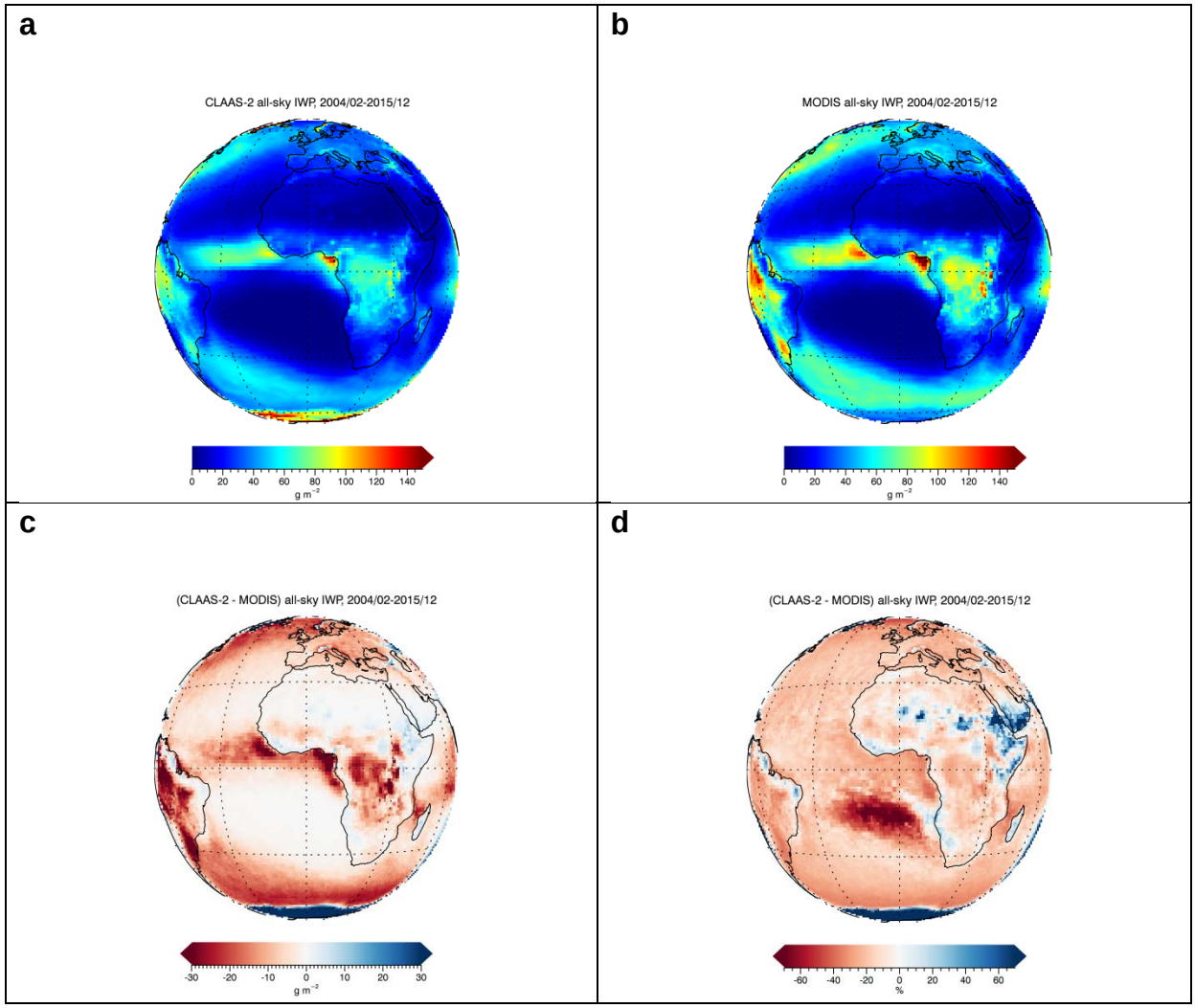


**Figure 7-16:** Spatial distribution of all-sky IWP, averaged from February 2004 until December 2015, from CLAAS-2 (a) and MODIS (b). Differences between CLAAS-2 and MODIS are also shown, in absolute values (c) and percent (d). (Panels a and b taken from Benas et al., 2016)

The lower CLAAS-2 IWP values are also apparent in the spatially averaged time series results of Figure 1.14, which lead to a bias fluctuating around -5 g $m^{-2}$, always below the 10 g $m^{-2}$ optimal threshold, while its standard deviation is also systematically below the optimal 20 g $m^{-2}$ requirement. The two data sets exhibit the same seasonal variation, with higher IWP values in winter and lower in summer.

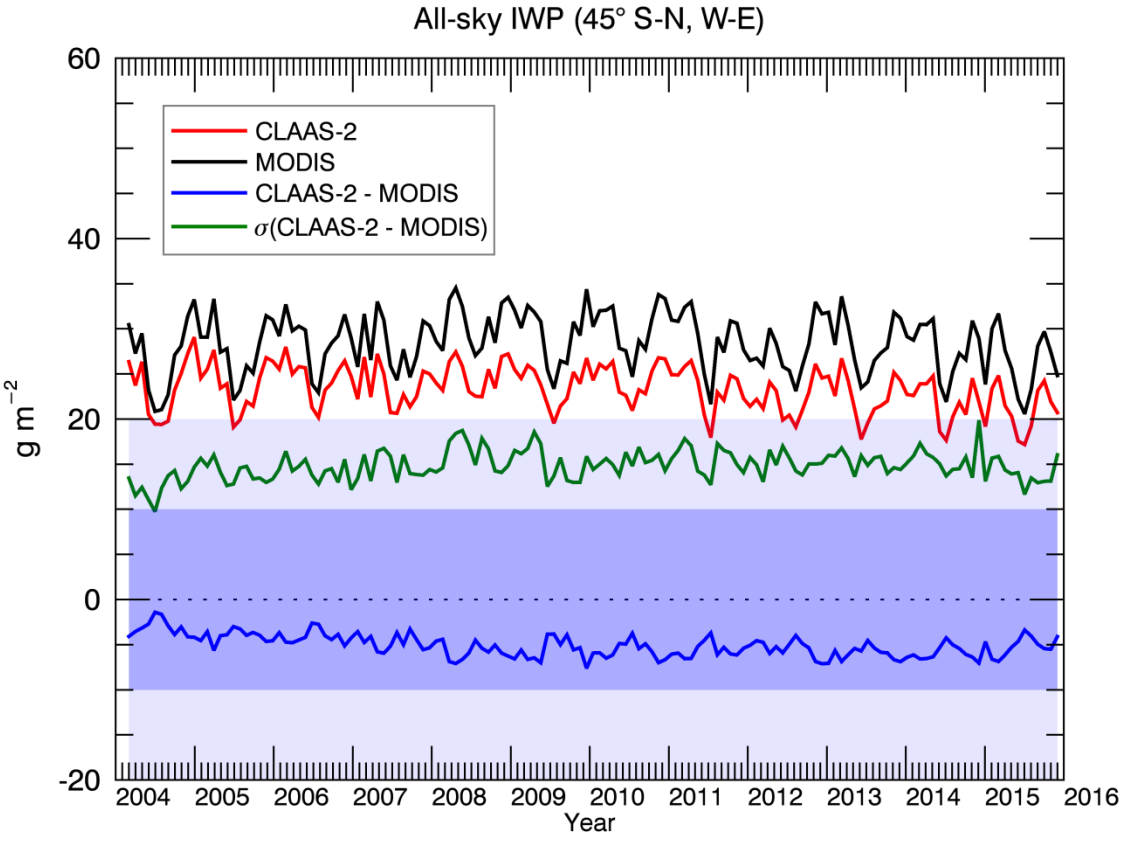


**Figure 7-17:** Time series of the 45° W-E and S-N area-averaged all-sky IWP from CLAAS-2 and MODIS, their bias and standard deviation of the bias. Optimal and target bias zones are indicated by dark and pale shading, respectively. The optimal standard deviation of the bias is 20 g m-2. (Figure taken from Benas et al., 2016)

#### 7.3.5.1 Evaluation of ice Cloud Optical Thickness and Effective Radius

As in the LWP case, COT and REFF of ice clouds were analyzed to further investigate results on the IWP evaluation. Spatial distributions of these variables are shown in Figure 7-18. Similarly to the LWP, the ice COT spatial characteristics are almost identical to those of IWP, showing that the former plays the primary role in determining the latter. The CLAAS-2 ice REFF, on the other hand, is systematically lower than the corresponding MODIS values. The best agreement between the two data sets is achieved in the marine Sc region of south Atlantic and parts of eastern Africa and South America, where ice REFF acquires minimum values.

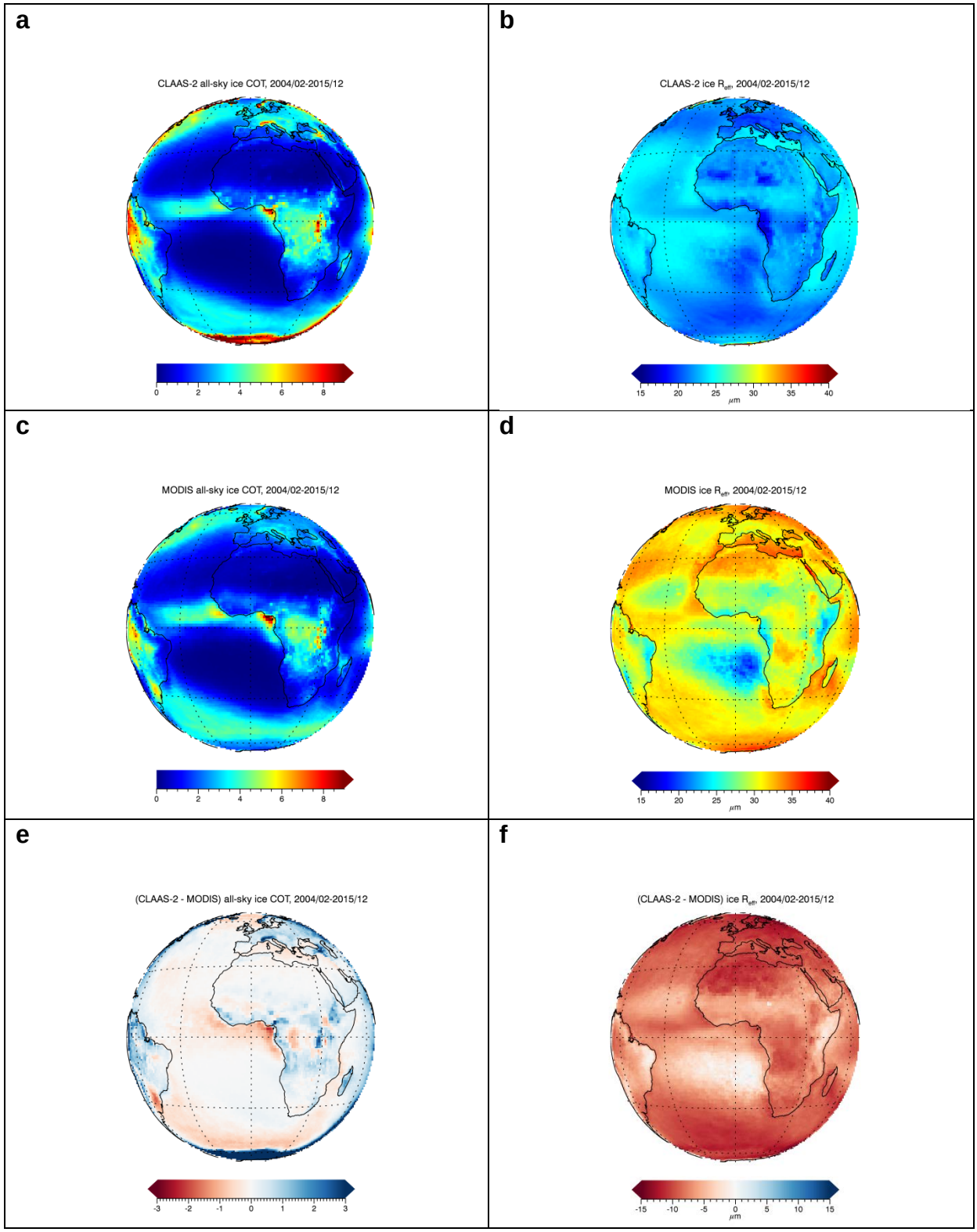


**Figure 7-18:** Spatial distribution of the all-sky ice COT and ice REFF, averaged from February 2004 until December 2015, from CLAAS-2 (a, b) and MODIS (c, d). Differences between CLAAS-2 and MODIS, for COT and REFF are also shown in absolute values (e and f, respectively).

#### 7.3.5.2 Summary of overall results

Table 7-9 summarizes the overall evaluation results for CLAAS-2 all-sky IWP in terms of the bias and bc-RMS with respect to the corresponding Terra and Aqua averaged MODIS product. Except for the selected 45° W-E and S-N area, averages from the full SEVIRI disk (90°) are also included. The compliance of these results against the predefined accuracy requirements is then checked. It is found that in both 45° and 90° cases, all-sky IWP fulfils the optimal requirement for bias. Regarding the bc-RMS, the optimal and target thresholds are fulfilled in the 45° and 90° cases, respectively.

**Table 7-9** Overall requirement compliance of the CLAAS-2 all-sky IWP product with respect to the Mean Error and the bias-corrected RMS (bc-RMS), calculated separately for the 45° S-N, W-E area and the full disk (90°). Consistency checks marked in blue. Units are g m-2.

| Ice Water Path | | | |
|---|---|---|---|
| Mean Error (g $m^{-2}$) 45°/90° | Fulfilling Threshold requirements (40) | Fulfilling Target Requirements (20) | Fulfilling Optimal Requirements (10) |
| -5.11/-3.21 | YES/YES | YES/YES | YES/YES |
| bc-RMS (g $m^{-2}$) | Fulfilling Threshold requirements (80) | Fulfilling Target Requirements (40) | Fulfilling Optimal Requirements (20) |
| 14.82/28.98 | YES/YES | YES/YES | YES/NO |

### 7.3.6 JCH: Joint Cloud property Histograms of CTP and COT

In this section, the Joint Cloud property Histogram (JCH) product will be compared with the joint histogram products provided by MODIS and the International Satellite Cloud Climatology Project (ISCCP; Rossow and Schiffer, 1999).

The CLAAS-2 joint histogram of COT and CTP was first evaluated against similar histograms from MODIS Level 3 Collection 6 data. Results are shown in Figure 7-19, separately for liquid and ice clouds. For both CLAAS-2 and MODIS data sets, the analysis focused on the 45° S-N, W-E area, and results were obtained from the entire CLAAS-2 temporal coverage (02/2004-12/2015). In the case of MODIS, data from Terra and Aqua platforms were aggregated, to best mimic the CLAAS-2 acquisition frequency. All histograms show the normalized number of occurrences for each COT/CTP bin.

It is apparent from Figure 7-19 that due to the different binning between CLAAS-2 and MODIS, only a qualitative comparison is possible. In fact, MODIS has also different CTP and COT bin boundaries for the liquid and ice clouds histograms, to better highlight their different characteristics. The majority of CLAAS-2 ice clouds is present in the 90-245 hPa pressure level, with relatively low COT, mostly in the range 0.6-3.6 (Figure 7-19a). Ice clouds from

MODIS appear slightly lower (150-300 hPa), in a similar COT range (Figure 7-19b). In the water clouds case, the CLAAS-2 majority also appear in lower pressure compared to MODIS (800-950 hPa, Figure 7-19c, compared to 800-1000 hPa, Figure 7-19d). Here, however, the majority of CLAAS-2 clouds also lies in higher COT values, compared to MODIS. These results are consistent with the CTP evaluation results, where systematically lower values were found from CLAAS-2 when intercompared with MODIS (Figure 7-10b).

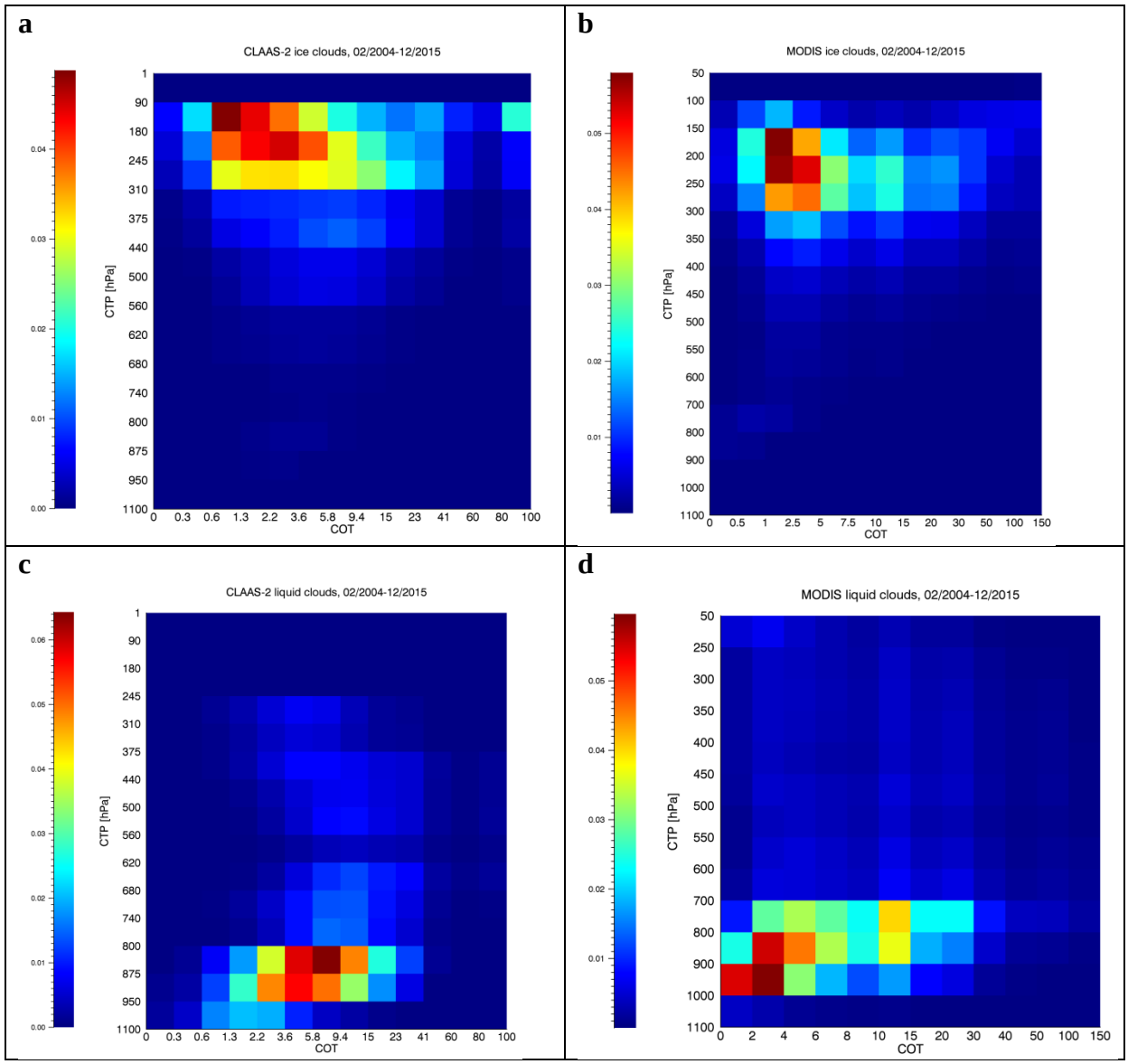


**Figure 7-19:** CTP/COT histograms of CLAAS-2 (left column) and MODIS (Terra and Aqua aggregated data, right column), separately for liquid (upper row) and ice (lower row) clouds, computed from the entire CLAAS-2 time range (02/2004-12/2015). Note the different COT- and CTP-axes.

In order to obtain a more meaningful evaluation between JCHs from CLAAS-2 and other data sets, the ISCCP CTP and COT bin boundaries were used. Although these boundaries are much coarser compared to CLAAS-2 and MODIS, they are also available in MODIS data sets, while the CLAAS-2 grid can also be directly converted to the former, through simple aggregation, allowing a more consistent intercomparison. This analysis, however, was limited to the 02/2004-12/2007 period, which is the only time range when data from all three data sets are available.

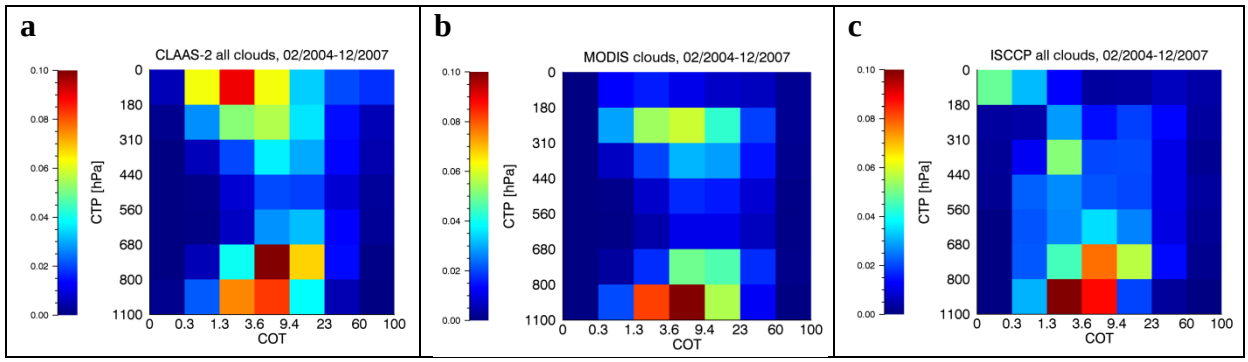


**Figure 7-20:** CTP/COT histograms of CLAAS-2 (a), MODIS (Terra and Aqua aggregated data, b) and ISCCP (c) for all clouds, computed from the period 02/2004-12/2007.

Figure 7-20 shows the CLAAS-2, MODIS and ISCCP histograms derived from this analysis at the same scale. As in the case of MODIS, ISCCP data were obtained by aggregating morning and afternoon data sets. The agreement between the three data sets is reasonable, especially regarding low clouds, with a great number of them occurring in the 800-1100 hPa pressure level, with COT ranging between 1.3 and 9.4. In the 680-800 hPa level, MODIS has less occurrences compared to CLAAS-2 and ISCCP, which again agree well. In high clouds, differences become larger, especially between ISCCP and the other two data sets. CLAAS-2 and MODIS cloud occurrences in the 180-310 hPa and 1.3-23 COT almost coincide, while this range is absent in ISCCP. On the other hand, higher clouds (CTP<180 hPa) appear in CLAAS-2 and ISCCP, the latter less frequently and with lower COT values.

The previous analysis highlighted the ability of CLAAS-2 JCHs to detect the multi-modal nature of COT/CTP-distributions and justified their necessity. Compared to corresponding MODIS products, CLAAS-2 showed qualitatively similar results for water and ice clouds. Results are also similar with ISCCP, especially for low clouds, when compared using the same COT and CTP bins resolution. Overall, the CLAAS-2 JCH adds valuable information to the data set from a more statistical point of view, e.g. in terms of the discrimination between different cloud regimes.

# 8 Conclusions

With this report we document the validation of CLAAS SEVIRI Edition 2 (CLAAS-2) cloud property data records. For the study we used reference datasets from independent observation sources, including different measurement strategies, as well as from similar satellite-based datasets from passive visible and infrared imagery. The used reference observation sources were: MODIS, CALIOP, DARDAR, AMSR-E, UWisc, and SYNOP datasets. This broad spectrum of reference measurements supports the required independence and variety in the evaluation process. As such a best possible effort to assess accuracy and precision of the derived cloud properties and products has been made.

The validation was based on products at different processing levels: Level 2 (instantaneous data on native satellite resolution and projection) and Level 3 (aggregated on equal-angle latitude/longitude grid with a spatial resolution of 0.05°. Including the instantaneous products (Level 2) in the evaluation brings further insight into the precision of the derived cloud products on high temporal resolution, while the accuracy (bias) is assumed to be similar to the Level 3 evaluations. In an additional section we evaluated the joint cloud property histogram product, by inter-comparison to MODIS and ISCCP, in order to illustrate the usefulness of this statistical approach.

Table 8-1 and Table 8-2 below give an overview of all results with respect to the target accuracies and precisions in [AD 1]. More information about the threshold and optimal product requirements, as also reported in [AD 1], is given in the individual product sections 6 and 7.

Validation results can be summarized as follows for each individual cloud product in the CLAAS-2 data record:

- **Fractional Cloud Cover (CFC)**
  - The CLAAS-2 level-3 CFC product fulfils the target requirements when compared with all references. Optimal requirements are also fulfilled for SYNOP and MODIS.
  - The level-2 cloud mask validation scores with CALIOP fulfil the threshold requirements.

- **Cloud Top level (CTO)**
  - The CLAAS-2 CTH product fulfils target requirements when compared to CALIOP (level-2) and optimal requirements for comparisons with MODIS (level-3). These results hold for both bias and bc-RMS.
  - The CLAAS-2 CTP product fulfils optimal accuracy requirements and threshold precision requirements against CALIOP (level-2). Against MODIS level-3 data the threshold accuracy requirement and target precision requirement are fulfilled.

- **Cloud Thermodynamic Phase (CPH)**
  - The CLAAS-2 CPH product mostly achieves target and optimal requirements for POD and FAR when compared to CALIOP. When evaluated against MODIS, optimal requirements for both bias and bc-RMS are fulfilled.

- **Liquid Water Path (LWP)**
  - The CLAAS-2 LWP product meets target requirements for bias and bc-RMS when validated against the UWisc data set. The bias and bc-RMS with respect to MODIS fulfil optimal requirements.
  - The level-2 target precision requirement is fulfilled against AMSR-E data.

- **Ice Water Path (IWP)**
  - The CLAAS-2 IWP product fulfils optimal bias and bc-RMS requirements when compared to MODIS. Both CLAAS-2 and MODIS IWP show similar trends.

- **Joint Cloud property Histograms (JCH)**
  - This product is excluded from specific requirement testing because it is composed of three already evaluated products (CPH, COT and CTP). Nevertheless, a demonstration of the product in inter-comparisons with MODIS and ISCCP products shows that it provides added value to the products by giving important clues on the statistical distribution of the involved parameters. It is believed that the access to this product representation will greatly enhance the usefulness of CLAAS-2 for some applications.

**Table 8-1:** Summary of CLAAS-2 validation results compared to target accuracy requirements for each cloud product. The accuracies are formulated in terms of biases. Results from consistency checks / inter-comparisons (using MODIS data, which, due to the sampling, cannot be seen as absolute reference) are marked in **blue**. * = ICOT>0 applied for CALIOP filtering; ** = ICOT>0.2 applied for CALIOP filtering.

| Product | | Accuracy requirement (bias) | Achieved accuracies |
|---|---|---|---|
| **Cloud Fractional Cover** | **(CFC)** | **10%** | **≈ 3% (CALIOP*)**<br>**3.8 % (SYNOP)**<br>**-1.1 % (MODIS)** |
| **Cloud Top Height** | **(CTH)** | **800 m** | **-520 m (CALIOP**)**<br>**307 m (MODIS)** |
| **Cloud Top Pressure** | **(CTP)** | **45 hPa** | **-2.2 hPa (CALIOP**)**<br>**-58.6 hPa (MODIS)** |
| **Cloud Phase** | **(CPH)** | **10%** | **≈ 0% (CALIOP**)**<br>**1% (MODIS)** |
| **Liquid Water Path** | **(LWP)** | **10 g $m^{-2}$** | **6.17 g $m^{-2}$ (UWisc)**<br>**2.05 g $m^{-2}$ (MODIS)** |

| | | | |
|---|---|---|---|
| **Ice Water Path** | **(IWP)** | **20 g m$^{-2}$** | **-5.11 g m$^{-2}$ (MODIS)** |
| **Joint Cloud Histogram** | **(JCH)** | **n/a** | **n/a** |

**Table 8-2:** Summary of CLAAS-2 validation results compared to target precision requirements for each cloud product. Consistency checks are marked in **blue**. * = ICOT>0 applied for CALIOP filtering; ** = ICOT>0.2 applied for CALIOP filtering.

| **Product** | | **Precision requirement** bc-RMS/POD/FAR | **Achieved precisions** |
|---|---|---|---|
| **Cloud Fractional Cover** | **(CFC)** | **L2 POD$_{cld}$ > 90%**<br>**L2 FAR$_{cld}$ < 15%** | **87.5% (CALIOP*)**<br>**16.9% (CALIOP*)** |
| | | **L3 bc-rms < 20%** | **10.0 % (SYNOP)**<br>**7.2 % (MODIS)** |
| **Cloud Top Height** | **(CTH)** | **L2 bc-rms < 2500 m** | **2398 m (CALIOP**)** |
| | | **L3 bc-rms < 1500 m** | **949 m (MODIS)** |
| **Cloud Top Pressure** | **(CTP)** | **L2 bc-rms < 110 hPa** | **134.1 hPa (CALIOP**)** |
| | | **L3 bc-rms < 70 hPa** | **62.7 hPa (MODIS)** |
| **Cloud Phase** | **(CPH)** | **L2 POD$_{liq}$ > 80%**<br>**L2 FAR$_{liq}$ < 20%**<br>**L2 POD$_{ice}$ > 80%**<br>**L2 FAR$_{ice}$ < 20%** | **85.5 % (CALIOP**)**<br>**10% (CALIOP**)**<br>**88.9% (CALIOP**)**<br>**16% (CALIOP**)** |
| | | **L3 bc-rms < 20 %** | **8.7 % (MODIS)** |
| **Liquid Water Path** | **(LWP)** | **L2 bc-rms < 50 g m$^{-2}$** | **34 g m$^{-2}$ (AMSR-E)** |
| | | **L3 bc-rms < 20 g m$^{-2}$** | **11.63 g m$^{-2}$ (UWisc)**<br>**6.50 g m$^{-2}$ (MODIS)** |
| **Ice Water Path** | **(IWP)** | **L2 bc-rms < 100 g m$^{-2}$** | **-** |
| | | **L3 bc-rms < 40 g m$^{-2}$** | **14.82 g m$^{-2}$ (MODIS)** |
| **Joint Cloud Histogram** | **(JCH)** | **n/a** | **n/a** |

# 9 Final remarks

The validated products are considered to be ready for publication. With this report we tried to describe the positive features as well as possible sources of error as accurately as possible within the scope of this document. We emphasised the positive aspects of the CLAAS-2 data record such as the high temporal resolution of the level-2 products and the resulting high sampling rate for the averaged products. The produced variables are available not only as daily and monthly means but also as monthly mean diurnal cycles thereby making use of the advantages of a geostationary imager. However, undesired features also occur when dealing with geostationary satellite imagery, e.g. the effect of an increasing retrieved cloud fraction towards the edge of the SEVIRI disc.

Even though the time-series is limited to 12 years, the amount of processed data was enormous and needed strongly parallelized script control. With this data record we demonstrated the capability of processing a spatially and temporally highly resolved satellite-derived time-series of spectral radiance information on the atmosphere's state. Thanks to its long-term commitment, CM SAF will reprocess SEVIRI based cloud property data records on a regular basis within the next years, i.e. the next edition of CLAAS is planned around 2021, then benefiting from potentially improved calibrations, further enhanced retrievals schemes, and a prolonged time coverage. Meanwhile, there are plans to extend the CLAAS-2 data record on a regular basis with frozen algorithms, in order to bridge the gap to the next edition.

## 10 References

Baum, B. A., W. P. Menzel, R. A. Frey, D. C. Tobin, R. E. Holz, S. A. Ackerman, A. K. Heidinger, and P. Yang, 2012: MODIS Cloud-Top Property Refinements for Collection 6. *J. Appl. Meteor. Climatol.*, **51**, 1145–1163, doi: 10.1175/JAMC-D-11-0203.1.

Baran, Anthony. J., Shcherbakov, V. N., Baker, B. A., Gayet, J. F. and Lawson, R. P., 2005: On the scattering phase-function of non-symmetric ice-crystals. *Q.J.R. Meteorol. Soc*., 131: 2609–2616. doi: 10.1256/qj.04.137.

Benas N., Finkensieper S., Stengel M., van Zadelhoff G.-J. ,Hanschmann T., Hollmann R., Meirink J.F., 2016: Evaluation of the new MSG-SEVIRI based cloud property data record CLAAS-2. In preparation - to be submitted to ACP

CALIPSO Science Team, 2015: CALIPSO/CALIOP Level 2, Lidar Aerosol Profile Data, version 3.30, Hampton, VA, USA: NASA Atmospheric Science Data Center (ASDC). Accessed 2016-04-15 at doi: 10.5067/CALIOP/CALIPSO/CAL_LID_L2_05kmAPro-Prov-V3-30_L2-003.30. (analogous documents for v3-01 and 3-02)

Chepfer H., S. Bony, D. M. Winker, G. Cesana, JL. Dufresne, P. Minnis, C.J. Stubenrauch, S. Zeng, 2010: The GCM Oriented CALIPSO Cloud Product (CALIPSO- GOCCP*), J. Geophys. Res*., **105**, D00H16, doi:10.1029/2009JD012251.

Delanoë, J., and R. J. Hogan, 2008: A variational scheme for retrieving ice cloud properties from combined radar, lidar, and infrared radiometer, *J. Geophys. Res.*, **113**, D07204, doi:10.1029/2007JD009000.

Derrien, M. and H.Le Gléau, 2010: Improvement of cloud detection near sunrise and sunset by temporal differencing and region-growing techniques with real-time SEVIRI, *Int. J. Remote Sens.*, **31**, No. 7, 1765-1780.

Eliasson, S., G. Holl, S. A. Buehler, T. Kuhn, M. Stengel, F. Iturbide-Sanchez, and M. Johnston, 2013: Systematic and random errors between collocated satellite ice water path observations, *J. Geophys. Res. Atm.*, 118, 2629–2642, *doi:*10.1029/2012JD018381.

Fairman, Jonathan G., Jr., Nair, Udaysankar S., Christopher, Sundar A. *et al.*, 2011: Land use change impacts on regional climate over Kilimanjaro, *J. Geophys. Res. Atmos.*, **116**, DOI: 10.1029/2010JD014712

GCOS, 2011: Systematic observation requirements for satellite-based products for climate http://www.wmo.int/pages/prog/gcos/Publications/gcos-154.pdf.

Hamann, U., et al., Remote sensing of cloud top pressure/height from SEVIRI: analysis of ten current retrieval algorithms, 2014: *Atmospheric Measurement Techniques*, 7, 2839-2867, doi:10.5194/amt-7-2839-2014.

Karlsson, K.-G., 2003: A ten-year cloud climatology over Scandinavia derived from NOAA AVHRR imagery. *Int. J. Climatol*., **23**, 1023-1044.

Karlsson, K.-G. and E. Johansson, 2013: On the optimal method for evaluating cloud products from passive satellite imagery using CALIPSO-CALIOP data: example investigating the CM SAF CLARA-A1 dataset, *Atmos. Meas. Tech.*, **6**, 1271-1286, doi:10.5194/amt-6-1271-2013.

Maddux, BC, Ackerman, SA, Platnick, S, 2010: Viewing Geometry Dependencies in MODIS Cloud Products, J. Atm. Ocean. Tech., 27(9), 1519-1528.

Meirink, J.F., R.A. Roebeling and P. Stammes, 2013: Inter-calibration of polar imager solar channels using SEVIRI, *Atm. Meas. Tech.*, **6**, 2495-2508, doi:10.5194/amt-6-2495-2013.

Nakajima, T. and M.D. King, 1990: Determination of optical thickness and effective particle radius of clouds from reflected solar radiation measurements. Part I: Theory, *Journal of the Atmospheric Sciences*, **47**, pp. 1878–1893.

O'Dell, C.W., F.J. Wentz, and R. Bennartz, 2008: Cloud Liquid Water Path from Satellite-Based Passive Microwave Observations: A New Climatology over the Global Oceans. *J. Climate*, **21**, 1721–1739, doi:10.1175/2007JCLI1958.1

Platnick, S., M. King, S. Ackerman, et al., 2003: The MODIS cloud products: Algorithms and examples from Terra., *IEEE Trans Geosci Remote Sens* 41 (2): 459-473.

Reuter, M., Thomas,W., Albert, P., Lockhoff, M.,Weber, R., Karlsson, K.-G., and Fischer, J.: The CM SAF and FUB Cloud Detection Schemes for SEVIRI: Validation with Synoptic Data and Initial Comparison with MODIS and CALIPSO, J. Appl. Meteorol. Climatol., 48, 301–316, doi:10.1175/2008JAMC1982.1, 2009.

Rossow, W. B., and R. A. Schiffer, 1999: Advances in understanding clouds from ISCCP, *Bull. Amer. Meteorol. Soc.*, **80**, 2261-2287.

Seethala, C., and Á. Horváth (2010), Global assessment of AMSRE and MODIS cloud liquid water path retrievals in warm oceanic clouds, *J. Geophys. Res.*, **115**, D13202, doi:10.1029/2009JD012662.

Stengel, M., Mieruch, S., Jerg, M., Karlsson, K.-G., Scheirer, R., B.Maddux, Meirink, J. F., Poulsen, C., Siddans, R., A.Walther, and Hollmann, R.:2013: The Clouds Climate Change Initiative: Assessment of state-of-the-art cloud property retrieval schemes applied to AVHRR heritage measurements, *Remote Sens. Environ.*, **162**, 363-379, doi: 10.1016/j.rse.2013.10.035.

Stengel, M., Kniffka, A., Meirink, J. F., Lockhoff, M., Tan, J., and Hollmann, R., 2014: CLAAS: the CM SAF cloud property data set using SEVIRI, *Atmos. Chem. Phys.*, 14, 4297–4311.

Stephens, G. L., D. G. Vane, R. J. Boain, G. G. Mace, K. Sassen, Z. Wang, A. J. Illingworth, E. J. O'Connor, W. B. Rossow, S. L. Durden, S. D. Miller, R. T. Austin, A. Benedetti, C. Mitrescu, The CloudSat Science Team, 2002: THE CLOUDSAT MISSION AND THE A-TRAIN, *Bull. Amer. Meteorol.* Soc., **83**, 12, 1771-1790.

Tackett, J. L., 2013: Impacts of Change in GEOS-5 Version on CALIOP Products. Accessed 2016-04-15 at http://www-calipso.larc.nasa.gov/resources/calipso_users_guide/data_summaries/pdfs/Impacts_of_Change_in_GEOS-5_Version_on_CALIOP_Products_rev01.pdf

Wentz, F. and T. Meissner. 2000. AMSR Ocean Algorithm. Algorithm Theoretical Basis Document, Version 2. Santa Rosa, California USA: Remote Sensing Systems.

## 11 Glossary

| | |
|---|---|
| AMSR-E | Advanced Microwave Scanning Radiometer for EOS |
| ATBD | Algorithm Theoretical Baseline Document |
| AVHRR | Advanced Very High Resolution Radiometer |
| BC-RMS | Bias-Corrected RMS |
| CALIPSO | Cloud-Aerosol Lidar and Infrared Pathfinder Satellite Observations |
| CALIOP | Cloud-Aerosol Lidar with Orthogonal Polarisation |
| CDO | Climate Data Operators |
| CDOP | Continuous Development and Operations Phase |
| CFC | Fractional Cloud Cover |
| CFOT | Cloud Feature Optical Depth |
| CLARA-A | CM SAF cLoud, Albedo and Radiation products, AVHRR-based |
| CLAAS | CM SAF cLoud dAtAset using SEVIRI |
| CM SAF | Satellite Application Facility on Climate Monitoring |
| COT | Cloud Optical Thickness |
| CPH | Cloud Phase |
| CPR | Cloud Profiling Radar |
| CTH | Cloud Top Height |
| CTO | Cloud Top product |
| CTP | Cloud Top Pressure |
| CTT | Cloud Top Temperature |
| CPP | Cloud Physical Properties |
| DAK | Doubling Adding KNMI (radiative transfer model) |
| DRR | Delivery Readiness Review |
| DWD | Deutscher Wetterdienst (German MetService) |
| ECMWF | European Centre for Medium Range Forecast |
| ECV | Essential Climate Variable |
| ERA-Interim | Second ECMWF Re-Analysis dataset |
| EUMETSAT | European Organisation for the Exploitation of Meteorological Satellites |
| FAR | False Alarm Ratio |
| FCDR | Fundamental Climate Data Record |
| FCI | Flexible Combined Imager |
| GAC | Global Area Coverage (AVHRR) |

| | |
|---|---|
| GCOS | Global Climate Observing System |
| GSICS | Global Space-Based Inter-Calibration System |
| ISCCP | International Satellite Cloud Climatology Project |
| ITCZ | Inter Tropical Convergence Zone |
| IWP | Ice Water Path |
| JCH | Joint Cloud properties Histogram |
| KNMI | Koninklijk Nederlands Meteorologisch Instituut |
| KSS | Hanssen-Kuiper Skill Score |
| LWP | Liquid Water Path |
| MODIS | Moderate Resolution Imaging Spectroradiometer |
| MSG | Meteosat Second Generation |
| MTG | Meteosat Third Generation |
| NOAA | National Oceanic & Atmospheric Administration |
| NWC SAF | SAF on Nowcasting and Very Short Range Forecasting |
| NWP | Numerical Weather Prediction |
| PATMOS-x | Pathfinder Atmospheres-Extended dataset (NOAA) |
| POD | Probability Of Detection |
| PPS | Polar Platform System (NWC SAF polar cloud software package) |
| PRD | Product Requirement Document |
| PUM | Product User Manual |
| REFF | Cloud particle effective radius |
| RMS | Root Mean Square (Error) |
| RTTOV | Radiative Transfer model for TOVS |
| SEVIRI | Spinning Enhanced Visible and InfraRed Imager |
| SAF | Satellite Application Facility |
| SMHI | Swedish Meteorological and Hydrological Institute |
| SYNOP | Synoptic observations |
| SZA | Solar Zenith Angle |
| UWisc | University of Wisconsin passive microwave based LWP dataset |
| VZA | Viewing Zenith Angle |